Fabrication of Nanocomposite Filaments for 3D-Printing of Water Treatment Membranes

by

Emad Shahnam

A thesis
presented to the University of Waterloo
in fulfillment of the
thesis requirement for the degree of
Masters of Applied Science
in
Mechanical and Mechatronics Engineering

Waterloo, Ontario, Canada, 2018

Examining Committee Membership

The following served on the Examining Committee for this thesis. The decision of the Examining Committee is by majority vote.

Supervisor:	Norman Y. Zhou Professor, Dept. of Mechanical and Mechatronics Engineering, University of Waterloo
Internal Member:	Mihaela Vlasea Assistant Professor, Dept. of Mechanical and Mechatronics Engineering, University of Waterloo
Internal-External Member:	Mark Servos Professor, Dept. of Biology, University of Waterloo

I hereby declare that I am the sole author of this thesis. This is a true copy of the thesis, including any required final revisions, as accepted by my examiners.

I understand that my thesis may be made electronically available to the public.

Abstract

The ever-increasing demand to provide fresh, potable water combined with the continued discharge of industrial and agricultural water pollutant chemicals in the water, require developments in conventional water and wastewater treatment operations. Bearing in mind the shortage and scarcity of fresh water sources, it is crucial to devise novel techniques, and design advanced materials to satisfy the growing demand for water and wastewater treatment.

A treatment method that can be enhanced is in the area of Advanced Oxidation Processes (AOPs). AOPs are promising techniques in degradation of organic contaminants through reduction-oxidation (redox) reactions. Through advanced oxidation, the organic materials are decomposed into their constituent molecules. Nevertheless, AOPs often use consumable hazardous chemicals that need to be added to the treatment constantly. Photocatalysis is an advanced oxidation process in which non-consumable sources (in this case photocatalysts) can be employed. Titanium dioxide is a chemically inert, non-consumable photocatalyst. TiO_2 nanomaterials can be used in water treatment in various applications. Aside from their photocatalytic oxidation ability which can degrade organic contaminants such as bacteria, algae, and pharmaceuticals, they can also be used to induce hydrophilicity, increase water flux and hinder membrane fouling. Despite their advantages, further improvements are required to immobilize TiO_2 nanomaterials onto substrates in order to retain them within the water treatment reactors and reuse them constantly. One approach is to introduce TiO_2 nanomaterials to water treatment membranes.

Membrane-based technologies have been used worldwide in various operations such as microfiltration, ultrafiltration, nanofiltration, and reverse osmosis, to serve in several applications including seawater desalination, water purification, and contaminant removal,

etc. Polymers are the most prevalent materials used in water treatment membranes. Despite the wide use of polymeric membranes, novel manufacturing methods are required to decrease energy consumption, use raw materials more efficiently, and possess advanced capabilities to obtain more complex designs. Moreover, membrane fouling is an important obstacle in maintaining the efficiency of the water treatment modules. Another challenge in the membrane treatment is the accumulation of the rejected species on the surface or within the pores of the membrane, which is referred to as 'fouling'. Fouling can reduce flux and intensify the trans-membrane pressure, resulting in energy consumption increase and the addition of chemicals to hinder the accumulation of the rejected particulates.

Nanomaterials can be blended with polymers to produce nanocomposite membranes. TiO_2 and bentonite nanomaterials can be added to the polymers to enhance their performance. Due to the significant developments in additive manufacturing (AM), the layer-by-layer production of water treatment membranes seems feasible. Fused deposition modeling (FDM) is an AM process that requires thin polymer filaments to feed a 3D-printer, to manufacture three-dimensional objects. Such filaments can be obtained by extruding polymer-based mixtures.

In this research, TiO_2 nanobelts were synthesized and together with purchased TiO_2 nanoparticles and bentonite nanoclay, were blended with four different polymers (PMMA, Nylon, PSU, PVDF) in twenty-four different compositions, all of which were extruded to produce nanocomposite filaments. Several experiments have been executed to characterize the mechanical and water treatment properties of the extruded filaments. The filaments showed the capability to degrade organic dyes due to the photocatalysis of TiO_2 nanomaterials and exhibited absorption because of the addition of bentonite nanoclay.

Overall, this research demonstrated that the extrusion of nanomaterial-enhanced polymer filaments is feasible, and the produced filaments show the ability and characteristics

to be employed in water treatment reactors. Such filaments can ultimately be fed into a 3D-printer to manufacture advanced water treatment membranes.

Acknowledgements

First and foremost, I would like to thank my supervisor, Dr. Norman Zhou, for his precious guidance and provisions that benefited me throughout my masters study. I want to thank Dr. Mark Servos who granted access to the Water Group to use his laboratory for research.

I would like to thank Dr. Robert Liang for all the help and advice he has given me during my study. I would like to thank the wonderful teammates in the Water Group who have helped me in research: Ivana Jaciw-Zurakowsky and Azar Fattahi. I am grateful to Dr. Ehsan Marzbanrad for all the insights and motivations he has given me. I would like to thank the co-op students: Olivia M. Schneider, James Tweel and Lena L. Chun Fong for their precious help.

I would like to thank all of my labmates and colleagues in the Centre for Advanced Materials Joining, whom I am truly honoured to work with (in no specific order): Ming Xiao, Hadi Razmpoosh, Amirali Shamsolhodaei, Pablo Enrique, Lorenzo Felix, Erica Wintjes, Paola Russo, Gitanjali Shanbhag, Xu Han and Alireza Mohamadizadeh. I would like to thank the Natural Sciences and Engineering Research Council of Canada (NSERC) for supporting our research.

I would like to thank my beloved family (father, mother and brother) and my wonderful friends for their endless love and support.

Dedication

To My Family

Table of Contents

List of Figures

List of Tables

Chapter 1

Introduction

1.1 Background

The ever-increasing demand to provide fresh, potable water on one hand and the emergence of water pollutant chemicals on the other hand, require developments in conventional water and wastewater treatment operations. Bearing in mind the shortage and scarcity of fresh water sources, devising novel techniques to supply the growing demand for water is crucial.

Advanced oxidation processes (AOPs) are promising techniques in degradation of organic contaminants through reduction-oxidation (redox) reactions. These processes require oxidant sources that are either consumable or non-consumable, whereby the consumable sources need to be supplied constantly while the non-consumable sources do not, provided that their recovery is feasible and efficient. Photocatalysis is an advanced oxidation process in which non-consumable sources (in this case photocatalysts) are employed. Photocatalysis is described as the formation of radical species due to the promotion of an electron from the valence band to the conduction band. These radicals can degrade organic materials

into their constituent molecules [2].

Titanium dioxide is a chemically inert, stable, bio-compatible and cost-effective photocatalyst. TiO_2 nanomaterials ($< 100\,nm$ in size) can be used in water treatment in various applications. Aside from their photocatalytic oxidation ability which can degrade organic contaminants, they can also be used to induce hydrophilicity, increase water flux and mitigate membrane fouling [3]. Despite their advantages, further improvements are required to immobilize TiO_2 nanomaterials onto substrates in order to keep them within the reactors and reuse them constantly. One approach is to introduce TiO_2 nanomaterials to water treatment membranes.

Membrane-based technologies have been widely used all the world over in various operations such as microfiltration, ultrafiltration, nanofiltration, and reverse osmosis, to serve in several applications including seawater desalination, water purification and contaminant removal, etc. Polymers are the most prevalent materials used in water treatment membranes, among which PMMA, Nylon, PSU and PVDF have the greatest contribution [4]. Despite the wide use of polymeric membranes, novel manufacturing methods are required to decrease energy consumption, use raw materials more efficiently, and possess advanced capabilities to obtain more complex designs. Moreover, membrane fouling is an important obstacle in maintaining the efficiency of the water treatment modules.

Fouling can be described as the accumulation of the rejected species on the surface or within the pores of the membrane. The rejected minerals or microorganisms will eventually reduce the flux and intensify the trans-membrane pressure, which would result in increasing the energy consumption to overcome the increase in the pressure and maintain a constant flux.

Nanomaterials can be blended with polymers to produce nanocomposite membranes.

TiO_2 and bentonite nanomaterials can be added to the polymers to enhance their performance. Due to the significant developments in additive manufacturing (AM), the layer-by-layer production of water treatment membranes seems feasible. Additive manufacturing has several great benefits such as the ability to produce more complex designs, as well as using less raw materials inherently by producing less waste [5].

Fused deposition modeling (FDM) is an AM process that requires thin polymer filaments to feed a 3D-printer, through which three dimensional objects can be printed in layers [6]. The filaments can be obtained by extruding polymer-based mixtures.

Incorporation of TiO_2 nanomaterials into polymer-based membranes can present an opportunity to overcome the flux reduction and fouling problems therein. Furthermore, extruding nanomaterial-enhanced composite filaments can pave the way to additive manufacturing of membranes with advanced properties for water and wastewater treatment.

1.2 Objectives

The aim of this research is to extrude TiO_2 nanoparticle-enhanced filaments and examine their properties in order to investigate their overall performance in water treatment applications, and their ability to be used in 3D-printing. The success of the dye degradation and TPA conversion tests will indicate the usefulness of this approach in the water treatment applications, while the mechanical properties of the produced filaments would illustrate the ability of them to be manufactured by advanced processes such as 3D-printing.

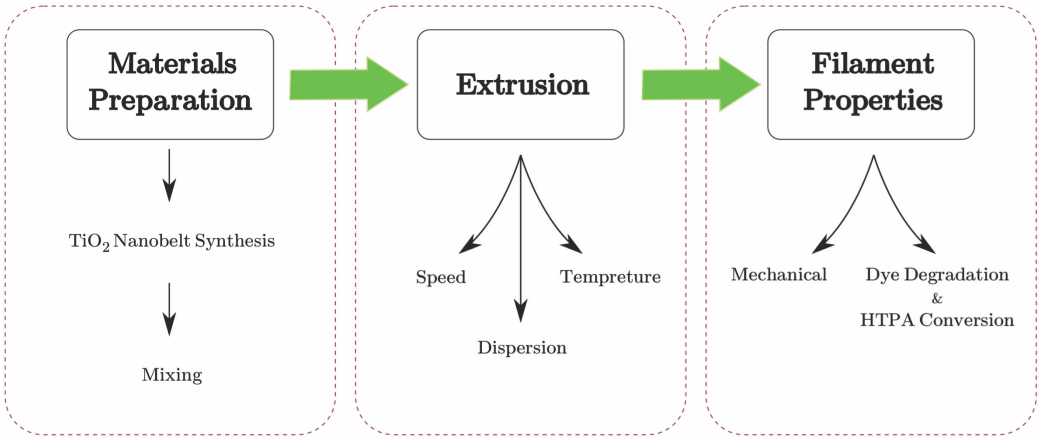

Figure 1.1: Research Overview

1.3 Thesis Organization

- **Chapter 1** introduces the main concepts such as advanced oxidation processes, photocatalysis, water treatment membranes, and advanced manufacturing of nanomaterial-enhanced water treatment membranes, as well as objectives behind this work.
- **Chapter 2** contains a literature review of photocatalysis in water treatment, TiO_2 nanomaterial properties and synthesis, water treatment membranes, and finally, extruding nanocomposite filaments for 3D-printing of water treatment membranes.
- **Chapter 3** describes the experimental methodology in the experiments, which include: material preparation, extruding process, and filament characterization methods.
- **Chapter 4** evaluates the process of filament extrusion, the mixing procedures, and the factors influencing a proper extrusion.

- **Chapter 5** discusses the mechanical and photocatalytic properties of the extruded filaments. The results of the tensile, methylene blue degradation and HTPA conversion tests are described in this chapter.
- **Chapter 6** reviews the conclusions and provides recommendations for future work.

Chapter 2

Literature Review

The population of the world has tripled over the past century and will continue to boost up by another half in the upcoming fifty years [7]. Bearing in mind that population growth results in further industrialization and raises the need for greater agricultural and livestock production, it is apparent that the demand for fresh, potable, and clean water is continuously and rapidly growing. On the contrary, the water supplies and resources all over the world are deteriorating as a result of the climate change and lack of proper use, recycling, and management. Thus, the fresh water shortage is an emerging problem affecting the development of many countries economically and socially.

In addition to the global water shortage, poor water quality is also a major concern in many developing countries. The World Health Organization (WHO) estimated that as of 2015, 663 million people the world over have only access to unimproved drinking water sources [8]. To tackle the mentioned problems, innovation of novel technologies for both water treatment and management is inevitable.

Many of the emerging technologies for water quality are based on photocatalysis. Pho-

tocatalysis is a process in which reduction-oxidation (redox) reactions are enhanced due to the presence of a catalyst that is excited upon receiving certain wavelengths of light. Titanium dioxide (TiO_2) has shown to be successfully effective in the photocatalysis applications because of its reactivity, low toxicity, as well as stability [3]. A complete review of photocatalysis applications in water treatment and the significant role of TiO_2 therein is provided in Section 2.1.

All of the innovations are useful and practical if only they show the possibility of production at an industrial scope, otherwise they are solely limited to the research level. In order for a technology to be applicable worldwide, there needs to be proper platforms to implement the new methods. In case of TiO_2 use in water treatment, some efforts have been done in order to immobilize them in the reactors to achieve extended life-times and prevent their discharge into the effluent which would cause the need for further filtration of the water in order to recover the released TiO_2 particles. A complete review of the path from slurry batch reactors to various immobilization techniques is done in Section 2.2.

Membrane filtration has been extensively used for water and wastewater treatment over the past few decades. Section 2.3 will take a closer look at the membrane production techniques and their applications in water treatment. Furthermore, keeping the great developments in material sciences in mind, novel composites can be produced from combination of ceramics, polymers, etc. that possess the potential to be utilized in water treatment applications. Section 2.3.1 discusses the efforts made to obtain advanced materials for water treatment and disinfection from the material science perspective.

Finally, Section 2.4 will study the application of nanomaterials together with advanced manufacturing techniques in order to introduce the next generation of smart water treatment membranes.

2.1 Photocatalysis applications in water treatment

Not all forms of pollution can be treated using filtration, adsorption, flocculation, or biological methods. Pollution caused by organic compounds such as pharmaceuticals, pesticides, and organic dyes in water is a widespread and important problem. Such compounds are very complicated to remove using the aforementioned conventional water treatment means [9, 10]. Advanced Oxidation Processes (AOPs) have been employed for several decades to remove organic pollutants by generating extremely oxidative radical agents such as hydroxyl ($^{\bullet}OH$), superoxide ($O_2^{\bullet -}$), and perhydroxyl ($HOO^{\bullet}$) radicals [11]. If sufficient exposure and time is given, these radicals could oxidize the target organic compounds and assist in their mineralization into carbon dioxide (CO_2), water (H_2O), or mineral acids [12].

AOPs may employ a consumable or renewable oxidant. Hydrogen peroxide (H_2O_2) for example, is a consumable oxidant. In semiconductor photocatalysis, the photocatalyst is a renewable source, as the term *catalyst* suggests its nature, meaning that since it involves the photo-excitation of electrons from the valence band to the conduction band, the photocatalyst itself is not used up at the end. Provided that the light of appropriate wavelength and energy illuminates the photocatalyst, an electron (e^-) excites to the conduction band and leaves a positive hole (h^+) —electron deficiency — behind in the valence band. The h^+ and e^- play as the oxidizing and reducing agents respectively which take part in redox reactions. The required potential of the organic compound is determined by the position of the valence band and the redox potential of the organic compound with regards to a standard electrode. If more negative than the redox level of the h^+, the organic compound would reduce the h^+, and becomes a positive radical as a result which can participate in further reactions at a faster rate. On the contrary, if the organic compound has a more positive redox potential, the h^+ will be reduced by water or adsorbed OH^- ions. In this

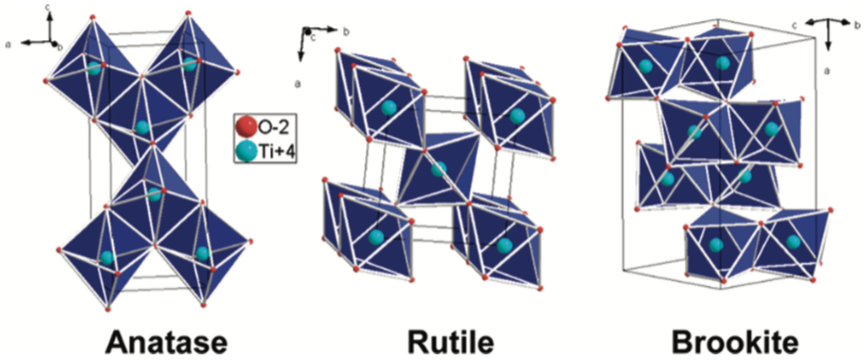

Figure 2.1: TiO_2 crystalline forms- Adapted with permission from ([1]). Copyright (2018) American Chemical Society."

case, $HO^{\bullet}$ or other radicals are produced as a result which in turn are able to oxidize organics [13].

Overall, semi-conductor photocatalysts have been among the most effective approaches for both water and wastewater treatment, because of their high efficiency and capability to eliminate bacteria and other organic pollutants. Moreover, photocatalysis is considered as a green, nondestructive and sustainable technology, keeping in mind that it only uses light as its source of energy and is a renewable source [14].

2.1.1 TiO_2 as a photocatalyst

Titanium dioxide (TiO_2) is perhaps the most widely used photocatalyst in water treatment [15]. It is a powerful oxidizer near-UV radiation. It is chemically stable in the acidic and basic environments, yet chemically inert in the absence of UV illumination [16]. TiO_2 exists in three crystalline forms: anatase, rutile, and brookite (Fig. 2.1). Anatase shows the best photocatalytic ability [17].TiO_2 possesses a wide band gap — 3.21 eV for anatase, 3.13

eV for brookite, and 3.00 eV for rutile [18] — with optical absorption in the ultraviolet spectrum (less than 400 nm). Under ultraviolet (UV) illumination, an electron from the valence band (VB) elevates to the conduction band (CB) which leaves an electron hole behind. The following processes can occur after electron excitation: (i) electron-hole recombination, (ii) trapping of electron and hole in meta-stable states, or (iii) reaction of electrons and holes with electron donors or acceptors in the vicinity of the nanomaterial surface.

In electron-hole recombination (i), an electron from the conduction band descends to the valence band and its energy is dissipated in the form of a photon (light). Moreover, in electron and hole trapping in meta-stable states (ii), the excess energy during recombination is transferred to the crystal lattice (phonon emission). This process is made possible because of the existence of traps between valence and conduction band due to lattice defects at the energy level (Et) [19]. Nonetheless, the goal of photocatalysis is to increase the reaction of electrons and holes with with the neighbouring organic molecules, as pointed in (iii).

Superhydrophilicity is another distinctive characteristic of TiO_2. A hydrophilic surface tends to favor water molecules whereas a hydrophobic one tends to repel water molecules. If TiO_2 is applied to a surface which is then illuminated by light, the superhydrophlic effect of TiO_2 is formed after certain time of exposing to the light, whereby the contact angle between the water droplets and the surface reaches zero degrees. Nevertheless, the hydrophilicity will disappear once the illumination stops [3].

TiO_2 particles having small sizes (below 100 nm) could exhibit high visible light transparency and UV light absorption [20]. The small size of nanoparticles can also improve the adsorption coefficients of organic molecules on their surfaces [21]. There are various methods of synthesizing TiO_2 nanomaterials. The most general classification of these

methods is by dividing them into two major categories of aqueous and non-aqueous methods. The first category includes "Sol-Gel" and "hydrothermal" approaches and the latter one is composed of "solvothermal" and "nonhydrolytic" methods [22]. Despite the fact that profounder study of all of the synthesis methods is beyond the scope of this review, since TiO_2 nanobelts in this research are synthesized with the hydrothermal method, it is covered in a greater depth. Nevertheless, it is imperative to learn that nanoparticles, nanorods, nanobelts, and other forms of nano-structures can be produced through different methods of synthesis [23].

2.1.1.1 Hydrothermal Synthesis

Hydrothermal method is a process used to synthesize one dimensional nanostructures, nanobelts, and nanotubes, by means of phase transformation. This method is usually conducted in steel vessels, called autoclaves with or without Teflon liners, under controlled temperature and pressure. The reaction happens in an aqueous solution. The amount of added solution together with the temperature produce the internal pressure in the autoclave. Hydrothermal synthesis is a method used extensively to produce small ceramic particles [23].

Most hydrothermal processes lack in efficiency in terms of solubility and uniformity of the materials. Even so, the crystallinity of the particles is distinctively enhanced compared to the sol-gel method. Most of the one-dimensional nanomaterials emanate from alkaline hydrothermal processes. Generally, ammonia or alkaline hydroxides are used to form titanium hydroxide, which is then dried to titania under high temperature in the autoclave. Equations 2.1 to 2.3 demonstrate the chemical reactions occurring in a typical hydrothermal synthesis of one dimensional TiO_2 nanostructures [2]:

$$3\,TiO_2 + 2NaOH \rightarrow Na_2Ti_3O_7 + H_2O \tag{2.1}$$

$$Na_2Ti_3O_7 + 2\,HCl \rightarrow H_2Ti_3O_7 + 2\,NaCl \tag{2.2}$$

$$H_2Ti_3O_7 \rightarrow 3\,TiO_2 + H_2O \tag{2.3}$$

pH of the solution, temperature, and the presence of counter ions dictate the nature of the TiO_2 structures in the solution. Stirring of the solution during hydrothermal treatment can also affect the nature of the titania. For instance, pure rutile phase can be achieved under vigorous stirring of the solution [22].

Overall, titanium dioxide materials produced by hydrothermal method can have a large diversity in terms of the type of the structures. Nanoparticles, nanorods, nanotubes, platelets and nanoplates, hollow microspheres, nanosheets, etc. are examples of the hydrothermally produced titania, which can be classified into three major categories of three, two, and one-dimensional forms. [22, 23, 24].

2.2 Application of TiO_2 in water and wastewater reactors

TiO_2 has often been used in slurry batch reactors [25, 26, 27] which resulted in reasonable organic degradation rates. Nevertheless, the use of photocatalysts in the slurry reactors has

a serious drawback, which is the need to remove the catalyst nanoparticles from the treated effluents. This step introduces considerable costs and efforts which hinders its practical use in water and wastewater treatment applications in large scales. For instance, several separation mechanisms (such as centrifuging and gravity settling) have been tested and proved to be costly and impracticable due to the very low density of TiO_2 nanoparticles [28].

As a consequence, various methods have been suggested to immobilize TiO_2 nanomaterials on different substrates [29, 30, 31, 32, 33, 34]. These substrates include metals [35], glass [36], activated carbon [37], alumina (Al_2O_3) [38], and mostly polymers [39, 40, 41, 42, 43]. These substrates could be thin films of solid or porous materials. More recently, coating of TiO_2 nanoparticles on quarts fibers has also been investigated [44]. These efforts have been complicated in terms of both preparation of the TiO_2 solutions as well as the substrates, and coating endeavors.

As a result, even though TiO_2 photocatalysis seems very promising in terms of organic removal from water and wastewater, its applications have not been prevalent at the industrial level. Novel methods and solutions are required to easily manufacture substrates containing immobilized TiO_2.

2.3 Membranes for water and wastewater treatment

Membrane-based technologies are used in various areas of engineering, and extensively, in water and wastewater treatment. In general, a membrane is a barrier that separates two phases and restrains the transportation of species based on their size [45]. Membranes are used in microfiltration, ultrafiltration and nanofiltration to produce fresh water and retain minerals and micro-species within the influent. Reverse osmosis membranes, on

the other hand, are used to stop minerals and salt ions in the water by applying high pressures. As a result, membranes need to possess certain characteristics such as chemical stability, mechanical durability, the ability to tolerate very high pressures and wide pH ranges. Overall, membrane water treatment is playing a significant role in different areas of drinking water, seawater desalination, and wastewater treatment and reuse, bearing in mind that its operation is simple, it does not need chemical additives, and is manufactured in modules for easy setup and maintenance [46, 47].

On the other hand, membrane fouling is one of the challenges in membrane water treatment. Fouling is defined as the accumulation of rejected particulates on the membrane surface or inside the pores therein. The feed water may contain concentrations of dissolved and suspended matter. Suspended solids include inorganic particles, and biological species such as bacteria and algae.During treatment operations, the concentration of such matters increases eventually. The settled suspended solids decrease water flux as they block the passage of water molecules through the membrane. In addition, the inorganic molecules precipitate on the surface as well as inside the pores and form scales in there and, consequently, they also contribute to the flux reduction. Beside decreasing in the flow rate, fouling can also increase the trans-membrane pressure, meaning that energy consumption would also rise correspondingly, to overcome the pressure difference. *Bio-fouling* describes the accumulation of microorganisms on the membrane surface. Not only microorganisms are amassed on the membrane, but also they continue to grow on the surface since enough water and nutrients are available in their vicinity. Therefore, on top of flux reduction, bio-fouling can also change the pH of water and degrade the polymer molecules of the membrane, thus, impair the performance [48]. TiO_2 photocatalysis is a promising method to mitigate membrane fouling as it can degrade organic microorganism on the membrane surface.

Hydrophobicity and hydrophilicity of the membrane materials are greatly studied in the literature. The hydrophobicity of membranes increases the rate of fouling due to the adhesion of particulates on to the surface [49]. Hydrophobicity is defined as the physical property of a molecule to repel a water molecule, as mentioned in 2.1. Nonetheless, there have been several approaches to increasing the hydrophilicity —tendency of molecules to prefer water molecules in their vicinity — of the membrane material and reducing the membrane fouling. They include blending hydrophilic materials with the membrane building polymer molecules, surface coating, photo- and thermal-induced grafting, plasma treatment, etc. [50].

2.3.1 Membrane Materials

Membranes are produced from variety of materials such as ceramics [46], metals [51, 52], polymers, or their combination (composites). Cellulose acetate (CA), polysulfone (PSU), polyethersulfone (PES), sulfonated PSU or PES, polyacrylonitrile (PAN), polypropylene (PP), polycarbonate (PC), polytetrafluoroethylene (PTFE, a.k.a Teflon), polyvinylidine fluoride (PVDF), and Nylons are the most common polymers (organic materials) used in membrane production [46, 53, 54].

Each membrane material has its own advantages and disadvantages. For examples, even though ceramics are thermally stable and chemically resistant, their high cost and fragility impedes their extensive use. Furthermore, stainless steel membranes posses good mechanical durability, but like ceramics, their expensive cost limits their application to certain processes.

Polymeric membranes are currently the most used membranes in water treatment. Significant pore forming mechanism, high flexibility, easy installation and lower cost compared

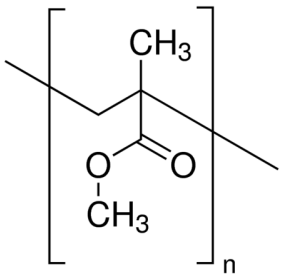

Figure 2.2: PMMA structure

to their inorganic counterparts are only few characteristics they offer [55]. Despite their advantages, several areas still seek improvements.

Polymethyl methacrylate (PMMA), polysulfone (PSU), polyvinylidine fluoride (PVDF), and nylon 6 are among the most widely used materials for water treatment membranes [4, 46]. These polymers are all thermoplastic, meaning that they all have the ability to being repeatedly melted and hardened by heating and cooling. The succeeding paragraphs describe the properties of the aforementioned polymers in regards to water treatment.

2.3.1.1 PMMA

Polymethyl methacrylate (PMMA), also known as acrylic, is a synthetic resin product of the polymerization of the liquid methyl methacrylate (MMA). The associated chemical formula for this polymer is $[CH_2C(CH_3)(CO_2CH_3)]_n$ or in the short form: $(C_5H_8O_2)_n$ as shown in Figure 2.2.

PMMA is a transparent and rigid thermoplastic. Its nearly perfect transparency in visible light range makes PMMA a good candidate to employ it in optical applications [56]. The glass transition temperature (T_g) for pure PMMA is 104.6 °C [57]. At temperatures above T_g, the polymer will act similar to the pastes and is able to move in the extruder

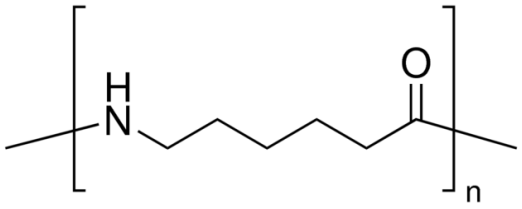

Figure 2.3: Nylon structure

chamber.

The water contact angle of PMMA is 67.8 °C [58]. Although contact angles below 90 degrees are considered hydrophilic in general, the closer their value to 0°, the more hydrophilic the material is.

2.3.1.2 Nylon

The term "nylon" describes a group of organic polymers containing the amide (-CONH) group, hence the group is also called "polyamides". The various membres of this family are distinguished by adding different numbers after the term nylon. Each number indicates the chemical composition of the polymer molecule. Nylon6 is one of the most important and widely used members of this family. From this point, 'nylon' and 'nylon 6' are used interchangeably, referring to nylon 6. Nylon 6 is a thermoplastic with the linear formula of $[CO(CH_2)_5NH]_n$ and the short formula of $(C_6ONH_{11})_n$ [59] (Fig. 2.3).

The glass transition temperature (T_g) of Nylon is 62.5 °C and the reported melting temperature (T_m) is 228.5 °C [60]. Nylon possesses good toughness and abrasion resistance that make it a noteworthy replacement choice for numerous applications to substitute in lieu of metals and rubbers [61]. Furthermore, nylon is a hydrophilic polymer intrinsically [62]. To conclude, all of these properties make nylon an ideal choice of material for both

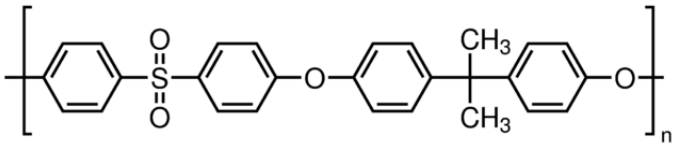

Figure 2.4: PSU structure

membranes and membrane support structures theoretically. However, more effort is needed to achieve greater and more developed manufacturing qualities.

2.3.1.3 PSU

Polysulfone (PSU or PSF) is a class of polymers with high thermal stability which is due to the diphenylene sulfone group in its structure. The linear chemical formula of PSU is $[C_6H_4\text{-}4\text{-}C(CH_3)_2C_6H_4\text{-}4\text{-}OC_6H_4\text{-}4\text{-}SO_2C_6H_4\text{-}4\text{-}O]_n$ and the associated short formula is $(C_{27}H_{22}O_4S)_n$ (Fig. 2.4). In addition to demonstrating high resistance to oxidation, PSU can tolerate chemicals and in fact is capable of withstanding long exposures to chlorinated water. Consequently, it can even endure free chlorine contact as much as 200 mg/L for shorter periods of time (e.g. during back wash). On top of its resistance to chemicals, PSU is also resistant to a wide pH range between 1 to 13 [63]. All of these characteristics make PSU an ideal material of choice in water treatment membranes.

The glass transition temperature (T_g) of PSU is 187 °C [64]. It is worth of mentioning that polysulfone is a thermoplastic and can be melted and hardened without losing its properties.Several grades of PSU are classified based on the melt viscosity, all of which can be employed in microfiltration (MF) and ultrafiltration (UF) membranes [65, 66]. Polysulfones are also utilized in microporous supports in thin film composite membranes especially in reverse osmosis (RO) support membranes [46].

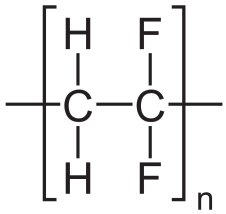

Figure 2.5: PVDF structure

PSU is a hydrophobic material [67], a quality that counts as a drawback in water treatment membrane applications. Therefore, efforts need to be taken so as to hydrophilize the surface of PSU membranes in order to hinder fouling rates and increase water flux through PSU-made membranes.

2.3.1.4 PVDF

Polyvinylidende fluoride (PVDF) is a stable thermoplastic polymer with linear and short chemical formulae of $(CH_2CF_2)_n$ and $(C_2H_2F_2)_n$, respectively (Fig. 2.5).

This fluoropolymer is obtained through polymerization of vinylidene difluoride and is highly inert, meaning that it can tolerate harsh chemicals for long periods of time. It can also withstand the contact to any concentration of free chlorine, as well as pH range of 2 to 10 [63]. Consequently, excellent heat and abrasion resistance on top of good mechanical strength result in wide applications of PVDF in pipes, fittings, and valves industry as well as semiconductor products [68]. Apart from these characteristics, PVDF also exhibits significant ultraviolet stability [69], a property that enables their cooperation with UV treatment applications.

Nonetheless, the 97.4° contact angle of PVDF classifies this polymer amongst hydrophobic materials [70]. Further modifications are needed to reduce the contact angle and en-

hance the hydrophilicity thereof. The glass transition temperature (T_g) for PVDF is -35 °C [71] and the associated melting point is 178 °C [72].
Due to the exceptional properties mentioned above, PVDF is vastly used in MF and UF. Moreover, regarding its strong chemical resistance, cleaning and disinfecting of such membranes can be vigorous without imposing any degradation to the membrane [63].

2.3.2 Nanocomposite Membranes

Promising to overcome challenges such as fouling mitigation, composite materials have gained interest in water treatment membrane production. Polymeric nanocomposite membranes are advanced membranes whereby nanomaterials are dispersed in the polymer matrix. On top of water treatment, such composite membranes are also used in gas-gas, liquid-liquid, and liquid-solid separations. In addition to the improved hydrophilicity and antifouling, the incorporation of nanomaterials into polymers would also enhance porosity, and chemical, mechanical and thermal stability [73].

The fabrication of the conventional nanocomposite membranes is mostly based on phase inversion (PI). In PI, the nanomaterials are first dispersed in the polymer solution, followed by the PI process, to produce flat sheets or hollow fiver configurations, which are mainly used in microfiltration or ultrafiltration, due to their potential porosity. The nanomaterials used therein (or: nanofillers) can be inorganic, organic, or bio- materials.

Inorganic materials can be metal oxides (eg. TiO_2 [74], SiO_2 [75], Al_2O_3 [76], Fe_3O_4 [77], ZrO_2 [78], ZnO [78]), metals (Ag [79], Cu [80], Se [81]), or non-metals (such as: zeolite [82], carbon nanotubes (CNTs) [83], clay [84]). Organic and biomaterial nanofillers are beyond the focus of this research.

Photocatalysis and antibacterial activities are phenomenal functionalities that are added

to the membranes due to the incorporation of nanomaterials in the matrices. TiO_2 has been added into various polymer matrices to provide photocatalytic properties. Rahimipour et al [85] studied TiO_2/PES membranes and showed that under the illumination of UV light, these membranes exhibited higher flux and enhanced antifouling, comparing to same conditions in the absence of UV. TiO_2/PVDF membranes too, appeared in several researches [86, 87], where the results suggested improved fouling resistance, antibacterial capability and better flux.

Clays are minerals occurring naturally, due to weathering of volcanic ashes. Depending on their groups and sources, they vary in chemical composition and characteristics, and are classified into several groups of montmorillonite, bentonite, kaolinite, etc. Consequently, nano-particles of layered mineral silicates are called nanoclay.Nanoclays have also been added to polymers to make nanocomposites. Even a small addition of nanoclay (3% wt) can enhance mechanical and thermal properties of the nanocomposites. Atop from this, several species in the organoclays (e.g. alkyle ammonium cations) could reduce the surface energy of the inorganic host and intensify weting properties of the polymer [88]. This ability to lower the surface energy of the host further helps them in adsorption. The lowest surface energy of the adsorbate and adsorbent is most stable according to adsorption isotherms.

The organic molecules bind to the ionic surface of the clay molecules and alter their hydrophilicity, transforming them to hydrophobe organophilic material that can adsorb hydrocarbons. In water treatment applications, oranoclays are often implemented in the adsorption of oil, heavy metals, organic matter (humic and fulvic acids), etc. The explanation behind organic molecule removal ability of the organoclays is that they consist of interspersing organic and inorganic layers, of which the hydrophobic organic layer tends to adsorb organic materials from water. It has been studied that nanoclays can significantly decrease turbidity and oil and grease concentrations in wastewater [88]. Notwithstanding

such advantages, recovering the nanoclay from water batches and reactors, and further recycling and regeneration of this adsorbent remains a challenge [89]. Ideally, nanoclay should be easily recovered from the product water, otherwise it hinders their widespread use. Intermixing of nanoclay with polymers in nanocomposites production is a solution to immobilize them in the matrix, preventing them from dispersion in water.

The most used clay in synthesizing of polymeric nanocomposites is montmorillonite (MMT). MMT is the major component of bentonite. Bentonite has different types of chemical formulae depending on the dominant element —aluminum, calcium, potassium and sodium. However, only the sodium- and calcium-bentonites are used at an industrial level, both having the potential to be implemented in water treatment applications. Hydrophobic interaction is the bentonite's main mechanism for removing organic micropollutants. Additionally, the bentonite has been proved to successfully adsorb several metallic cations such as Zn^{2+}, Ca^{2+}, and Co^{2+} in aqueous solutions [89].

2.4 Advanced techniques for water membrane manufacturing

Nanoparticle reinforced composite materials and rapid prototyping/manufacturing are two growing technologies in materials and manufacturing [90]. Nanoparticle reinforced polymers not only exhibit enhanced characteristics, as mentioned in 2.3.2, but also retain their processibility properties during extrusion and molding [91]. Nanoparticle-based membranes can be produced by blending nanomaterials into the polymer matrix. The conventional method for producing such membranes is the phase inversion, 2.3.2. However, with the great developments in the field of additive manufacturing during the last two decades, man-

ufacturing nanocomposite membranes seems feasible. Additive manufacturing is basically the creation of a three-dimensional object in a layer by layer manner. Fused deposition modeling (FDM) is an additive manufacturing process in which a polymer filament is fed into a machine (also known as: 3D-printer) where the nozzle melts the filament and deposits it in layers [6]. By engineering the filament materials and properties, it is possible to extrude advanced nanomaterial-enhanced filaments, and later 3D-print them.

Extrusion is a mechanical process for creating objects with a fixed cross-section. Infinitely long wires or bars can be extruded in either of the hot or cold environments. In the hot extrusion, the material of choice is heated up to near melting temperatures, as opposed to the cold extrusion which occurs at ambient conditions. Metals, ceramics, polymers, and more recently, composites can be produced through this method. In extrusion, the desired material is pressed to pass through a die, thus gaining its two-dimensional geometry. The ability to produce fixed cross-sectional profiles is due to utilization of such dies.

Extrusion of polymer-based filaments is executed in hot temperatures. The need to control the temperature rises due to the difference in the glass transition temperature of different materials. Therefore, it is imperative to achieve the desired extrusion temperature of the materials, both theoretically and experimentally. Previous researchers have tried to integrate polymers with TiO_2 nanomaterials. They extruded TiO_2 enhanced filaments with ABS ([92]), PMMA([56]), and polypropylene ([93]). However, a complete comparison between different polymers is still needed. In addition, the incorporation of bentonite nanoclay into such compositions also needs deeper study.

Development of nanomaterial-enhanced polymeric filaments that possess sound mechanical and chemical properties is the first step to be able to successfully 3D-print nanocomposite membranes with improved water flux and antifouling properties for water and wastewater treatment.

Chapter 3

Experimental Methodology

3.1 Materials Preparation

Prior the extrusions, required materials were either purchased or synthesized. The materials are classified into three groups of titania nanomaterials, polymers, and bentonite nanoclay. Preparation of each material is elaborated in the succeeding parts. Ultimately, in the last part of this subsection, the composition percentages are discussed.

3.1.1 Titanium dioxide nanomaterials

3.1.1.1 TiO_2 Nanobelts

In addition to the nanopowder, titania was also used in the nanobelt form. TiO_2 nanobelts were synthesized in the lab from P_{25} precursor through hydrothermal synthesis method which was introduced earlier in 2.1.1.1. Here, the exact method applied in synthesizing the titania nanobelts is described.

Twenty-four grams of NaOH pelletes (99%) and 2 grams of P_{25} both from Sigma-Aldrich [94], and concentrated HCl (36 - 38%) were prepared. NaOH was poured into 60 mL of MilliQ water to produce 10 M NaOH solution, and dissolved by sonicating in an ultrasonic bath. Furthermore, the solution was also stirred manually using a glass rod in order to prevent pellets from clustering together. The NaOH solution was then poured into a Teflon-lined autoclave, followed by transferring the P_{25} powder therein. After stirring vigorously, the autoclave was sealed properly and the steel cap was completely tightened. The autoclave was then put inside an isothermal furnace for twenty-four hours under the temperature of 240°C to produce nanobelts. After the heating time was over, the furnace was turned off and opened to let the autoclave cool down in the ambient temperature.

Once at ambient temperature, the autoclave was opened up and the alkaline liquid in the vessel was drained. The white $Na_2Ti_3O_7$ nanobelts were scraped off the vessel and transferred into a 500 mL beaker. By adding MilliQ water, the volume of the solution reached 400 mL. The solution was mixed and poured into 50 mL centrifuge tubes which were centrifuged at 3500 rpm for 30 minutes. When finished, the liquid in the tubes was discharged and fresh MilliQ water was added instead. This procedure was repeated three times to remove excess sodium and hydroxyl ions from the solution. Consequently, the the nanoparticles were transferred into a beaker and immersed in 400 mL of 0.1 M HCl acid. The solution was sonicated for one hour and left intact for 12 hours.

A Whatman filter (Grade 1, 185 mm) was inserted into a funnel and placed on an Erlenmeyer flask. All the $H_2Ti_3O_7$ nanobelt solution was poured on the filter and the nanobelts were rinsed by MilliQ water until pH 7 was achieved. After this step, the filter with its nanobelts content was placed in an oven at 70 °C for four hours in order to dry.

After the $H_2Ti_3O_7$ nanobelts were dried, they were scraped off the filter into a mortar, followed by grinding them using a pestle until fine powder with no clumps was achieved.

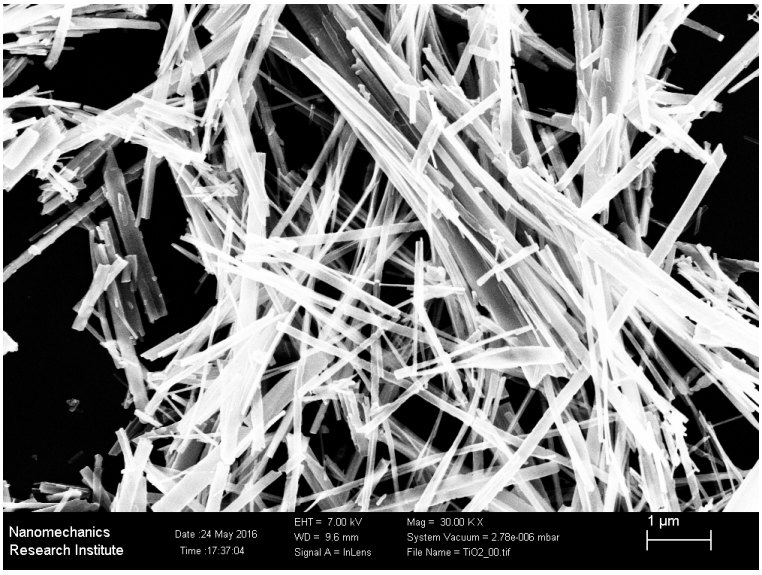

Figure 3.1: SEM image of TiO_2 nanobelts synthesized by the hydrothermal method

The powder was transferred into an alumina cup which was then capped by a disk of the same material and placed in a furnace at 700 °C for four hours. After this heat treatment, the door of the furnace was opened to allow the alumina cup and its content gradually cool down in the ambient temperature.

Finally, TiO_2 nanobelts were removed from the alumina cup and transferred into scintillation vials for storage and future use. Figure 3.1 demonstrates the TiO_2 nanobelts synthesized through hydrothermal method.

3.1.2 Composite mixtures

Titanium (IV) oxide nanopowder (Aeroxide^{TM} P_{25}) with the average particle size of 21 nm was acquired from Sigma-Aldrich. Hydrophilic bentonite nanoclay was purchased from Sigma-Aldrich. The size of the particle was less than 25 μm as indicated on the product

container and website [95]. The four polymers used in the experiments were polymethyl methacrylate (PMMA), polysulfone (PSU), polyvinylidine fluoride (PVDF), and nylon 6 (2.3.1). All of these polymers were purchased from Sigma-Aldrich. Except PSU that was initially in the pellet form, all the rest were powder.

3.2 Compositions

Each polymer was proposed to be tested in six different compositions which include: polymer plus P_{25}; polymer plus TiO_2 nanobelts; combination of polymer, P_{25}, and bentonite nanoclay; combination of polymer, TiO_2 nanobelts, and bentonite nanoclay; pure polymer; and at last, polymer plus bentonite nanoclay without the presence of TiO_2 in any form.

Polymers constitute the main part of the filaments. Not only they act as the binding agent to keep the nanomaterials in place throughout the composite, but also provide flexibility and formability to produce sophisticated mechanical designs, as discussed in (2.3.1). Hence, for the mixtures that include TiO_2, the polymers compose 95% and 93% of the weight in bipartite and tripartite compositions, respectively. In the 'polymer and nanoclay' blends however, the polymer weight increases to 98%. It goes without saying that in the composition involving pure polymer, the associated weight is 100%. The TiO_2, whether in P_{25} or nanobelt form, is used at 5% by weight constantly when present in the mix. On the other hand, if used, bentonite only makes up 2% of the weight of the compositions. All of the aforementioned information is summarized in Table 3.1. For convenience in naming, a short code is attributed to each composition.

Code	**Polymer**	**Wt%**	**TiO_2**	**Wt%**	**Nanoclay**	**Wt%**
M_1	PMMA	95	P_{25}	5	—	0
M_2	PMMA	95	Nanobelts	5	—	0
M_3	PMMA	93	P_{25}	5	Bentonite	2
M_4	PMMA	93	Nanobelts	5	Bentonite	2
M_5	PMMA	100	—	0	—	0
M_6	PMMA	98	—	0	Bentonite	2
N_1	Nylon	95	P_{25}	5	—	0
N_2	Nylon	95	Nanobelts	5	—	0
N_3	Nylon	93	P_{25}	5	Bentonite	2
N_4	Nylon	93	Nanobelts	5	Bentonite	2
N_5	Nylon	100	—	0	—	0
N_6	Nylon	98	—	0	Bentonite	2
S_1	PSU	95	P_{25}	5	—	0
S_2	PSU	95	Nanobelts	5	—	0
S_3	PSU	93	P_{25}	5	Bentonite	2
S_4	PSU	93	Nanobelts	5	Bentonite	2
S_5	PSU	100	—	0	—	0
S_6	PSU	98	—	0	Bentonite	2
V_1	PVDF	95	P_{25}	5	—	0
V_2	PVDF	95	Nanobelts	5	—	0
V_3	PVDF	93	P_{25}	5	Bentonite	2
V_4	PVDF	93	Nanobelts	5	Bentonite	2
V_5	PVDF	100	—	0	—	0
V_6	PVDF	98	—	0	Bentonite	2

Table 3.1: Composition of the materials

3.2.1 Initial Mixing

Twenty-four compositions were prepared according to Table 3.1. The materials were weighed to reach the total mass of 20 grams for each batch. After achieving the desired mass proportions, the powder was admixed manually using a spatula for sixty seconds. By this point in time, the mixture appeared homogeneous in terms of overall colour. The reason behind naming this step as "initial mixing" is that the overall blending is not limited to the manual endeavor only. As will be discussed in the next subsection, a superior extent of mixing will be accomplished during the next steps of extrusion. Thus far however, the premix is ready to be fed into the extruder.

3.3 Extrusion Process

3.3.1 Procedure

Filabot EX2 Filament Extruder was purchased from Filabot company. This device has an hopper for material input. The feeding material maximum particle size is one eighth of an inch, where finer powder is favored since it limits the stress exertion to the main screw. At the bottom of the inlet, the feed will enter a cylindrical chamber in which a screw (approximately the same diameter as the internal diameter of the chamber) is connected to the motor and rotates. The rotation of the screw transfers the feed forward toward the nozzle. As the feed moves forward, it creates empty space behind, leading to intake of more feed material into the chamber due to the force of gravity. The extruder mechanism is basically moving the intake feed forward in the screw chamber, while simultaneously heating the material. The heating causes the thermoplastic polymer powder/pellets to

reach temperatures higher than their glass transition temperature and deform from their previous solid state shape. Close to the nozzle outlet, the pressure exerted by the rotation of the screw forces the fluid-like material to exit the nozzle, adapting the shape and diameter of the nozzle hole. Various shapes and sizes can be produced at the nozzle. The nozzles used for this type of extruder can possess dyes between 1 to 4.5 mm in diameter. In this research, the nozzle dye had a 1-millimeter-diameter circular shape.

Once outside the nozzle, the ambient air cools down the extruded flow and solidifies it, resulting in 'filaments'. Other than natural cooling, the filament can also be cooled by either passing it through a water pool or by blowing air into it using a fan. In production of filaments for this dissertation, the latter method —utilizing a fan to cool down the filament —was employed. In general, rapid cooling is suggested so the filament retains the desired diameter and shape.

The extruder has two control knobs, to adjust temperature and speed. The temperature ranges between the room temperature to the maximum of 450°C. Consequently, the rotation speed ranges between 0 to 35 rounds per minute (rpm). Both the temperature and speed control are explained in 3.3.6 and 4.2 in greater depth because of their importance.

3.3.2 Secondary and Tertiary Mixing

Secondary and tertiary mixing take place inside the extruder. Due to the constant rotation of the screw, a great blending of the powder/pellets occurs inside the screw chamber. After the manually-mixed feed material 3.2.1 are fed into the extruder, the particles are thoroughly mixed in the chamber. Taking advantage of the blending ability of the feed screw, the produced filament was cut into 1-cm pieces and the whole extrusion process was repeated once more in order to guarantee a complete mix. As a result, after the initial

manual mixing, the components are blended two more times in the extruder.

3.3.3 Dispersion

In order to investigate the quality of blending and dispersion of different components of the compositions, several tests were performed which are described in the following sections (3.3.4 and 3.3.5).

3.3.4 Scanning Electron Microscopy + Energy-Dispersive X-ray spectroscopy

All of the filaments were examined by Scanning Electronic Microscopy (SEM) and Energy-Dispersive X-ray spectroscopy (EDX). Energy-Dispersive X-ray spectroscopy (EDX) analysis was performed to obtain a general understanding about the chemical elements within all of the compositions. Moreover, this analysis was also done to examine the likely-hood of the presence of undesired materials in the compositions. The preparation procedure for the samples and the microscopy methodology is described as follows:

3.3.4.1 Sample Preparation

The 24 filaments were divided into four groups, based on the polymer type. Each group (6 filaments) was cut using a wire cutter and placed onto a clay stick inside a mounting cup. After this step, Struers^{TM} epoxy resin was acquired. Struers' epoxy system composes two components: a resin and a curing agent (hardener). If mixed in the appropriate proportion, the mixture will solidify and harden in less than an hour.

The epoxy resin and the hardener were added to a separate cup and stirred with a wooden popsicle stick for one minute, after which the solution was added to the original mounting cup containing the filaments. The mounting cup was put under the fume hood for at least two hours. Once the polymerization was complete and a solid rigid mount was achieved, it was removed from the mount.

The next step involved grinding and polishing the surface of the mount in order to accomplish a smooth scratch-free surface to be examined under SEM. The grinding procedure began using a 1200 grit sandpaper on a Struers^{TM} grinding machine. After about 3 minutes, the sandpaper was substituted by a finer one. 800, 600, 400 grit sandpapers were used in this process. Every time, the orientation of the mount was rotated perpendicularly in order to enhance the grinding quality and leaving no micro-trenches on the surface.

After grinding with sandpapers, 6 μm, 3 μm and 1 μm polishing pads were installed on a Struers polishing machine in the same order as mentioned—from coarser to finer, and the mount was placed in the mount holder of the machine to start polishing. Each polishing step was executed for 3 minutes. Meanwhile, the appropriate diamond solution (6, 3 or 1 μm) was sprayed onto the pads to provide abrasive particles to polish the mount. Occasionally, ultra-pure water was added in small amounts to keep the pads wet.

Once the mount polishing was done, it was inspected under a laboratory microscope to check if the surface is polished thoroughly and whether any scratch is visible. Provided that the quality was satisfactory, the mount was ready for the next step, gold coating.

Since neither the mounting resin nor the composite filaments within the mount were conductors of electricity, a layer of an electrically-conducting metal —in this case gold (Au), was needed to coat the surface of the mount. In the SEM, the surface of the sample is bombarded by high voltage electrons and if it fails to provide both electrical

and thermal conductivity, the charge buildup will cause thermal damage to the affected area, and proper images cannot be produced. Correspondingly, the added conduction will cause reduced beam penetration which enhances the image quality as well. As a result, the already polished mounts were placed in a vacuum plasma gold coating machine, followed by sputtering an ultra-thin layer of gold on the surface. At this point, the mount was ready to be inserted into the SEM sample holder.

3.3.4.2 SEM and EDX Procedure

Starting with the secondary electrons detector (SE) at $10\,kV$ and working distance of 10 mm, the SEM was performed and back-scattered electrons (BSE) detector was also used as needed. After the desired image quality was achieved, it was analyzed by EDX to explore the elements.

3.3.5 Thermogravimetric Analysis

Thermogravimetry is a type of thermal analysis in which changes in the mass of a sample are examined either as a function of temperature, or as a function of time (isothermal). In dynamic thermal gravimetric analysis (TGA), the furnace is subjected to a continuous increase in the temperature at a constant heating rate, which usually goes up linearly.

In TGA, the samples are placed onto a precision balance which is later inserted into the furnace to undergo heating. The balance measures the mass over time and sends the data to the software to plot a TGA curve. TGA curves represent mass change percentages over the increase in the temperature, providing beneficial information about the decomposition stages, intermediate products, atmospheric reactions — oxidation reactions which result in a mass increase, the retained ash at the end of the experiments, etc. Furthermore,

TGA can be used to fingerprint materials for identification, as well as to investigate the composition of the composite materials, since different materials behave differently when treated in such thermal conditions.

3.3.5.1 Test Setup

TA Instruments Q500 Thermogravimetric Analyzer was used to perform the TGA experiments. The following settings were selected for this research:

- Method:
    1. Equilibrate at $30\,°C$
    2. Ramp $10.00\,°C/min$ to $800\,°C$
- Data sampling interval: 1.00 s/pt
- Post test: Air cooling —10 min
- Balance: Nitrogen 60 mL/min
- Sample: Air 40 mL/min
- Pan Type: Platinum

Minimum of $10\,mg$ of each filament type was prepared and cut into small pieces of about 2-3 mm in length, then loaded onto the a platinum pan. Each pan was tared by the Q500 TGA device. After taring was successfully finished, the thermal gravimetric analysis began and each sample took a few hours to complete. Had all the samples been analyzed, the data was saved and the pans were cleaned for the next user.

It is noteworthy that all the filaments except the PMMA group were heated up to $800°C$. For the PMMA samples (M series), the maximum temperature was adequately set to $600°C$, because the decomposition of the polymer had long been finished before reaching this temperature.

3.3.6 Temperature Control

The temperature of the extruder can reach as high as 450 °C. Adjustment of the temperature allows having control over the viscosity of the material inside the extruder and thus, enables enhancing the flow of the material through nozzle. The temperature is simply modified by turning the temperature knob on the device. A thermocouple is connected to the extruder barrel and reads the real-time temperature thereof.

The need to control the temperature rises due to the difference in glass transition temperature of different materials. Therefore, it is imperative to achieve the desired extrusion temperature of the materials, both theoretically and experimentally.

3.3.7 Speed Control

The Filabot EX2 Extruder speed ranges between 0 to 35 rounds per minute (rpm). There is a knob on top of the extruder that enables the user to adjust the speed of the screw rotation and consequently, the extrusion. The real-time speed cannot be read from the device. Despite this, the approximate values can be calculated by dividing the distance between where the knob stops at the two ends of its rotation path, giving the first end the value of zero and the other one the value of 35 rpm. On the device, this distance is originally scaled and divided into six equal segments by the Filabot manufacturer, with

each segment further divided into four parts for ease of reading. Therefore, each segment relates to a 6 rpm increment.

3.4 Filament Properties

3.4.1 Tensile Test

3.4.1.1 Tensile Test Machine

The machine used to perform the tensile tests in this research is Instron™ 5548 Universal Micro-tester which was on top of a steady table in the lab. The temperature of the lab maintained approximately between 21-25 °C the entire time. A 500 N load cell was used to hold the jaws. Smooth-face jaws were used to clasp the filaments, as the rougher jaws caused fracture in the earlier samples. However, a small piece of sandpaper was folded around the filament to provide the required fraction in order to keep the sample in place and hinder slippage.

3.4.1.2 Sample Preparation

Based on Table 3.1, twenty-four filaments have been extruded. In order to acquire statistically reliable data, at least five samples were prepared for each filament in order to collect multiple results. All the samples were cut (using a wire cutter) in 8-centimeters-long pieces. The samples were marked on at a 1.5 cm distance from both ends to give a 5 cm length in between. This step was done to facilitate the loading of the samples into the jaws of the tensile machine. The height of the jaws was almost 1 cm, therefore, having a 1.5 cm length at each end of the sample led to a perfect entrapment by the jaws, and half

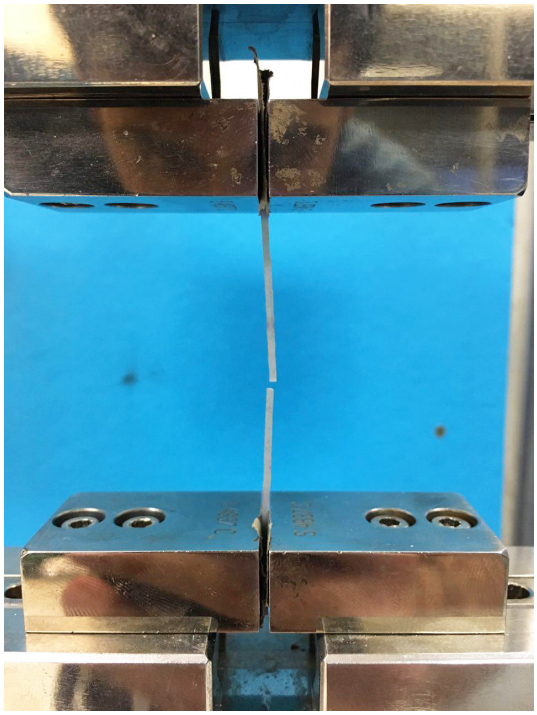

Figure 3.2: A filament held between micro-tensile machine jaws (after failure)

a centimeter would remain intact at the very end of the filament. Consequently, the air pressure which presses the jaws together was set to 35 psi. This pressure was high enough to hold the sample tightly, preventing it from slipping between the jaws, yet low enough not to press the sample fiercely, which might cause damage and deformation. Figure 3.2 shows a filament tightly placed between the tensile machine jaws.

Test Method

The machine was set to exert a tension force with the speed of v=1 mm/min, and stop after failure (fracture) of the sample. The settings were adjusted for the wire sample type, with the diameter of 1 mm. As mentioned, the length of the sample between the gauges was 50 mm. Keeping in mind that v=1 mm/min, the strain rate ($\dot{\epsilon}$) can be calculated as

follows:

$$\epsilon(t) = \frac{L(t) - L_0}{L_0} \tag{3.1}$$

Equation 3.1 is the general formula for the strain. L_t represents the length of the sample at time (t) and L_0 is the initial length.

$$\dot{\epsilon} = \frac{\mathrm{d}\epsilon}{\mathrm{d}t} = \frac{\mathrm{d}}{\mathrm{d}t}\left(\frac{L(t) - L_0}{L_0}\right) = \frac{1}{L_0}\frac{\mathrm{d}L}{\mathrm{d}t}(t) = \frac{v(t)}{L_0} \tag{3.2}$$

The short form of equation 3.2 would be:

$$\dot{\epsilon} = \frac{v(t)}{L_0} \tag{3.3}$$

As a result, the strain rate for the current setting would be:

$$\dot{\epsilon} = \frac{1\,mm/min \times 1\,min/60\,s}{50\,mm} = 3.33 \times 10^{-4}\,s^{-1}$$

Another parameter in this test method was to choose the wire-type sample option, since the filaments resembled wire.

3.4.2 Dye Degradation

The purpose of performing dye degradation tests is to understand if the TiO_2 is visible on the surface of the filaments and not fully entrapped by the polymer. Provided that TiO_2 nanoparticles or nanobelts have partially uncovered surfaces, the ultraviolet light can illuminate the exposed areas and thus, titania can undergo photocatalysis. Furthermore, the rate of photocatalysis can be calculated by measuring the rate of degradation over time. After all, the ultimate goal of studying photocatalysis properties of TiO_2 in the filaments is to investigate its performance in water treatment applications. In this research, photodegradation of methylene blue (MB) is investigated. This dye can be considered as a model pollutant in real water treatment applications. In the following parts, the test setup for the dye degradation experiments is explained.

3.4.2.1 Experiment Setup and Preparation

Test Setup

The photocatalytic degradation experiment was conducted in a slurry batch reactor setup, on a counter top in the laboratory in room temperature. The setup consisted of a quadruple-position stir plate, a UV-LED setup, and beakers which were placed on the stir plate and in which the solution was to be poured. Each UV-LED lamp was attached underneath an aluminum heat sink. In addition, a column (non-degradable black tube) was attached to the heat sink in order to act as a collimator and only direct the vertical beams down towards the beaker.

Solution Preparation

Bearing in mind that four beakers are needed to be placed on the stir plate and each of them is supposed to be filled with 300 mL of solution, total of 1.2 L of 10 mg/L methylene blue in MilliQ water was prepared. In order to do so, 1 mL of the 10 g/L stock MB was transferred to a 1 L volumetric flask using a pipette and the remaining volume was filled with MiliQ water up to the flask line, followed by sonication for 10 minutes. In order to prepare the remaining 0.2 L of the solution, 200 μL of 10 g/L MB stock was added to 200 mL of MilliQ water in a 0.4 L beaker and sonicated for ten minutes.

Each filament type was cut into 1 cm pieces using a wire cutter. One gram of the pieces was weighed and added into each reactor (beaker). The cutting step was done so as to increase the surface area of the filament and thus maximize the chance of illumination of TiO_2 by UV. Due to experiencing slight variations in the weighed samples at the milligram level, the weighed mass was recorded for later calculations.

After the addition of sample pieces to the reactors, 300 mL of the MB solution was

also poured into each beaker. The beakers were covered with aluminum foil alongside the wall to block the ambient light entering the reactor. Furthermore, pH of the content of the beakers was also measured and recorded. At this moment, the reactors were ready to be placed on the stir plate and begin the experiment.

Performing the Experiment

The beakers were then placed on the Talboys^{TM} digital quadruple-position magnetic stirrer. Three of the four positions on the UV-LED setup contained a UV-LED lamp (λ= 365 nm). The remaining position had no UV-LED to compare the results in the dark and under UV illumination.

For the three spots with UV-LED, the lamps were located 11 cm above the starting water level in the reactors. The beakers were under steady illumination of ultraviolet light, as well as constant stirring throughout the experiment.

At each time-point, 1 mL samples were taken out of each reactor (using a pipette) and stored in micro-centrifuge tubes, which were placed under a cover afterwards to keep them in the dark. Once all the samples were taken in every time-point, 300 μL aliquots were transferred into a clear 96-well plate and the layout of the plates was recorded.
The plate was then placed in a SpectraMax M3^{TM} plate reader to read the absorbance. Two distinctive readings was performed: the endpoint analysis and the range analysis. In the range analysis, the absorbance was read in the range of 550-750 nm wavelength. However, the peak absorbance for MB was at 660 nm. As a consequence, the endpoint analysis was taken at λ= 660 nm separately which was in accordance to the results from the range analysis. The latter results (endpoint results) took part in later calculations.

Fter the dye degradation test, the remaining solution inside the beakers was disposed properly and the filament pieces were retrieved. The MB solution was safe to be dumped

in the sink because of its very low concentration. Four scintillation vials were weighed and labeled. The retained filament pieces of each beaker was transferred into the corresponding vial. The vials were weighed with the wet sample inside them and the masses were recorded. After that, they were placed in the incubator to dry over the night. The vials were weighed again in the next morning and the mass of the dried pieces was calculated by subtracting the before and after mass of the vials with the filament pieces inside. The dry mass was recorded to observe the mass difference (if any) before and after the whole experiment.

3.4.3 Adsorption Kinetics

After the spectroscopy of the samples, the abosrbance data at λ =660 nm was taken to pursue further calculations. As of this moment, the absorbance at different time-points was available. However, the concentration of the dye needed to be calculated from the raw absorbance data. In order to obtain the concentration, the standard curve of the absorbance over known concentrations plot was measured. For this step, 10 different concentrations (0, 0.1, 0.25, 0.5, 1, 2, 6, 10, 15, 20 mgL^{-1}) of the dye were prepared and the absorbance of them was measured using the plate reader. After the aforementioned graph was plotted, the slope and y-intercept was measured. With the slope and y-intercept available, the concentrations of the original samples could be calculated using Eq. 3.4:

$$A = mC + b \tag{3.4}$$

Where A is the absorbance read from the spectrometer, m is the slope achieved together with b, the y-intercept, from plotting absorbance of the known concentrations, and C is the unknown concentration that needs to be calculated. After the concentrations of the samples at all time-points were obtained,the Langmuir-Hinshelwood isotherm was used to achieve the kinetic rates.

Langmuir-Hinshelwood kinetics can be simplified to pseudo-first order equation when the concentration of the pollutants is low, so as to determine the kinetic rate coefficients [96]. The simplified equation is as follows 3.5, where 'r' represents the rate of the reaction in ($\mathrm{mg\,L^{-1}min^{-1}}$):

$$-r = \frac{dC}{dt} = -k_{app}C \tag{3.5}$$

$$ln(\frac{C}{C_o}) = k_{app}t \tag{3.6}$$

In Eq. 3.6: k_{app} ($\mathrm{min^{-1}}$) is the apparent first-order reaction rate,

C is the concentration ($\mathrm{mg\,L^{-1}}$) at time t, and

$C_\circ$ is the initial concentration ($\mathrm{mg\,L^{-1}}$).

The apparent kinetic constant k_{app} is achieved by taking the slope of the $ln(\frac{C}{C_\circ})$ versus t plot.

3.4.4 Mass Difference

The mass of the filaments before and after the MB degradation tests was measured in order to investigate the changes therein throughout the experiment. In order to weigh the filaments after the tests finished, the following procedure was executed. First, an empty micro-centrifuge tube was weighed and the mass was recorded. Then the wet pieces of filament in the reactors were collected in the micro-centrifuge tubes. The tubes were kept in an incubator over the night to dry. In the next morning, the micro-centrifuge tubes with filament pieces inside them were weighed again. The mass of dry filaments was calculated by subtracting the mass of the empty micro-centrifuge tube from the mass of the micro-centrifuge tube containing pieces of filament.

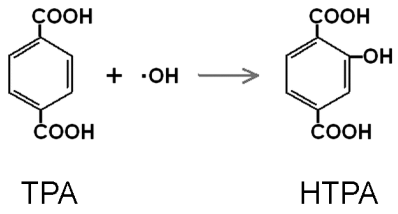

Figure 3.3: HTPA formation due to reaction of TPA with $^{\bullet}$OH

3.4.5 HTPA Conversion

Terephthalic acid (TPA) oxidizes to hydroxyterephthalic acid (HTPA) upon receiving a photo-generated positive hole (h^+) due to TiO_2 photocatalysis. Hence, the production of HTPA can be indicative of photocatalysis and the rates can be measured through fluorescence detection [97]. Figure (3.3) depicts the formation of HTPA due to the reaction between TPA and a hydroxyl radical.

3.4.5.1 Experiment Setup and Preparation

Test Setup The same setup as for the one in dye degradation tests 3.4.2.1 was used for the TPA tests. It basically consisted of a quadruple-position stir plate, UV-LEDs and beakers. The only differences between the dye-degradation and TPA tests are the solutions therein, sampling time-points, as well as the post-analysis of the results.

Solution Preparation

One liter of the TPA solution was needed to perform the experiments. Thus, 0.831 g TPA (Sigma-Aldrich) was weighed and dissolved in 6 mL of 1 M NaOH in a volumetric flask. MilliQ water was added afterwards to increase the volume to 1 L. The solution was then

sonicated for ten minutes. Finally, 300 mL portions of the solution were poured into three 400 mL-beakers.

Similar to dye-degradation tests, 3.4.2.1, 1 cm pieces of each filament type were cut using a wire-cutter, and were added into the beakers, 1 g in each. The magnetic stirrers were also put inside the reactors which then were placed on to the stir plate, under UV-LED lights.

Performing the Experiment

The power outputs of each individual light was measured through PM100/200 Utility program. The pH of each reactor was also measured and recorded. The first samples were taken from all the beakers. Sixty minutes later, the lights were turned on and the rest of the samples were taken based on the desired time-points in up to five hours.

Standards of HTPA from 60 μM stock solution to achieve the standard curve was prepared. The concentrations and the procedure to obtain them is summarized in Table 3.7. In order to make the blank concentration, 2 μL of 1 M NaOH in 998 μL of water per solution was prepared.

At each time point, 300 μL sample of every beaker was taken. Together with the standard solution, the samples were replaced into a plate reader. The spectrum range was set to 350 - 550 nm, in which, λ=420 nm exhibited the maximum fluorescence.

Finally, at the end of the experiment, the pH of the solution in the reactors was measured again. The TPA solution was disposed properly whereas the filament pieces were retrieved and dried in an incubator over the night. The dry pieces were weighed and recorded in the next morning.

The fluorescence intensity of the samples were measured in the plate reader. The following formula, (Eq. 3.7), was used to obtain the concentration of HTPA in the solutions.

C (4 μM)	V of higher concentration (mL)	V of MilliQ water/solution (mL)
20	0.333	0.667
10	0.5	0.5
6	0.6	0.4
2	0.333	0.667
1	0.5	0.5
0.5	0.5	0.5
0.25	0.5	0.5
0.1	0.4	0.6

Table 3.2: Concentration of HTPA standards — C: Concentration, V: Volume

Prior to this calculation, however, the slope and y-intercept needed to be calculated. For this purpose, the known concentrations based on Table 3.7, were plotted on the horizontal axis while the corresponding fluorescence values were placed on the vertical axis. The slope and y-intercepts were found afterwards. Having the missing values calculated, Eq. 3.7 was used to obtain concentrations (C).

$$F = mC + b \tag{3.7}$$

In Eq. 3.7, F is the fluorescence read from the spectrometer, m is the slope and b is the y-intercept achieved from the blank sample at concentration 0 μM. Both m and b were calculated as described above. The concentration was achieved by solving the equation. Nevertheless, concentration was not the sole interest of this experiment. The final goal was to calculate the rate of the HTPA conversion, k_1. Consequently, the k_2 represents TPA degradation. The simplified model kinetic model, suggested by Cernigoj et el [97], is used to calculate k_1 and k_2 (Eq. 3.8). Moreover, this equation can be integrated to obtain

Equation 3.9:

$$\frac{\mathrm{d}C_{HTPA}}{\mathrm{d}t} = k_1 - k_2\, C_{HTPA} \tag{3.8}$$

$$C_{HTPA} = \frac{k_1}{k_2}\,(1 - e^{-k_2 t}) \tag{3.9}$$

Chapter 4

Extrusion Properties

4.1 Temperature Control

The working temperatures for the extrusions in this research vary depending on the composition. The pure polymer samples (M_5, N_5, S_5,V_5) were extruded at temperatures noticeably higher than their glass transition temperatures. For the nylon and PVDF samples, it was observed that their extrusion temperatures was 265 °C and 205 °C, respectively, which is higher than their melting points. It is noteworthy that the extrusion temperature is higher than T_g and in some cases T_m because the thermocouple is not directly connected to the material in the barrel, and the material might be a few degrees cooler. Furthermore, the extrusion temperature also relates to the extrusion speed. Higher temperature leads to lower viscosity, thus higher extrusion rate. Therefore, in the production of the filaments, maintaining a steady flow and constant diameter had a higher priority than minimizing the temperature to stick with the T_g and T_m values. The speed control is discussed separately in the next section (4.2).

Table 4.1 summarizes the extrusion temperatures of the twenty-four compositions. Overall, it can be understood that most of the filaments were extruded between 200 °C and 250 °C, which is much hotter than their mentioned T_gs. In addition, it can also be observed that in those samples composed of nanoclay, the extrusion temperature is usually higher than the ones without it. One possible explanation for this observation is that the dry nature of the nanoclay particles causes more clogging in the mixture within the barrel. As a result, a less viscous melt is needed to overcome this problem and facilitate the blending of different powders and further extruding them. Such an enhanced flow is achieved by increasing the temperature even more.

In terms of tolerating high temperatures without undergoing degradation, polymers are more susceptible than TiO_2 and nanoclay. Hence, when raising the extruder temperature, polymer would be the limiting factor. On the other hand, a paste-like extrusion is preferred for maintaining a steady diameter and flow, as well as having the ability to draw the filament out of the extruder. When the temperature rises too much, the mixture exhibits behavior more similar to that of liquids, and accumulates in the chamber, followed by sudden erupting out of the nozzle with uncontrollable form and diameter. The values mentioned in Table 4.1 are the temperatures at which a steady flow with nearly constant diameter was successfully produced.

As discussed in previous subsections, all the compositions were mixed manually at first, fed into the extruder, mixed in the chamber and extruded, followed by cutting the filaments and re-feeding them to the extruder to achieve a profounder blending. Almost always, the first extrusion took longer and required higher temperatures. Again, the suggested explanation for this behaviour is that in the first round, the feed composes less mixed powder, and several small clogging occur within the feed. The hotter temperature causes the polymer to melt evenly and enhance the flow. In the second rounds, however, the

Code	**Extrusion Temperature** ($^{\circ}C$)	**Code**	**Extrusion Temperature** ($^{\circ}C$)
M_1	205 - 210	S_1	250 - 255
M_2	205 - 210	S_2	250
M_3	240 - 245	S_3	250 - 260
M_4	228 - 235	S_4	260 - 265
M_5	190 - 200	S_5	250 - 260
M_6	237 - 245	S_6	255 - 260
N_1	260	V_1	180 - 185
N_2	264 - 270	V_2	185 - 190
N_3	262 - 270	V_3	191 - 195
N_4	270	V_4	210- 215
N_5	265	V_5	199 - 205
N_6	270	V_6	245 - 250

Table 4.1: Extrusion temperatures of the twenty-four compositions

composite is already thoroughly mixed, and with lower temperatures, the filament pieces can melt and re-extrude with no clogging around the screw.

One other observation was that PVDF had the fastest extrusion speed. Having a very low glass transition temperature of -35 °C, it most likely melted down faster than the other counterparts. While other polymers took at least 20 minutes of mixing inside the extruder before exiting from the nozzle, PVDF took only a few minutes before coming out of the extruder.

4.2 Speed Control

In the first round of mixing —right after feeding the manually mixed powder, higher speeds (24-35 rpm) were favoured. This would impose greater transmission and collision of particles within the pre-mix which enhances the blending thereof. On the other hand, the horizontal velocity of the pre-mix is usually low due to the fact that the titania and nanoclay powder are very dry, and the polymer, as the binding agent responsible for the flow of the extrusion, is not thoroughly dispersed yet. Therefore, raising the screw rotation speed would not result in the sudden discharge of the raw material out of the nozzle as the feed has a relatively low horizontal velocity.

As opposed to the first round of extrusion, the second round requires lower speed (12-24 rpm) as in this step, the feed, which composes of initial filaments that have been cut into tiny pieces and re-fed into the extruder, has already been mixed two times (first manually and then through the first extrusion) so that the dispersion is relatively perfect at this point. The well dispersion and uniformity in the feed contributes to a faster horizontal velocity of the batch towards the outlet (nozzle). Therefore, lower screw speeds are needed to control the overall extrusion rate.

Another factor that plays a part in the extrusion rate is the temperature of the feed that was described separately in 3.3.6. In conclusion, the rate of the extrusion depends on both the temperature and the rotation speed of the screw. Temperature causes the polymer to melt and easily move forward towards the outlet and consequently, take the form of the nozzle, and the screw speed causes a drive to push the material faster toward the end of the chamber. During the extrusions, both the temperature and speed were adjusted multiple times to achieve the best combination under which a steady extrusion rate and constant diameter could be accomplished.

In this research, all of the filaments were extruded using a single screw extruder at very low speeds (24-36 rpm). However, based on similar works such as [98] and [99], better mechanical properties and dispersion achieved by twin screw extruders at significantly higher speeds ($>$ 150 rpm). The higher screw speeds can attribute to better dispersion, because higher shear rates can be achieved correspondingly, which will break the big nanomaterial clusters into smaller agglomerates [98]. Table 4.2 compares the obtained mechanical properties of nylon 6 and nylon + organoclay (bentonite) between a work done by Cho et al [100] and this research. Based on this comparison, higher speeds are more successful in achieving enhanced dispersion and thus, better mechanical characteristics. Section 5.1 discusses the tensile strength in a greater depth.

Composition	Reference	Extruder type	Temp. (°C)	Speed (rpm)	UTS (MPa)	Elongation %
Nylon 6	[100]	Twin screw	240	180	64.2±0.8	40±8
Nylon 6	this research	Single screw	265	24	8.83±1.3	47±5.6
Nylon 6 + bentonite (5 wt%)	[100]	Twin screw	240	180	83.4±0.7	38±19
Nylon 6 + bentonite (2 wt%)	this research	Single screw	270	24	6.92±0.35	47±2.4

Table 4.2: Comparison of the mechanical properties between two extruder types and different speeds

4.3 Formability

In this dissertation, formability is defined as the ability of the extruded filament to maintain the diameter of the nozzle after the extrusion, and possess enough flexibility and tensile strength not to break under spooling. The aforementioned factors, temperature and extrusion speed, affect the formability of the produced filaments. Atop from this, the physical and mechanical characteristics of the polymers also play an important role in regards to formability. Tensile strength tests have been done on the filaments and are discussed in depth in the subsection 5.1.

At the time of the extrusion, it was observed that the correct combination of temperature and speed is obtained by trial and error. The temperature was increased gradually to allow the composition in the chamber heat up. The screw speed was set to higher rates (24-35 rpm) to enhance blending and transferring the materials forward. The sound of the device also gave some information about the extrusion stage. The blending sound differed with the sound of the materials entering the void chamber where they are accumulated before reaching the nozzle. Anyway, it was learned that if the sound of the extruder was not smooth, a higher temperature was needed to enhance polymer melting and overcome abrasion of the rigid materials with the walls of the chamber.

When the filament was about to exit the nozzle, extra attention was paid to observe and control the diameter. Since the hole in the nozzle is circular, the filament takes a circular cross sectional form too. Right after the nozzle, up to at least twenty centimeters apart from it, the filament is still hot. At this distance, on one hand if the filament is drawn too much, its diameter is going to decrease. On the other hand, if there is no pulling, the diameter tends to expand. That is the reason behind drawing the filament, to keep its diameter constant until the filament cools down and maintains its geometry.

The diameter of the filaments was randomly checked using a caliper. Figure 4.1 shows the extruded filament right after the nozzle. Among the four types of polymers extruded in this research, none exhibited identical behaviour. PVDF samples were extruded faster than the other ones, especially in the first round of extrusion. Nevertheless, they lacked strength after the first extrusion and broke easily by a gentle pull. The PVDF group was soft and flexible overall, but the control over diameter was relatively good after the second round.

PMMA samples stayed a longer period of time in the chamber before coming out. However, the control over diameter was moderately good even in the first round of extrusion. Nonetheless, the PMMA samples were also a bit brittle and easy to break, comparing to their PSU and Nylon counterparts. The polysulfone (PSU) group were noticeably easier to control. All of the compositions (S_1-S_6), exhibited good extrusion control, especially at low speeds (6-12 rpm). However, in order to maintain the diameter under such a low speed, longer time was needed.

The last group of the polymers, Nylon, was challenging at first, since the proper combination of temperature and extrusion speed was obtained with more effort and was more exhausting. Despite this, after the right temperature and speed was reached, the control over the diameter became facile and the flow got steady. The Nylon samples too, showed great formability and flexibility. Both PSU and Nylon samples retained their diameter after cooling down and had good strength in that it was hard to break them apart by exerting manual tensile force. As mentioned earlier, all of the produced filaments underwent tensile strength tests which are elaborated in later sections.

Figure 4.1: Extruded filament- the caliper reads a diameter of 1.08 mm

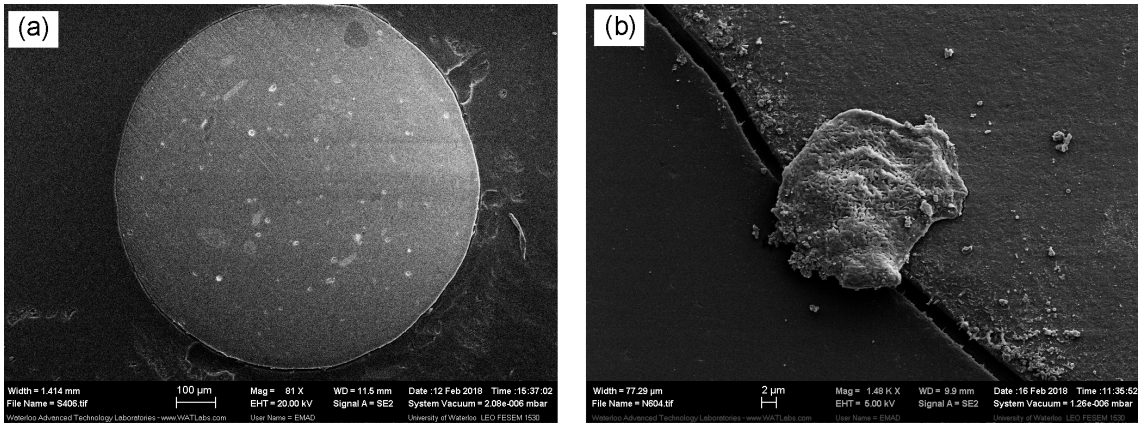

Figure 4.2: The circular cross-section of PSU (S_4) to the left (a), and agglomeration of bentonite nanoclay on the Nylon filament (N_6) to the right (b)

4.4 Dispersion

4.4.1 SEM Results

Since the observed filament cross-sections were chosen randomly, the SEM images showed a relatively successful blend, as well as almost perfect circular shapes for the cross sections (Fig.4.2-a). Various nanomaterial clustering were observed for TiO_2 nanoparticles, nanobelts, and bentonite nanoclay (Fig. 4.2-b). Overall, based on the SEM images, the dispersion usually seemed to be evenly spread throughout the surface. The rest of the SEM images can be found in A.1.

4.4.2 EDX Results

In the analysis of the EDX results, the approach is to analyze the filaments individually, starting with the PMMA group. It is worth to mention that based on the stoichiometry of

the compositions, there should exist $3\,wt\%$ titanium in the filaments. Hence, percentages close to this value for Ti on the cross section of the filaments evince a thorough mixing.

M_1 showed approximately 3 wt% titanium on its surface, which matches the initial composition prior to extrusion. However, 2 wt% Fe (steel) was discovered in the EDX results. The only explanation for this discovery might be either the scraping of the extruder screw to the walls of the screw chamber of the extruder, or picking up steel debris off the automatic polishing machine that might have been there from previous steel parts of other users. Nevertheless, observing iron in the filaments is limited to only a few of the samples. M_2 nearly showed an identical behaviour as M_1, with roughly 3 wt% titanium visible in the cross-section.

M_3 and M_4 followed the same trend as M_1 and M_2 and the 3 wt% Ti was observed in their compositions. In addition, aluminum and silicon elements were also noticed, which proves the dispersion of bentonite nanoclay in these filaments since bentonite composed of these elements.

M_5, consisting of pure PMMA polymer, showed an average of 67% carbon and 33% oxygen on EDX. This result is presumably in accordance to the 60 wt% and 32 wt% carbon and oxygen in the PMMA chemical formula ($C_5H_8O_2$), respectively. The small difference is due to ignoring the hydrogen weight percentage on the these results, as hydrogen is too light to be detected on the EDX setup. M_6 also proved the presence of aluminum and silicon on its surface. In addition, Fe was seen in several tiny areas.

Moving forward to the Nylon group, N_1 did not exhibit Ti amounts close to 3 wt%, yet the existence of titanium in addition to carbon, oxygen and nitrogen on the surface is undeniable. Nitrogen happens to be in the Nylon formula ($C_6H_{11}N$) and is seen in all the Nylon filaments. In N_2, various areas had 2% Ti while other parts had 5%, whereas

in N_3 and $_4$, an average of 3 wt% Ti was apparent. Moreover, Al and Si wre also detected as these two filaments had bentonite in their compositions. N_5 and N_6 followed a similar fashion as M_5 and M_6, in that they did not have titanium on their surfaces, as expected. N_6 also possessed several different percentages of Al and Si along the surface.

Polysulfone samples have a sulfur atom in their chemical formula —$C_{25}H_{22}O_4S$. Thus, aside from the other elements, sulfur was also seen in all of the filaments in this group. Samples S_1 to S_4 showed a similar behaviour as their counterparts in the PMMA and Nylon groups. They all confirmed having 2-4 wt% titanium in their compositions. Only S_1 had a slight difference, with an extra iron portion somewhere on the cross-section. S_5 and S_6 too, acted as anticipated. They showed carbon, oxygen and sulfur in their matrices, with S_6 having aluminum and silicon in addition due to the bentonite in its formula.

In a similar way, PVDF specimens acted like the other peers in the other groups. This time, because of a fluorine atom in the chemical formula (C_2H_2F), noticeable percentages of this element were also observed.

4.4.3 TGA Results

The weight over temperature graphs were obtained from thermogravimetric analysis, and demonstrated that the degradation started at similar temperatures in each group of polymers. However, the addition of nanomaterials into the compositions was expected to alter the degradation temperatures. An explanation might be that the dispersion was not 100% homogeneous throughout the length of the filaments, so the properties would not be constant over the length.

On the other hand, TGA results also showed the remaining ash weight percentages. Based on the initial compositions, the ash was expected to belong to the TiO_2 nanomate-

rials and the bentonite nanoparticles, because in TGA analysis, the temperature rises to a extent that the polymer fully degrades, and produces gases such as CO, CO_2, etc. Table 4.3 illustrates both the anticipated and achieved remaining ash percentages. Based on this table, it can be understood that although several times the obtained results were higher or lower than the anticipated values, usually the expected and the obtained results were in agreement. Furthermore, it can be learned that the dispersion needs further developments.

Sample	Anticipated Ash %	Obtained Ash %	Sample	Anticipated Ash %	Obtained Ash %
M_1	5	6.23	S_1	5	7.36
M_2	5	5.85	S_2	5	6.12
M_3	7	9.89	S_3	7	6.97
M_4	7	6.34	S_4	7	5.85
M_5	0	1.6	S_5	0	0.37
M_6	2	2.55	S_6	2	4.29
N_1	5	4.15	V_1	5	3.25
N_2	5	5.09	V_2	5	3.22
N_3	7	4.67	V_3	7	1.19
N_4	7	6.21	V_4	7	0.11
N_5	0	0.87	V_5	0	- 1.46
N_6	2	2.49	V_6	2	- 0.95

Table 4.3: Anticipated and obtained ash weight percentages after TGA

4.5 Summary

The correct combination of temperature and speed was obtained by trial and error. Even though properties of the polymers can be found easily in the literature, the properties of all the composites with different compositions (if available) are difficult to find.

At the time when the filament is about to exit the nozzle, extra attention is required to observe and control the diameter. Because the die in the nozzle is circular, the filament passing through the die forms a circular cross-section. From the nozzle up to at least twenty centimeters away, the filament is still very hot and soft. Throughout this length, if the filament is drawn excessively, the diameter will decrease. On the other hand, in the absence of a tension force, the diameter would expand because of a sudden pressure drop as it comes out of a small die. Therefore, drawing the filament is needed to keep its diameter constant until the filament cools down and is dense enough to maintain its geometry.

Based on the results of the SEM and EDX analyses, in filaments having TiO_2 nanomaterials in their compositions, an average of $3\,wt\%$ titanium was observed on EDX analysis, which matches the initial desired stoichiometry. Nevertheless, based on the SEM images, the nanomaterials have been clustered in some cases. These clusters indicate the need to propose enhanced mixing methods, to prevent nanomaterials clumping. Otherwise, it will increase the particulate size which can deteriorate their characteristics at the nano scale.

TGA results showed that the addition of the nanomaterials did not alter the heat degradation of polymers significantly. A possible reason might be lack of a homogeneous dispersion throughout the length. The ash percentages mostly showed the anticipated results. However, several results were not as expected, which can intensify the hypothesis about the lack of a complete, thorough dispersion.

Chapter 5

Filament Properties

In the preceding chapter, 4, properties of the extrusion were discussed. In this chapter, characteristics of the produced filament are studied. First, the tensile strength of the filaments is examined. Then, in the succeeding sections, 3.4.2 and 3.4.5, the photocatalytic properties of the nanocomposite filaments are explained.

5.1 Tensile Strength

Tensile strength of the filaments was tested as described in 5.1 to obtain a profound understanding about their mechanical behaviour. The achieved results spread over a wide range. Therefore, in the beginning, the five results (or six, in some cases) for each filament were evaluated while the outlier data were eliminated. The remaining numbers were analyzed next. The maximum load for each specimen was found and the corresponding extension value was also distinguished. After this step, the average of all of the maximum loads and the associated extension values were calculated separately and tabulated. It is noteworthy

to mention that the proper mechanical term describing this maximum load is the ultimate tensile strength (UTS) provided that the load divides by the cross-sectional area of the specimen. UTS defines the maximum load a sample could tolerate without undergoing plastic deformation. After this point, only the extension will continue to increase whereas the force load remains the same or decreases, until failure occurs and the specimen breaks. If the specimen is more brittle, the fracture happens faster without noticeable necking. On the other hand, if the specimen is less brittle and more flexible, the necking happens and it experiences longer extensions.

5.1.1 Tensile strength and strain results

Final average ultimate tensile strengths and the corresponding average extensions were compared in two ways. The first approach is juxtaposing the load force values within the samples in each group of polymers (M, N, S, and V) and observing possible trends. The other approach, however, is comparing the acquired values between the members of each category — all the M_1, N_1, S_1, and V_1 filaments for instance, to compare the results of each composition among various polymers.

Method 1 The first analysis method is to compare the tensile force load values between specimens within each polymer group: Figure 5.1 depicts the load for members in the PMMA group. The force load values range between 15.4 to 48.5 newtons. Comparing to the M_5 which is pure polymer, M_2 and M_3 show higher results. M_2 with 5% nanobelt TiO_2 has the maximum load of all. Furthermore, M_2 also shows the most extension (1.69 mm, 3.4%). Other extensions range between 0.8 to 1.8%. Figure 5.2 shows the load values for filaments in the Nylon group. Comparing to the PMMA filaments, Nylon counterparts vary in a smaller range. The maximum load force belongs to N_1 (28.9 N) that has TiO_2

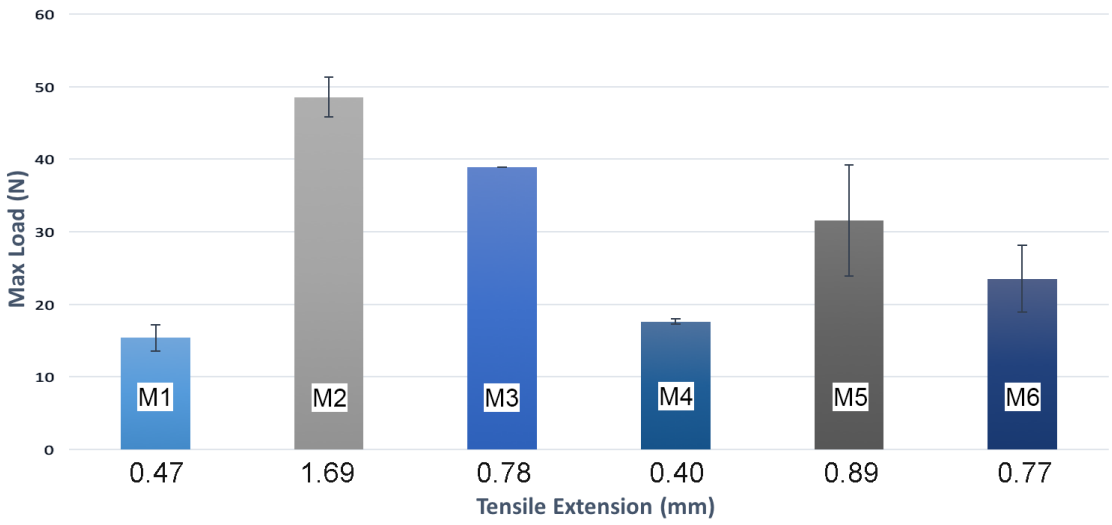

Figure 5.1: Load vs. extension for PMMA filaments

nanoparticles. N_6 having only PMMA and bentonite, has the minimum amount (21.7 N). In contrast, the extension values in the Nylon group vary significantly, so as their standard deviation. While N_3 elongated 3.8 mm in average (7.6%), N_6 which showed the least load toleration possesses the highest elongation (23.4 mm, 46.8%), followed by N_5 (pure nylon) with 23.3mm extension (46.6%). Apparently, the N_5 and N_6 that had no TiO_2 in their matrix showed the longest extensions, suggesting that the nanomaterials have possibly made them more brittle. Figure 5.3 demonstrates the load over extension for the PSU filaments. Both of the maximum force (61.6 N) and maximum extension (2.43 mm, 4.9%) belong to the S_3 specimen which has both titanium dioxide and bentonite in its matrix, as opposed to S_2 (with nanobelts added) which exhibits the minimum load (32.5 N) and extension (1.46 mm, 2.9%). The remaining four filaments showed a mediocre behaviour compared to S_2 and S_3. In these samples, when the load force increased, so did the extension. Overall, the average force for the PSU family was highest between all of

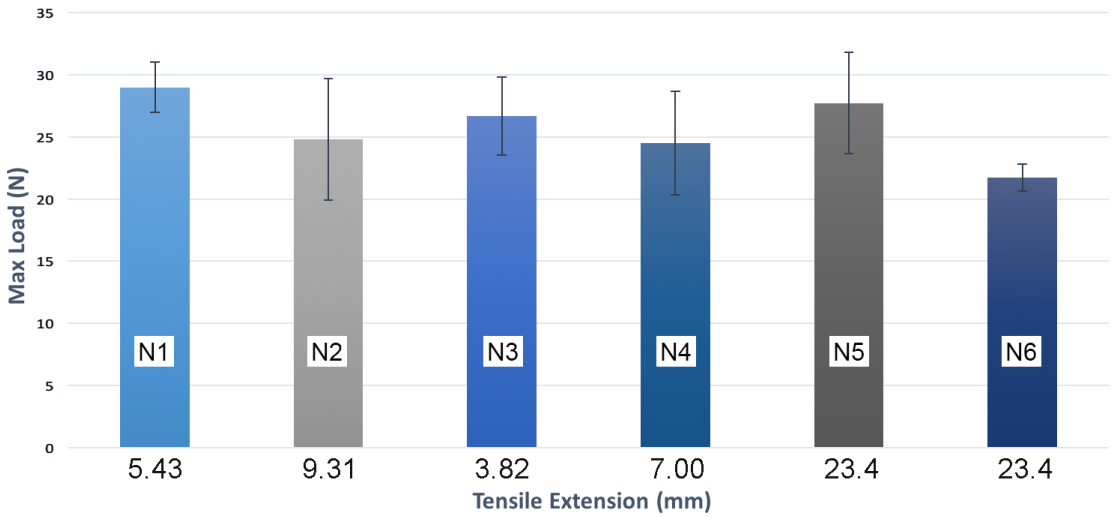

Figure 5.2: Load vs. extension for Nylon filaments

the four groups of polymers in this research. In the remaining filaments belonging to the PVDF family, V_4 (nanobelts and bentonite plus PVDF) tolerated the least force (16.5 N), as well as the minimum extension (1.06 mm, 2.1%). On the contrary, V_5 (pure polymer) withstood the maximum load (33.94 N) followed by V_6 (polymer and bentonite) (33.66 N). Nonetheless, the maximum elongation belongs to V_2 which extended approximately 5 mm, 9.99%. Apparently, the nanobelts in these specimens enhanced the extension. The nearly identical behaviour of V_5 and V_6 which did not compose any TiO_2 is noteworthy. The only difference in their composition is the 2%-weight nanoclay that V_6 possesses. Either the nanoclay did not have any effect in tolerating the load and extension of V_6, or the dispersion was not completely uniform despite the fact that different specimens were cut from different points in the manufactured filaments and the shown values are an average. Figure 5.4 summarized the maximum loads and extension values of the PVDF family.

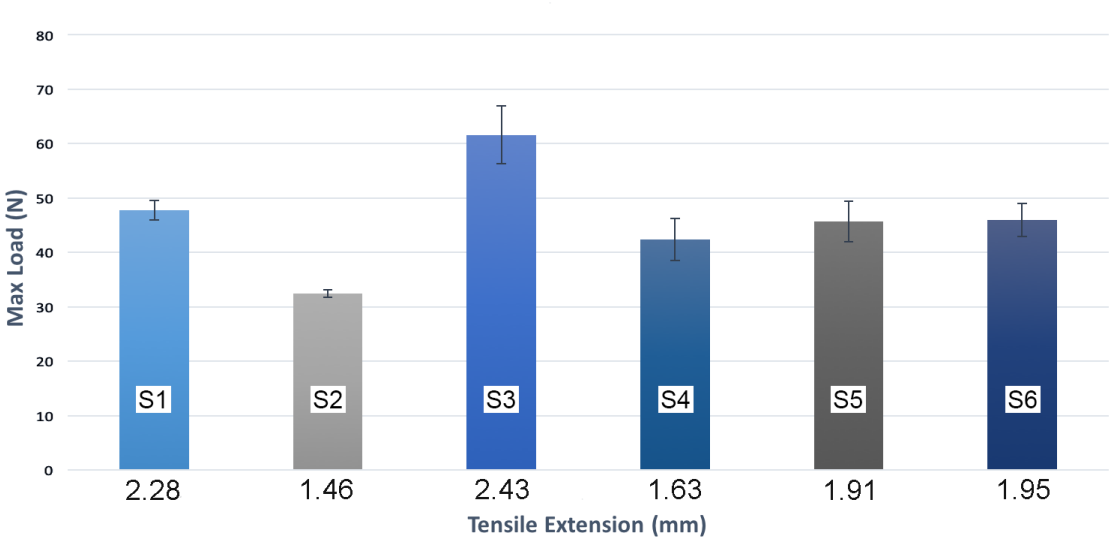

Figure 5.3: Load vs. extension for PSU filaments

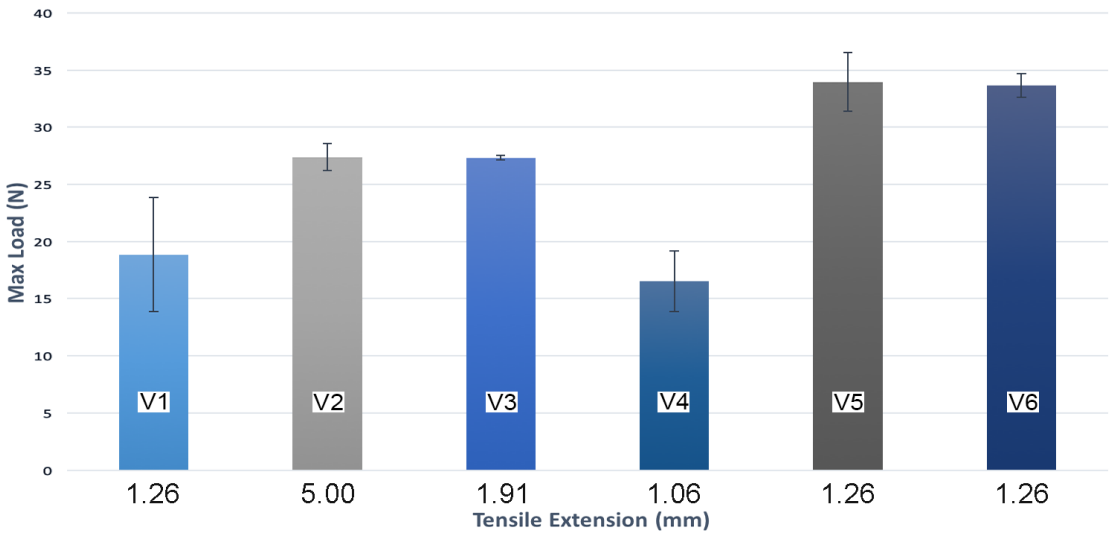

Figure 5.4: Load vs. extension for PVDF filaments

Method 2 In method two, the focus is on comparing the results from various filaments having the same composition except for the polymer type —M_1, N_1, S_1, and V_1 for example. For convenience, all the categories and their compositions are tabulated in Table 5.1. In

Category	Samples	Compositions
A	M_1, N_1, S_1, V_1	Polymer + TiO_2 nanoparticles
B	M_2, N_2, S_2, V_2	Polymer + TiO_2 nanobelts
C	M_3, N_3, S_3, V_3	Polymer + TiO_2 nanoparticles + nanoclay
D	M_4, N_4, S_4, V_4	Polymer + TiO_2 nanobelts + nanoclay
E	M_5, N_5, S_5, V_5	Polymer
F	M_6, N_6, S_6, V_6	Polymer + nanoclay

Table 5.1: Categories based on filament compositions with the same added nanomaterials

category A (TiO_2 nanoparticles + polymer), the highest ultimate tensile strength and extension belong to S_1 and N_1 respectively. The least UTS and extension belong to M_1. In category B which has TiO_2 nanobelts in the compositions, the Nylon filament (N_2) has the highest extension, while the largest UTS value is for the PMMA specimens. In this category, the samples either showed high UTS and low extension (such as M_2 and S_2), or the other way around, low UTS and high extension (N_2 and V_2). Hence, neither is could be considered as the best material of choice. Figure 5.5 shows the corresponding values for the first two categories. In the third category, in which TiO_2 nanoparticles and bentonite are added to the polymers, the Nylon sample still possesses the highest elongation (Fig. 5.6- a). Similar to category A which only had TiO_2 nanoparticles added, the highest UTS belongs to the PSU sample. Should any material be chosen as the best in this category, it definitely would be the S_3, because not only it withstands the highest UTS (19.6 MPa), but also exhibits acceptable extension and flexibility.

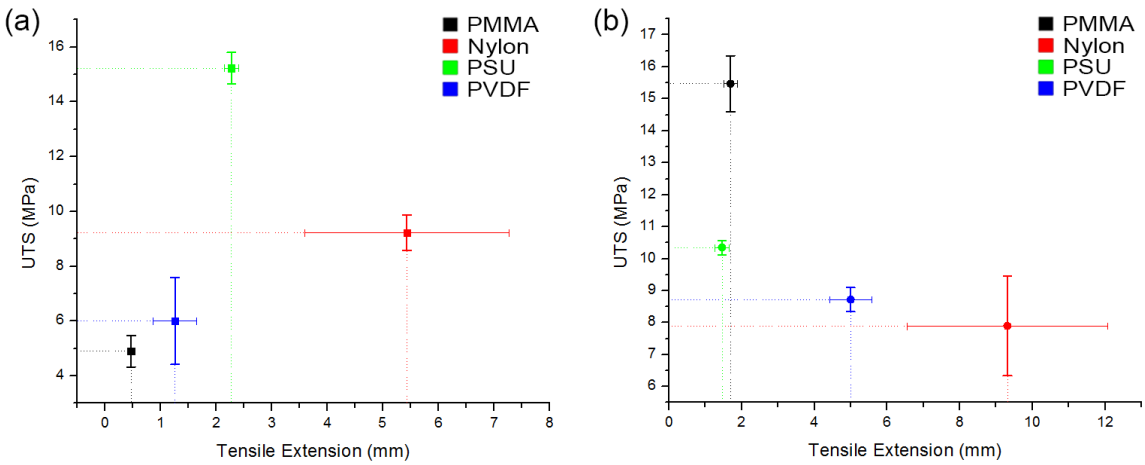

Figure 5.5: UTS over extension values- Category A (a) and Category B (b)

In category D, whereby TiO_2 nanobelts and bentonite were added to the polymers, the highest UTS and strain belong to the PSU and Nylon family, respectively. They followed the same trend as the categories with added TiO_2 nanoparticles. Having the UTS of 13.5 MPa, S_4 (PSU) is by far the most tolerant filament to tensile load. Furthermore, while the other samples have extensions less than $2mm$, or 4%, extension of the Nylon filament was $7mm$, or 14% which is significantly higher than the rest. M_4 and V_4 behaved similarly in both UTS and strain values (Fig. 5.6- b). Category E consists of pure polymers and Category F has bentonite-added filaments. As seen in Figure 5.7, the PSU members show the highest UTS and the Nylon counterparts show longest extensions, similar to categories A,C, and D.

Table 5.2 summarizes the whole comparison in that it demonstrates the members of each category ranked in both UTS and strain values. In general, the PSU family exhibited the highest UTS values, while the Nylon filaments demonstrated the maximum elongations. The PMMA samples were the most brittle filaments in these experiments.

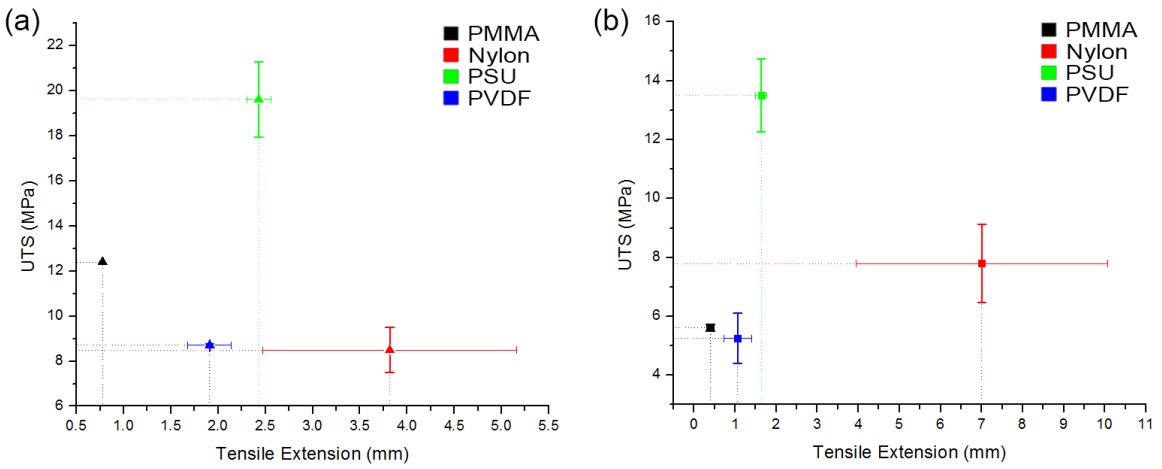

Figure 5.6: UTS over extension values- Category C (a) and Category D (b)

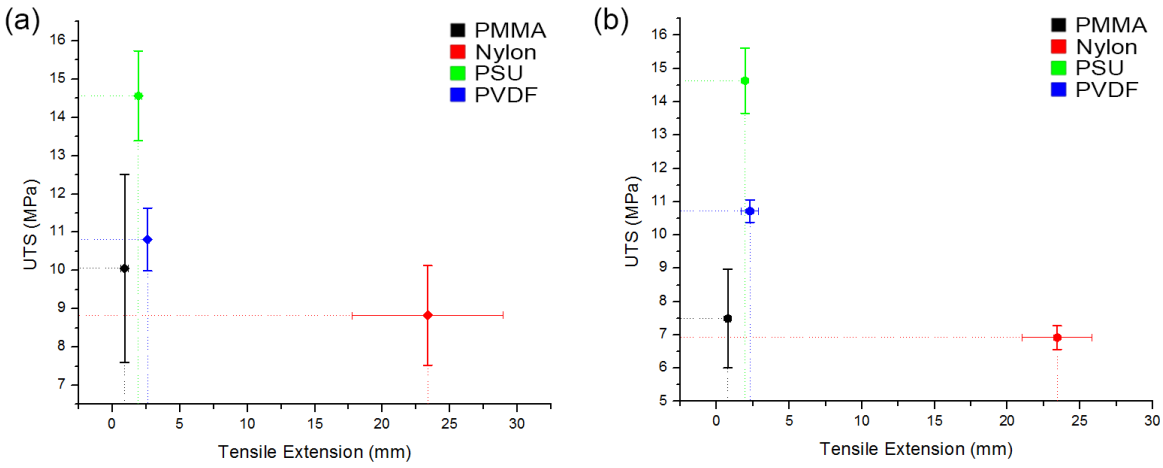

Figure 5.7: UTS over extension values- Category E (a) and Category F (b)

Category	UTS	Strain
A	S>N>V>M	N>S>V>M
B	M>S>V>N	N>V>M>S
C	S>M>V>N	N>S>V>M
D	S>M>V>N	N>S>V>M
E	S>V>M>N	N>V>S>M
F	S>V>M>N	N>V>S>M

Table 5.2: UTS and Strain assortment in each filament category

5.1.2 Tensile properties summary

Table 5.2 demonstrates the UTS and strain assortment of all the filaments magnificently and can be studied in order to arrive to a rapid conclusion. Polysulfone shows the highest UPS values for all the categories except category B. Even so, in category B, it is still the second best. On the other hand, Nylon is the weakest filament in terms of tensile strength. PVDF and PMMA show similar behavior in terms of UTS and are placed in the middle of PSU and Nylon interchangeably. Consequently, in regards to the Strain column, Nylon is by far the most extendable filament in this research. Although standard deviations for each filament specimens was observed, the gap between the Nylon strain values and those of the other counterparts in every category is considerably distinctive. On the contrary, the PMMA samples exhibited the least strain. In fact, they were very brittle and easy to break even by a gentle force when handling or between the micro-tensile machine jaws. The remaining filaments (PSU and PVDF) fall in between Nylon and PMMA and show similar strain results.

Overall, polysulfone displayed the highest ultimate tensile strengths and nearly high

strains, followed by PVDF. In regards to water treatment filtration structures or membranes, both of the characteristics —high UTS and high strain —are imperative. They have to withstand high water pressures without failure and possess endurance and durability under different conditions.

5.2 Methylyne Blue Degradation

The results of the methylene blue degradation tests comprise data on mass difference and the absorption constants that are described in the following sections.

5.2.1 Mass Difference

The average mass differences for all of the samples are calculated as explained in 3.4.4 and are recorded in Table 5.3.

Based on the mass differences recorded in Table 5.3, it can be seen that the values are infinitesimal comparing to the initial mass of the pieces of filaments ($1g$) that were placed in the reactors. Nonetheless, another observation that can be made is that approximately most of the values are negative, suggesting that there has been very small mass loss in orders of 10^{-3} and $10^{-4}g$ which is again, negligible with regards to the initial $1g$ mass. On the other hand, different sources of error (collecting the pieces of filaments, multiple weighing, etc.) might affect the final results. Overall, the mass difference in these experiments can be neglected, concluding that the filaments maintained their shape and mass over the time both during the tests and afterwards during the drying and weighing process.

Sample	UV	Dark	Sample	UV	Dark
M_1	-0.0054	-0.0063	S_1	0.0552	-0.1545
M_2	-0.0751	-0.0148	S_2	0.0031	-0.0078
M_3	0.0069	-0.0007	S_3	0.0027	0.0021
M_4	-	-	S_4	-0.0090	-0.0002
M_5	-	-	S_5	0.0008	0.0048
M_6	-0.0049	-0.0017	S_6	0.0042	-0.0046
N_1	-0.0033	-0.0191	V_1	-0.0073	-0.0578
N_2	0.0020	0.0033	V_2	0.0003	-0.3087
N_3	0.0005	-0.0109	V_3	-0.0147	0.0003
N_4	0.0006	-0.007	V_4	-	-
N_5	-0.0027	-0.0113	V_5	-0.0252	-0.0005
N_6	-0.0317	-0.00568	V_6	0.0003	0.0031

Table 5.3: Average mass difference (after - before) of the samples in the degradation test, both under UV and in the dark (in grams)

5.2.2 MB Degradation

The average rate of the reaction for all of the twenty-four filaments is calculated (as explained in 3.4.2.1). Bearing in mind that only the negative rates indicate the degradation of the dye, the positive values are neglected on this graph. However, the absolute value of the degradation rates are plotted in Figure 5.8. Despite this, several suggestions are made to interpret the positive results. They include:

(i) the TiO_2 nanomaterials have been fully entrapped inside the sample and have no contact with the solution surrounding the filament. Therefore, they cannot perform satisfactorily

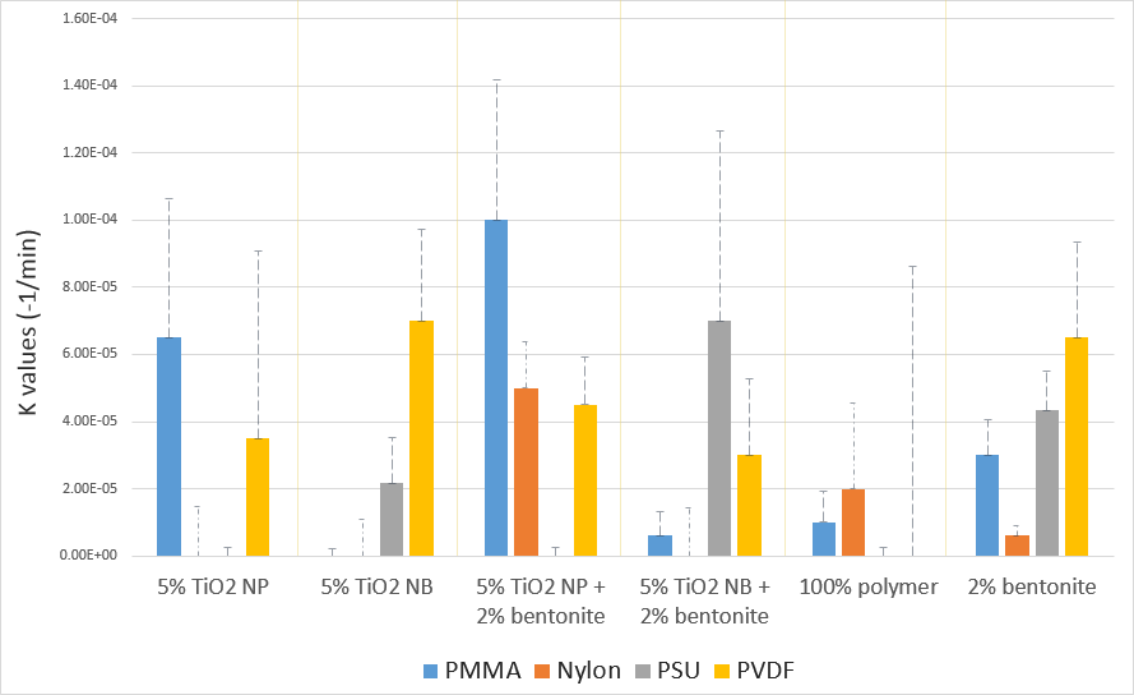

Figure 5.8: Absolute values of the methylene blue degradation rates- the initial positive results are eliminated

in releasing free radicals into the solution and as a result, cannot undergo photocatalysis.
(ii) Various types of samples such as S_5 and V_5 have absolutely no TiO_2 in their compositions, and if there exists any sign of degradation by any chance, in M_5 and N_5 for example, it might be due to reasons other that TiO_2 photocatalysis.
(iii) Human errors are also possible. Upon sampling the solution, the micro-centrifuge tubes were covered and sat on the counter top in order for all the samples to be taken and transported to the spectrometer. The sudden exposure of the samples to the ambient light might be another reason for errors. This explanation, however, is not as strong as the two preceding suggestions because extra care was taken to perform all the experiments with caution and in the same manner.

Nevertheless, most of the samples lead to negative values —indicating dye degradation. The results of Figure 5.8 vary significantly and fail to follow a certain trend. However, several observations are discussed as follows:

1. Only half of the samples that only had TiO_2 nanoparticles or nanobelts added into their matrix showed degradation. Apparently, a large portion of the added nanomaterials is inside the filament where no contact is available to the solution.

2. Three-quarter of the samples in categories C and D exhibited degradation. These categories include the same ingredients as of categories A and B, plus the addition of 2% bentonite nanoclay. Presumably, the addition of nanoclay increased the adsorption capacity of the filaments.

3. All of the samples in category F (polymer + bentonite) showed negative K values despite the fact that there was no TiO_2 in their matrix. Therefore, the observed degradation is not because of titania photocatalysis activity. The bentonite nanoclay has effectively influenced on the adsorption of the dye.

4. It is noteworthy of stating that all the values are very small comparing to the values achieved in slurry batch experiments where the nanomaterials are added to the solution in a powder form [101], as opposed to their enmeshment in the polymer filaments in this research.

Based on the aforementioned facts, the addition of bentonite nanoclay enhanced the adsorption of the dye, even though its amount was as low as 2 wt% of the compositions. Furthermore, the TiO_2 nanomaterials did not have as much success, and it is unclear whether the K values are due to the photocatalysis of titanium dioxide or to the adsorption

capacity of the nanoclay. The comparison plots based on each of the polymer groups can be found in the B.1.

5.3 HTPA Conversion Results

After calculating the conversion rates by Eq. 3.9, the following observations could be made. (In order to perform an in-depth comparison between the samples, they are analyzed based on the aforementioned categorization in Table 3.1.)

In Category A which had 5% TiO_2 nanoparticles, the PMMA sample showed the most conversion rate ($6.33 \times 10^{-4}\,\mu$M/min). V_1 succeeded M_1 with a $5.11 \times 10^{-4}\,\mu$M/min rate. On the other hand, N_1 and S_1, showed poor performance in the HTPA conversion. In Category B, the filaments had 5% TiO_2 nanobelts. N_2, S_2, and V_2 behaved similarly, all exceeding $5.0 \times 10^{-4}\,\mu$M/min, while M_2 showed a very low conversion rate. Overall, the largest K_1 value belongs to N_2 ($K_1 = 5.67 \times 10^{-4}\,\mu$M/min). Comparing between nanoparticles and nanobelts, the nanobelts showed a better average rate between the four polymers. The results for Categories A and B are depicted in Figure 5.9.

In Categories C and D, filaments had 2% bentonite added in their composition. The trend is similar between filaments with nanoparticles (Category C) and the ones with nanobelts (Category D). The PVDF samples showed the best HTPA conversion while the PMMA demonstrated the least amount. The addition of bentonite did not influence the conversion rates apparently. Figure 5.10 illustrates the conversion rates for these categories.

There were no TiO_2 nanomaterials in Categories E and F. Members of Category E are composed of pure polymer, whereas in Category F, 2% bentonite is also added to the polymer. Nylon filaments showed the best performance in both of the categories, but no

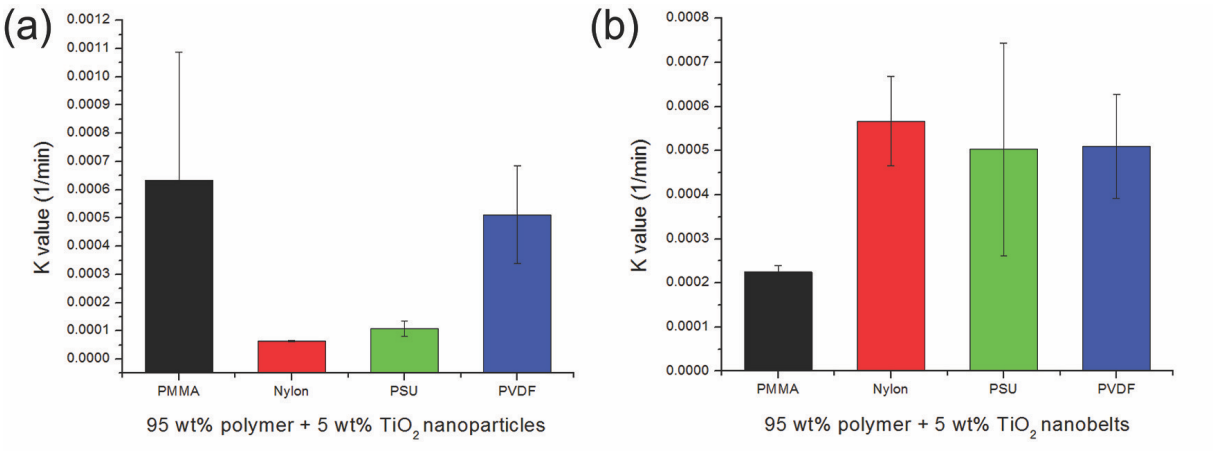

Figure 5.9: HTPA conversion rates for categories A (a) and B (b)

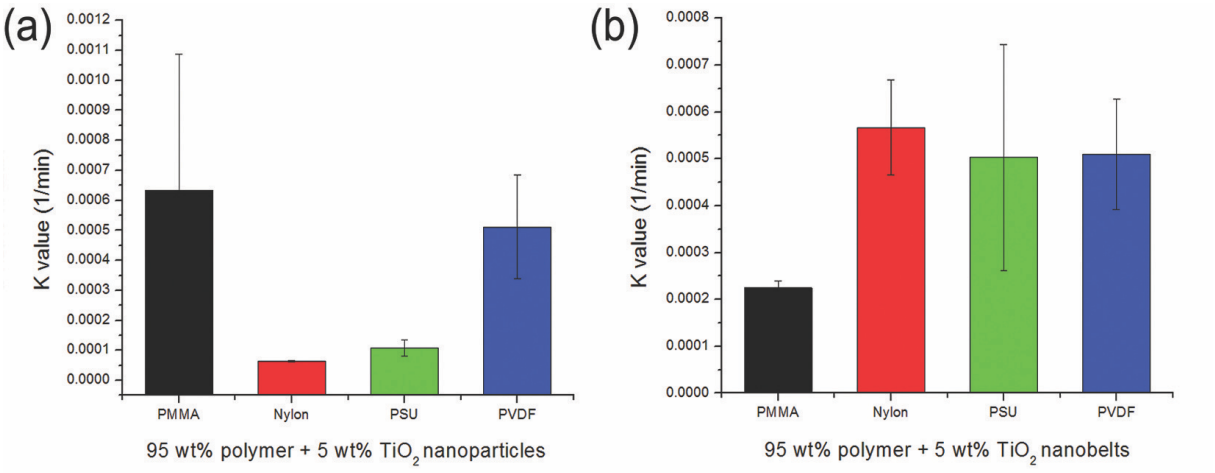

Figure 5.10: HTPA conversion rates for categories C (a) and D (b)

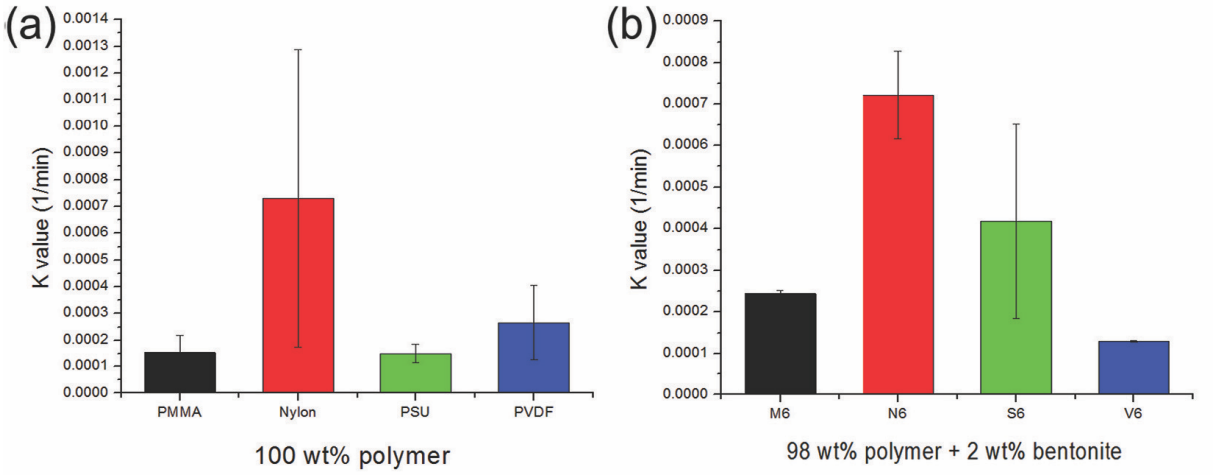

Figure 5.11: HTPA conversion rates for categories E (a) and F (b)

other apparent trend can be seen. The photocatalysis was not expected to happen in the pure polymer samples, and the achieved values are subject for future study. Furthermore, its noteworthy to mention that the addition of bentonite slightly increased the conversion rates (Figure 5.11).

5.4 Summary

A better dispersion of the nanomaterials in the polymer matrix can improve the mechanical properties of the extruded filaments. Extruding at higher speeds is an approach to obtain enhanced blending, because at higher speeds, higher shear rates are imposed on the mixture which will fragment the nanomaterial clumping and result in a more homogeneous mixture.

Regardless of the intensity and amount of the k_1 values, the conversion of TPA to HTPA is occurring due to the fact that HTPA conversion is observed in the experiments. However, no significant trend could be seen between different groups. Various assumptions

could explain the inferior results obtained in these experiments. First of all, photocatalysis only happens if the TiO_2 nanoparticles get the chance to be illuminated by the UV rays, and have direct contact with water —having part of their surface exposed to the solution, not completely entrapped in the polymer matrix —so that after receiving the required band-gap energy, the generated electron-holes can be released into the solution and play their part in further chemical reactions. Consequently, if any of the aforementioned conditions is not met, the photocatalysis cannot occur perfectly.

The dispersion of the nanomaterials in the polymer matrix is hypothetically throughout the whole volume of the filament, suggesting that only a small portion can be situated on the surface. Thus, the photocatalysis is not very likely to happen while most of the TiO_2 nanoparticles are enmeshed inside the matrix, not having any form of direct contact with the solution.

One suggestion to improve the exposure of the nanomaterials to the solution is by introducing porosity to the filaments. Porosity can increase the probability of TiO_2 nanoparticles having contact with the solution molecules, which can, as a result, enhance the possibility of releasing electron-hole pairs into the solution.

Chapter 6

Conclusions and Future Work

In this thesis, the extrusion of nanocomposite filaments for 3D-printing of water treatment membranes was explored. Furthermore, the addition of TiO_2 nanomaterials —nanoparticles and nanobelts—alongside bentonite nanoclay to the polymer matrices in order to extrude filaments was investigated. It was shown that extrusion of nanomaterial-enhanced filaments is achievable. The characteristics of both the extrusion and the extruded filaments were also studied. This chapter reviews major conclusions from this work an provides recommendations for future research and development.

6.1 Conclusions

6.1.1 Dispersion and Extrusion Processes

During the extrusion of the filaments, the initial temperature was proposed based on the glass transition and melting temperatures of pure polymers, but the working temperatures

were obtained by trial and error. The addition of nanomaterials into the polymer matrices increased their glass temperatures. The higher the temperature, the lower the viscosity of the composites would get. The perfect combination of the working temperature and proper speed was achieved experimentally.

Extra attention is required to observe and control the diameter of the filament as it exits the nozzle. Since the die in the nozzle is circular, the filament takes a circular cross sectional form consequently. From the nozzle up to at least twenty centimeters away, the filament is still very hot and soft. Throughout this length, if the filament is drawn excessively, the diameter will decrease. On the other hand, in the absence of a tension force, the diameter would expand because of a sudden pressure drop as it comes out of a small die. Therefore, drawing the filament is needed to keep its diameter constant until the filament cools down and is dense enough to maintain its geometry.

EDX analyses showed that an average of $3\,wt\%$ titanium element exists on the cross-sections (of the filaments that had TiO_2 in their formula), which corresponds to the initial stoichiometry of the compositions. Since the examined cross-sections were chosen randomly, the assumption is that such dispersion exists throughout the length of the filament and that TiO_2 nanomaterials have been thoroughly mixed.

Based on the SEM images, nanomaterial clustering was observed several times. Even with multiple mixing attempts (manual, secondary and tertiary mixing), the binding of nanomaterials seemed inevitable. Enhanced mixing methods need to be developed. Otherwise, the nanomaterial clustering can deteriorate their characteristics at the nano scale.

6.1.2 Filament Properties

Polysulfone filaments demonstrated the highest ultimate tensile strengths, whereas nylon counterparts showed the least. Moreover, based on the strain values, nylon filaments had the most extension rates. Consequently, PMMA samples were very brittle. Overall, PSU displayed the highest UTS and a reasonable strain. PVDF ranked second in these criteria.

Based on photocatalysis-based experiments, it can be understood that dye degradation and HTPA conversion occurred, which proves the functionality of the TiO_2 nanomaterials in the filaments. However, the low degradation/conversion rates suggest that the exposed TiO_2 nanomaterials were limited in number, and most of them were most likely entrapped inside the filament. On the other hand, the results also showed the removal of the dye in filaments without TiO_2, suggesting that the bentonite nanoclay participated in adsorption.

6.2 Future Work

Several pathways are suggested for future research to enhance the properties of the extruded filaments:

Dispersion of nanomaterials with polymers can be improved in the following ways:

- Due to the fact that nanomaterials tend to form clusters, preventative approaches can be developed to hinder this problem.
- Mixing procedures can be improved to obtain a better blending of the materials. Solution casting might be a more effective approach to achieve homogeneous mixes.

Introduction of porosity to the filaments can enhance the UV illumination on TiO_2 nanomaterials, and increase the contact opportunity between nanomaterials and the solution. Addition of a new soluble nano- or micro-material to the composition can be a method to increase porosity. In this approach, once the filaments are extruded, they can be submerged and sonicated in a proper solvent, so that the soluble particulates dissolve and leave void spaces (pores) behind.

Coating the 3D-printed membranes with TiO_2 nanomaterials can further enhance the photocatalytic properties of the membranes.

Developing methods to standardize the extrusion speed and temperature for different compositions is also an area that seeks further exploration. Since no database has all the necessary information about the aforementioned parameters, experimental research can be executed to create proper databases.

The tests of this research can be repeated with different weight percentages of nanomaterials (whether TiO_2 or bentonite) to investigate the effect of the compositions on final characteristics of the polymers, as well as on the extrusion properties.

References

[1] D. Dambournet, I. Belharouak, and K. Amine, "Tailored preparation methods of tio2 anatase, rutile, brookite: mechanism of formation and electrochemical properties," *Chemistry of Materials*, vol. 22, no. 3, pp. 1173–1179, 2009.

[2] R. Liang, A. Hu, M. Hatat-Fraile, and N. Zhou, *Development of TiO2 Nanowires for Membrane Filtration Applications*. Cham: Springer International Publishing, 2014, pp. 47–77. [Online]. Available: https://doi.org/10.1007/978-3-319-06578-6_2

[3] A. Fujishima, T. N. Rao, and D. A. Tryk, "Titanium dioxide photocatalysis," *Journal of Photochemistry and Photobiology C: Photochemistry reviews*, vol. 1, no. 1, pp. 1–21, 2000.

[4] N. Ochoa, M. Masuelli, and J. Marchese, "Effect of hydrophilicity on fouling of an emulsified oil wastewater with pvdf/pmma membranes," *Journal of Membrane Science*, vol. 226, no. 1-2, pp. 203–211, 2003.

[5] B. Mueller, "Additive manufacturing technologies–rapid prototyping to direct digital manufacturing," *Assembly Automation*, vol. 32, no. 2, 2012.

[6] K. V. Wong and A. Hernandez, "A review of additive manufacturing," *ISRN Mechanical Engineering*, vol. 2012, 2012.

[7] G.-d. Kang and Y.-m. Cao, "Development of antifouling reverse osmosis membranes for water treatment: a review," *Water Research*, vol. 46, no. 3, pp. 584–600, 2012.

[8] W. H. Organization, W. J. W. Supply, and S. M. Programme, *Progress on sanitation and drinking water: 2015 update and MDG assessment*. World Health Organization, 2015.

[9] C. A. Gouvea, F. Wypych, S. G. Moraes, N. Duran, N. Nagata, and P. Peralta-Zamora, "Semiconductor-assisted photocatalytic degradation of reactive dyes in aqueous solution," *Chemosphere*, vol. 40, no. 4, pp. 433–440, 2000.

[10] P. Cooper, "Removing colour from dyehouse waste watersa critical review of technology available," *Journal of the Society of Dyers and Colourists*, vol. 109, no. 3, pp. 97–100, 1993.

[11] M. A. Oturan, N. Oturan, M. C. Edelahi, F. I. Podvorica, and K. El Kacemi, "Oxidative degradation of herbicide diuron in aqueous medium by fenton's reaction based advanced oxidation processes," *Chemical Engineering Journal*, vol. 171, no. 1, pp. 127–135, 2011.

[12] A. Mills and S. Le Hunte, "An overview of semiconductor photocatalysis," *Journal of Photochemistry and Photobiology A: Chemistry*, vol. 108, no. 1, pp. 1–35, 1997.

[13] M. Castellote and N. Bengtsson, "Principles of tio 2 photocatalysis," in *Applications of Titanium Dioxide Photocatalysis to Construction Materials*. Springer, 2011, pp. 5–10.

[14] F. Opoku, K. K. Govender, C. G. C. E. van Sittert, and P. P. Govender, "Recent progress in the development of semiconductor-based photocatalyst materials for ap-

plications in photocatalytic water splitting and degradation of pollutants," *Advanced Sustainable Systems*, 2017.

[15] J. Ovenstone, "Preparation of novel titania photocatalysts with high activity," *Journal of Materials Science*, vol. 36, no. 6, pp. 1325–1329, 2001.

[16] L. Cassar, "Photocatalysis of cementitious materials: clean buildings and clean air," *Mrs Bulletin*, vol. 29, no. 5, pp. 328–331, 2004.

[17] A. Fujishima, K. Hashimoto, T. Watanabe, and Y. V. Pleskov, "Tio2 photocatalysis: Fundamentals and applications, tokyo: Bks, inc, 1999," *Russian Journal of Electrochemistry*, vol. 35, no. 10, pp. 1137–1138, 1999.

[18] D. Reyes-Coronado, G. Rodríguez-Gattorno, M. Espinosa-Pesqueira, C. Cab, R. d. de Coss, and G. Oskam, "Phase-pure tio2 nanoparticles: anatase, brookite and rutile," *Nanotechnology*, vol. 19, no. 14, p. 145605, 2008.

[19] R. Entner, "Modeling and simulation of negative bias temperature instability," 2007.

[20] J. E. Wijnhoven and W. L. Vos, "Preparation of photonic crystals made of air spheres in titania," *Science*, vol. 281, no. 5378, pp. 802–804, 1998.

[21] H. Zhang, R. L. Penn, R. J. Hamers, and J. F. Banfield, "Enhanced adsorption of molecules on surfaces of nanocrystalline particles," *The Journal of Physical Chemistry B*, vol. 103, no. 22, pp. 4656–4662, 1999.

[22] M. Cargnello, T. R. Gordon, and C. B. Murray, "Solution-phase synthesis of titanium dioxide nanoparticles and nanocrystals," *Chemical Reviews*, vol. 114, no. 19, pp. 9319–9345, 2014.

[23] X. Chen and S. S. Mao, "Titanium dioxide nanomaterials: synthesis, properties, modifications, and applications," *Chemical Reviews*, vol. 107, no. 7, pp. 2891–2959, 2007.

[24] Y. Yu, X. Wang, H. Sun, and M. Ahmad, "3d anatase tio 2 hollow microspheres assembled with high-energy {001} facets for lithium-ion batteries," *Rsc Advances*, vol. 2, no. 20, pp. 7901–7905, 2012.

[25] R. Liang, A. Hu, W. Li, and Y. N. Zhou, "Enhanced degradation of persistent pharmaceuticals found in wastewater treatment effluents using tio 2 nanobelt photocatalysts," *Journal of Nanoparticle Research*, vol. 15, no. 10, p. 1990, 2013.

[26] M. A. Henderson, "A surface science perspective on tio2 photocatalysis," *Surface Science Reports*, vol. 66, no. 6-7, pp. 185–297, 2011.

[27] M. Faisal, M. A. Tariq, A. Khan, K. Umar, and M. Muneer, "Photochemical reactions of 2, 4-dichloroaniline and 4-nitroanisole in aqueous suspension of titanium dioxide," *Science of Advanced Materials*, vol. 3, no. 2, pp. 269–275, 2011.

[28] K. Tennakone, C. Tilakaratne, and I. Kottegoda, "Photocatalytic degradation of organic contaminants in water with tio2 supported on polythene films," *Journal of Photochemistry and Photobiology A: Chemistry*, vol. 87, no. 2, pp. 177–179, 1995.

[29] M. G. Antoniou, P. A. Nicolaou, J. A. Shoemaker, A. Armah, and D. D. Dionysiou, "Impact of the morphological properties of thin tio2 photocatalytic films on the detoxification of water contaminated with the cyanotoxin, microcystin-lr," *Applied Catalysis B: Environmental*, vol. 91, no. 1-2, pp. 165–173, 2009.

[30] H. Choi, E. Stathatos, and D. D. Dionysiou, "Photocatalytic tio2 films and membranes for the development of efficient wastewater treatment and reuse systems," *Desalination*, vol. 202, no. 1-3, pp. 199–206, 2007.

[31] R. Azouani, A. Michau, K. Hassouni, K. Chhor, J.-F. Bocquet, J.-L. Vignes, and A. Kanaev, "Elaboration of pure and doped tio2 nanoparticles in sol–gel reactor with turbulent micromixing: Application to nanocoatings and photocatalysis," *Chemical Engineering Research and Design*, vol. 88, no. 9, pp. 1123–1130, 2010.

[32] P. Pucher, M. Benmami, R. Azouani, G. Krammer, K. Chhor, J.-F. Bocquet, and A. Kanaev, "Nano-tio2 sols immobilized on porous silica as new efficient photocatalyst," *Applied Catalysis A: General*, vol. 332, no. 2, pp. 297–303, 2007.

[33] R. Molinari, A. Caruso, and T. Poerio, "Direct benzene conversion to phenol in a hybrid photocatalytic membrane reactor," *Catalysis Today*, vol. 144, no. 1-2, pp. 81–86, 2009.

[34] H. Zhang, X. Quan, S. Chen, H. Zhao, and Y. Zhao, "Fabrication of photocatalytic membrane and evaluation its efficiency in removal of organic pollutants from water," *Separation and Purification Technology*, vol. 50, no. 2, pp. 147–155, 2006.

[35] A. Fernandez, G. Lassaletta, V. Jimenez, A. Justo, A. Gonzalez-Elipe, J.-M. Herrmann, H. Tahiri, and Y. Ait-Ichou, "Preparation and characterization of tio2 photocatalysts supported on various rigid supports (glass, quartz and stainless steel). comparative studies of photocatalytic activity in water purification," *Applied Catalysis B: Environmental*, vol. 7, no. 1-2, pp. 49–63, 1995.

[36] M. Benmami, K. Chhor, and A. Kanaev, "High photocatalytic activity of monolayer nanocoatings prepared from non-crystalline titanium oxide sol nanoparticles," *Chemical Physics Letters*, vol. 422, no. 4-6, pp. 552–557, 2006.

[37] N. Takeda, N. Iwata, T. Torimoto, and H. Yoneyama, "Influence of carbon black as an adsorbent used in tio2 photocatalyst films on photodegradation behaviors of propyzamide," *Journal of Catalysis*, vol. 177, no. 2, pp. 240–246, 1998.

[38] M. Hatat-Fraile, J. Mendret, M. Rivallin, and S. Brosillon, "Effect of hydrodynamics during sol–gel synthesis of tio2 nanoparticles: From morphology to photocatalytic properties," *Chemical Engineering Research and Design*, vol. 91, no. 12, pp. 2389–2400, 2013.

[39] G. E. Romanos, C. Athanasekou, F. Katsaros, N. Kanellopoulos, D. Dionysiou, V. Likodimos, and P. Falaras, "Double-side active tio2-modified nanofiltration membranes in continuous flow photocatalytic reactors for effective water purification," *Journal of Hazardous materials*, vol. 211, pp. 304–316, 2012.

[40] S. Papageorgiou, F. Katsaros, E. Favvas, G. E. Romanos, C. Athanasekou, K. Beltsios, O. Tzialla, and P. Falaras, "Alginate fibers as photocatalyst immobilizing agents applied in hybrid photocatalytic/ultrafiltration water treatment processes," *Water Research*, vol. 46, no. 6, pp. 1858–1872, 2012.

[41] R. Molinari, M. Mungari, E. Drioli, A. Di Paola, V. Loddo, L. Palmisano, and M. Schiavello, "Study on a photocatalytic membrane reactor for water purification," *Catalysis Today*, vol. 55, no. 1-2, pp. 71–78, 2000.

[42] C. Athanasekou, G. Romanos, F. Katsaros, K. Kordatos, V. Likodimos, and P. Falaras, "Very efficient composite titania membranes in hybrid ultrafiltra-

tion/photocatalysis water treatment processes," *Journal of Membrane Science*, vol. 392, pp. 192–203, 2012.

[43] G. Romanos, C. Athanasekou, V. Likodimos, P. Aloupogiannis, and P. Falaras, "Hybrid ultrafiltration/photocatalytic membranes for efficient water treatment," *Industrial & Engineering Chemistry Research*, vol. 52, no. 39, pp. 13 938–13 947, 2013.

[44] M. Hatat-Fraile, R. Liang, M. J. Arlos, R. X. He, P. Peng, M. R. Servos, and Y. N. Zhou, "Concurrent photocatalytic and filtration processes using doped tio2 coated quartz fiber membranes in a photocatalytic membrane reactor," *Chemical Engineering Journal*, vol. 330, pp. 531–540, 2017.

[45] S. Madaeni, "The application of membrane technology for water disinfection," *Water Research*, vol. 33, no. 2, pp. 301–308, 1999.

[46] M. M. Pendergast and E. M. Hoek, "A review of water treatment membrane nanotechnologies," *Energy & Environmental Science*, vol. 4, no. 6, pp. 1946–1971, 2011.

[47] M. Elimelech and W. A. Phillip, "The future of seawater desalination: energy, technology, and the environment," *Science*, vol. 333, no. 6043, pp. 712–717, 2011.

[48] S. S. Ghayeni, P. Beatson, R. Schneider, and A. Fane, "Water reclamation from municipal wastewater using combined microfiltration-reverse osmosis (me-ro): preliminary performance data and microbiological aspects of system operation," *Desalination*, vol. 116, no. 1, pp. 65–80, 1998.

[49] B. Van der Bruggen, "Chemical modification of polyethersulfone nanofiltration membranes: a review," *Journal of Applied Polymer Science*, vol. 114, no. 1, pp. 630–642, 2009.

[50] D. Zhang, A. Karkooti, L. Liu, M. Sadrzadeh, T. Thundat, Y. Liu, and R. Narain, "Fabrication of antifouling and antibacterial polyethersulfone (pes)/cellulose nanocrystals (cnc) nanocomposite membranes," *Journal of Membrane Science*, vol. 549, pp. 350–356, 2018.

[51] S. Adhikari and S. Fernando, "Hydrogen membrane separation techniques," *Industrial & Engineering Chemistry Research*, vol. 45, no. 3, pp. 875–881, 2006.

[52] D. Wang, J. Tong, H. Xu, and Y. Matsumura, "Preparation of palladium membrane over porous stainless steel tube modified with zirconium oxide," *Catalysis Today*, vol. 93, pp. 689–693, 2004.

[53] A. Sagle and B. Freeman, "Fundamentals of membranes for water treatment," *The Future of Desalination in Texas*, vol. 2, no. 363, p. 137, 2004.

[54] J. Ren and R. Wang, "Preparation of polymeric membranes," in *Membrane and desalination technologies*. Springer, 2011, pp. 47–100.

[55] L. Y. Ng, A. W. Mohammad, C. P. Leo, and N. Hilal, "Polymeric membranes incorporated with metal/metal oxide nanoparticles: a comprehensive review," *Desalination*, vol. 308, pp. 15–33, 2013.

[56] A. Chatterjee, "Properties improvement of pmma using nano tio2," *Journal of Applied Polymer Science*, vol. 118, no. 5, pp. 2890–2897, 2010.

[57] P. Meneghetti and S. Qutubuddin, "Synthesis, thermal properties and applications of polymer-clay nanocomposites," *Thermochimica Acta*, vol. 442, no. 1-2, pp. 74–77, 2006.

[58] Y. Ma, X. Cao, X. Feng, Y. Ma, and H. Zou, "Fabrication of super-hydrophobic film from pmma with intrinsic water contact angle below 90," *Polymer*, vol. 48, no. 26, pp. 7455–7460, 2007.

[59] T. Gale, "Nylon 6 and nylon 66," http://www.encyclopedia.com/science/academic-and-educational-journals/nylon-6-and-nylon-66, accessed: 2018-04-21.

[60] "nylon 6," https://www.sigmaaldrich.com/catalog/product/aldrich/181110?lang=en&region=CA, accessed: 2018-04-23.

[61] H. Mahfuz, M. Hasan, V. Dhanak, G. Beamson, J. Stewart, V. Rangari, X. Wei, V. Khabashesku, and S. Jeelani, "Reinforcement of nylon 6 with functionalized silica nanoparticles for enhanced tensile strength and modulus," *Nanotechnology*, vol. 19, no. 44, p. 445702, 2008.

[62] L. Huang and J. R. McCutcheon, "Hydrophilic nylon 6, 6 nanofibers supported thin film composite membranes for engineered osmosis," *Journal of Membrane Science*, vol. 457, pp. 162–169, 2014.

[63] R. W. Baker, *Membrane Technology*. Wiley Online Library, 2000.

[64] K. Schult and D. Paul, "Water sorption and transport in a series of polysulfones," *Journal of Polymer Science Part B: Polymer Physics*, vol. 34, no. 16, pp. 2805–2817, 1996.

[65] "Poly(ether)sulfones," http://polymerdatabase.com/polymer%20classes/Polysulfone%20type.html, accessed: 2018-04-23.

[66] "Transparent plastic with high strength rigidity," https://www.solvay.com/en/markets-and-products/featured-products/udel.html, accessed: 2018-04-23.

[67] Q. Yu, Y. Tao, Y. Huang, Z. Lin, Y. Zhuang, L. Ge, Y. Shen, M. Hong, and A. Xie, "Preparation of porous polysulfone microspheres and their application in removal of oil from water," *Industrial & Engineering Chemistry Research*, vol. 51, no. 23, pp. 8117–8122, 2012.

[68] "What is polyvinylidene fluoride? (pvdf)," http://www.fluorocarbon.co.uk/news-and-events/post/19/what-is-polyvinylidene-fluoride, accessed: 2018-04-24.

[69] X. Gu, C. Michaels, D. Nguyen, Y. Jean, J. Martin, and T. Nguyen, "Surface and interfacial properties of pvdf/acrylic copolymer blends before and after uv exposure," *Applied Surface Science*, vol. 252, no. 14, pp. 5168–5181, 2006.

[70] L.-P. Zhu, J.-Z. Yu, Y.-Y. Xu, Z.-Y. Xi, and B.-K. Zhu, "Surface modification of pvdf porous membranes via poly (dopa) coating and heparin immobilization," *Colloids and Surfaces B: Biointerfaces*, vol. 69, no. 1, pp. 152–155, 2009.

[71] C. C. Ibeh, *Thermoplastic materials: properties, manufacturing methods, and applications*. CRC Press, 2011.

[72] M. Kobayashi, K. Tashiro, and H. Tadokoro, "Molecular vibrations of three crystal forms of poly (vinylidene fluoride)," *Macromolecules*, vol. 8, no. 2, pp. 158–171, 1975.

[73] J. Yin and B. Deng, "Polymer-matrix nanocomposite membranes for water treatment," *Journal of Membrane Science*, vol. 479, pp. 256–275, 2015.

[74] S. J. Oh, N. Kim, and Y. T. Lee, "Preparation and characterization of pvdf/tio2 organic–inorganic composite membranes for fouling resistance improvement," *Journal of Membrane Science*, vol. 345, no. 1-2, pp. 13–20, 2009.

[75] J.-n. Shen, H.-m. Ruan, L.-g. Wu, and C.-j. Gao, "Preparation and characterization of pes–sio2 organic–inorganic composite ultrafiltration membrane for raw water pretreatment," *Chemical Engineering Journal*, vol. 168, no. 3, pp. 1272–1278, 2011.

[76] L. Yan, S. Hong, M. L. Li, and Y. S. Li, "Application of the al2o3–pvdf nanocomposite tubular ultrafiltration (uf) membrane for oily wastewater treatment and its antifouling research," *Separation and Purification Technology*, vol. 66, no. 2, pp. 347–352, 2009.

[77] A. Gholami, A. Moghadassi, S. Hosseini, S. Shabani, and F. Gholami, "Preparation and characterization of polyvinyl chloride based nanocomposite nanofiltration-membrane modified by iron oxide nanoparticles for lead removal from water," *Journal of Industrial and Engineering Chemistry*, vol. 20, no. 4, pp. 1517–1522, 2014.

[78] N. Maximous, G. Nakhla, W. Wan, and K. Wong, "Effect of the metal oxide particle distributions on modified pes membranes characteristics and performance," *Journal of Membrane Science*, vol. 361, no. 1-2, pp. 213–222, 2010.

[79] H. Basri, A. F. Ismail, and M. Aziz, "Polyethersulfone (pes)–silver composite uf membrane: Effect of silver loading and pvp molecular weight on membrane morphology and antibacterial activity," *Desalination*, vol. 273, no. 1, pp. 72–80, 2011.

[80] A. Dasari, J. Quirós, B. Herrero, K. Boltes, E. García-Calvo, and R. Rosal, "Antifouling membranes prepared by electrospinning polylactic acid containing biocidal nanoparticles," *Journal of membrane science*, vol. 405, pp. 134–140, 2012.

[81] N. Akar, B. Asar, N. Dizge, and I. Koyuncu, "Investigation of characterization and biofouling properties of pes membrane containing selenium and copper nanoparticles," *Journal of membrane science*, vol. 437, pp. 216–226, 2013.

[82] F. Liu, B.-R. Ma, D. Zhou, Y.-h. Xiang, and L.-x. Xue, "Breaking through tradeoff of polysulfone ultrafiltration membranes by zeolite 4a," *Microporous and Mesoporous Materials*, vol. 186, pp. 113–120, 2014.

[83] V. Vatanpour, S. S. Madaeni, R. Moradian, S. Zinadini, and B. Astinchap, "Fabrication and characterization of novel antifouling nanofiltration membrane prepared from oxidized multiwalled carbon nanotube/polyethersulfone nanocomposite," *Journal of Membrane Science*, vol. 375, no. 1-2, pp. 284–294, 2011.

[84] N. Ghaemi, S. S. Madaeni, A. Alizadeh, H. Rajabi, and P. Daraei, "Preparation, characterization and performance of polyethersulfone/organically modified montmorillonite nanocomposite membranes in removal of pesticides," *Journal of Membrane Science*, vol. 382, no. 1-2, pp. 135–147, 2011.

[85] A. Rahimpour, S. Madaeni, A. Taheri, and Y. Mansourpanah, "Coupling tio2 nanoparticles with uv irradiation for modification of polyethersulfone ultrafiltration membranes," *Journal of Membrane Science*, vol. 313, no. 1-2, pp. 158–169, 2008.

[86] F. Zhang, W. Zhang, Y. Yu, B. Deng, J. Li, and J. Jin, "Sol–gel preparation of paa-g-pvdf/tio2 nanocomposite hollow fiber membranes with extremely high water flux and improved antifouling property," *Journal of Membrane Science*, vol. 432, pp. 25–32, 2013.

[87] H. Ngang, B. Ooi, A. Ahmad, and S. Lai, "Preparation of pvdf–tio2 mixed-matrix membrane and its evaluation on dye adsorption and uv-cleaning properties," *Chemical Engineering Journal*, vol. 197, pp. 359–367, 2012.

[88] H. A. Patel, R. S. Somani, H. C. Bajaj, and R. V. Jasra, "Nanoclays for polymer nanocomposites, paints, inks, greases and cosmetics formulations, drug delivery ve-

hicle and waste water treatment," *Bulletin of Materials Science*, vol. 29, no. 2, pp. 133–145, 2006.

[89] E. I. Unuabonah and A. Taubert, "Clay–polymer nanocomposites (cpns): Adsorbents of the future for water treatment," *Applied Clay Science*, vol. 99, pp. 83–92, 2014.

[90] J. Kim and T. Creasy, "Selective laser sintering characteristics of nylon 6/clay-reinforced nanocomposite," *Polymer Testing*, vol. 23, no. 6, pp. 629–636, 2004.

[91] J. W. Gilman, S. Bourbigot, J. R. Shields, M. Nyden, T. Kashiwagi, R. D. Davis, D. L. Vanderhart, W. Demory, C. A. Wilkie, A. B. Morgan *et al.*, "High throughput methods for polymer nanocomposites research: Extrusion, nmr characterization and flammability property screening," *Journal of Materials Science*, vol. 38, no. 22, pp. 4451–4460, 2003.

[92] M. R. Skorski, J. M. Esenther, Z. Ahmed, A. E. Miller, and M. R. Hartings, "The chemical, mechanical, and physical properties of 3d printed materials composed of tio2-abs nanocomposites," *Science and Technology of Advanced Materials*, vol. 17, no. 1, pp. 89–97, 2016.

[93] S. Chaudhari, T. N. Shaikh, B. Patel, and P. Pandey, "Engineering polypropylene tio2 nanocomposite filament to improve uv resistance," *International Journal of Advances in Management, Technology & Engineering Science*, vol. 4, no. 1, pp. 22–25, 2014.

[94] *Sigma Aldrich*, 2018 (accessed August 24, 2018). [Online]. Available: https://www.sigmaaldrich.com/canada-english.html

[95] "Nano minerals: Nanoclays," https://www.sigmaaldrich.com/technical-documents/articles/materials-science/nanomaterials/nano-minerals-nanoclays.html, accessed: 2018-04-25.

[96] C. S. Turchi and D. F. Ollis, "Photocatalytic degradation of organic water contaminants: mechanisms involving hydroxyl radical attack," *Journal of Catalysis*, vol. 122, no. 1, pp. 178–192, 1990.

[97] U. Černigoj, M. Kete, and U. L. Štangar, "Development of a fluorescence-based method for evaluation of self-cleaning properties of photocatalytic layers," *Catalysis Today*, vol. 151, no. 1-2, pp. 46–52, 2010.

[98] P. Kumar, K. Sandeep, S. Alavi, V. Truong, and R. Gorga, "Preparation and characterization of bio-nanocomposite films based on soy protein isolate and montmorillonite using melt extrusion," *Journal of Food Engineering*, vol. 100, no. 3, pp. 480–489, 2010.

[99] K. Oksman, A. P. Mathew, D. Bondeson, and I. Kvien, "Manufacturing process of cellulose whiskers/polylactic acid nanocomposites," *Composites Science and Technology*, vol. 66, no. 15, pp. 2776–2784, 2006.

[100] J. Cho and D. Paul, "Nylon 6 nanocomposites by melt compounding," *Polymer*, vol. 42, no. 3, pp. 1083–1094, 2001.

[101] R. Liang, L. C. L. C. Fong, M. J. Arlos, J. Van Leeuwen, E. Shahnam, P. Peng, M. R. Servos, and Y. N. Zhou, "Photocatalytic degradation using one-dimensional tio2 and ag-tio2 nanobelts under uv-led controlled periodic illumination," *Journal of Environmental Chemical Engineering*, vol. 5, no. 5, pp. 4365–4373, 2017.

[102] D. Macwan, P. N. Dave, and S. Chaturvedi, "A review on nano-tio2 sol–gel type syntheses and its applications," *Journal of Materials Science*, vol. 46, no. 11, pp. 3669–3686, 2011.

[103] G. Oskam, A. Nellore, R. L. Penn, and P. C. Searson, "The growth kinetics of tio2 nanoparticles from titanium (iv) alkoxide at high water/titanium ratio," *The Journal of Physical Chemistry B*, vol. 107, no. 8, pp. 1734–1738, 2003.

[104] A. Al-Kdasi, A. Idris, K. Saed, and C. T. Guan, "Treatment of textile wastewater by advanced oxidation processesa review," *Global Nest: the Int. J*, vol. 6, no. 3, pp. 222–230, 2004.

[105] L. Zhang, R. Dillert, D. Bahnemann, and M. Vormoor, "Photo-induced hydrophilicity and self-cleaning: models and reality," *Energy & Environmental Science*, vol. 5, no. 6, pp. 7491–7507, 2012.

[106] R. Chokshi and H. Zia, "Hot-melt extrusion technique: a review," *Iranian Journal of Pharmaceutical Research*, pp. 3–16, 2010.

[107] M. Salazar, "Polymer material selection and testing of resistive wire arrangement for a transparent infant warming blanket," Ph.D. dissertation, Massachusetts Institute of Technology, 2013.

[108] C. Wilkes and P. Handbook, "Hanser verlag., 2005," ISBN 1-56990-379-4 Search PubMed, Tech. Rep.

[109] C. Aitken, J. McHattie, and D. Paul, "Dynamic mechanical behavior of polysulfones," *Macromolecules*, vol. 25, no. 11, pp. 2910–2922, 1992.

[110] J. E. Dohany, "Fluorine-containing polymers, poly (vinylidene fluoride)," *Kirk-Othmer encyclopedia of chemical technology*, 2000.

[111] F. W. Billmeyer, "Textbook of polymer science, john wiley & sons," *Inc., New York*, p. 339, 1984.

[112] P. Daraei, S. S. Madaeni, N. Ghaemi, M. A. Khadivi, B. Astinchap, and R. Moradian, "Fouling resistant mixed matrix polyethersulfone membranes blended with magnetic nanoparticles: study of magnetic field induced casting," *Separation and Purification Technology*, vol. 109, pp. 111–121, 2013.

[113] J.-P. Qu, Z.-T. Yang, X.-C. Yin, H.-Z. He, and Y.-H. Feng, "Characteristics study of polymer melt conveying capacity in vane plasticization extruder," *Polymer-Plastics Technology and Engineering*, vol. 48, no. 12, pp. 1269–1274, 2009.

Appendix A

A.1 SEM Images

Below are the SEM images of all the samples to the left, with the corresponding EDX analysis to the right.

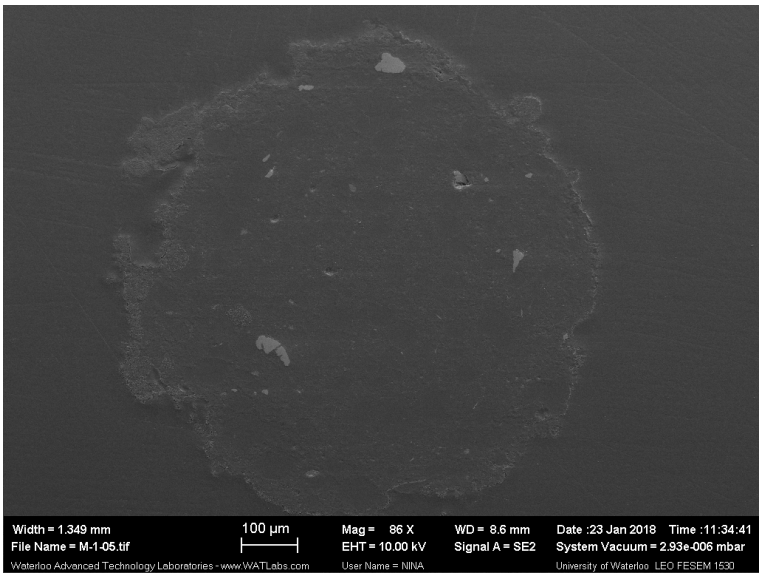

Figure A.1: M1: PMMA + TiO_2 NP

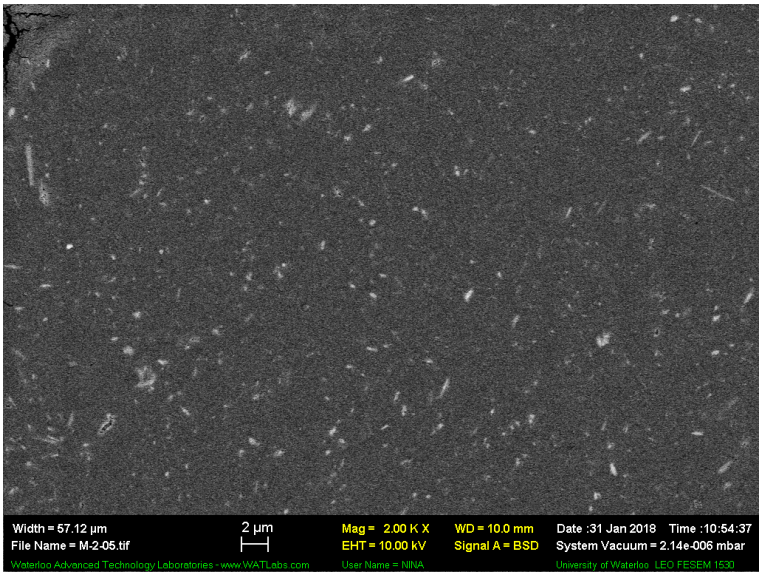

Figure A.2: M2: PMMA + TiO_2 NB

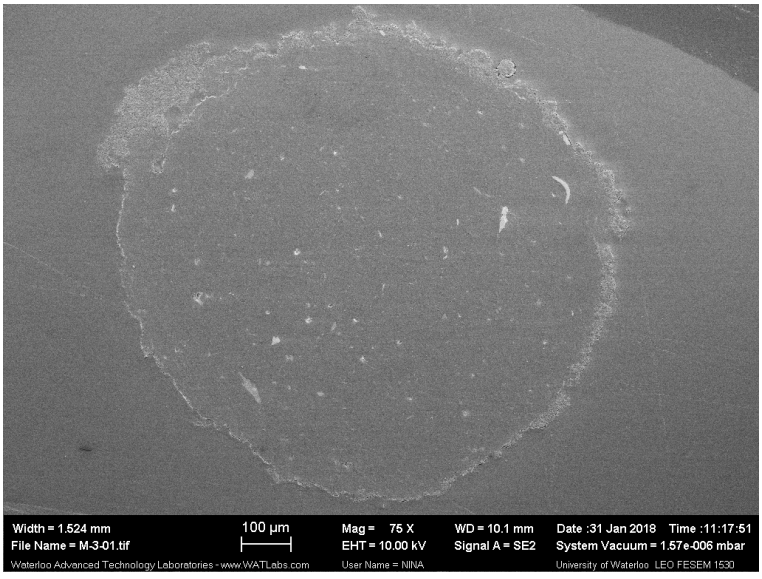

Figure A.3: M3: PMMA + TiO_2 NP + bentonite nanoclay

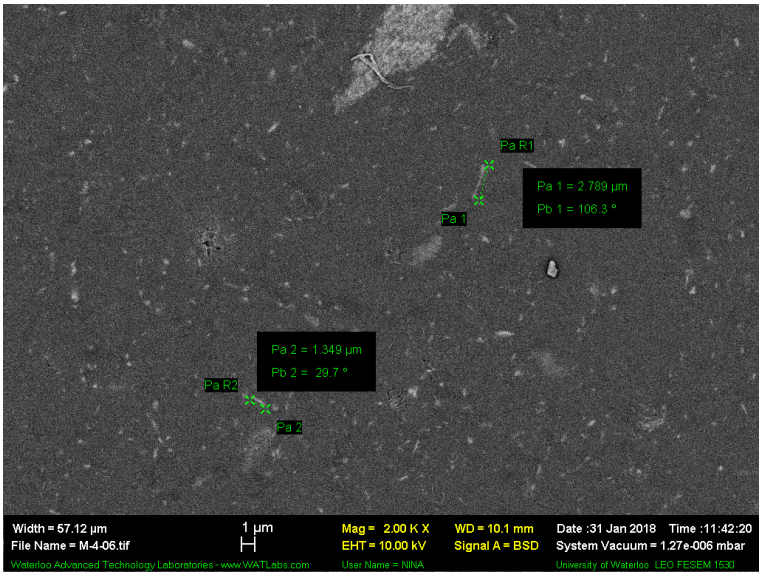

Figure A.4: M4: PMMA + TiO_2 NB + bentonite nanoclay

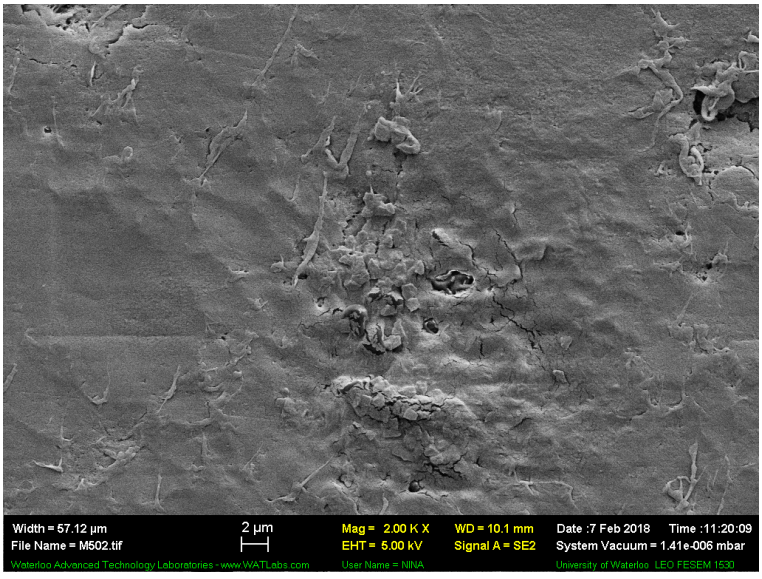

Figure A.5: M5: pure PMMA

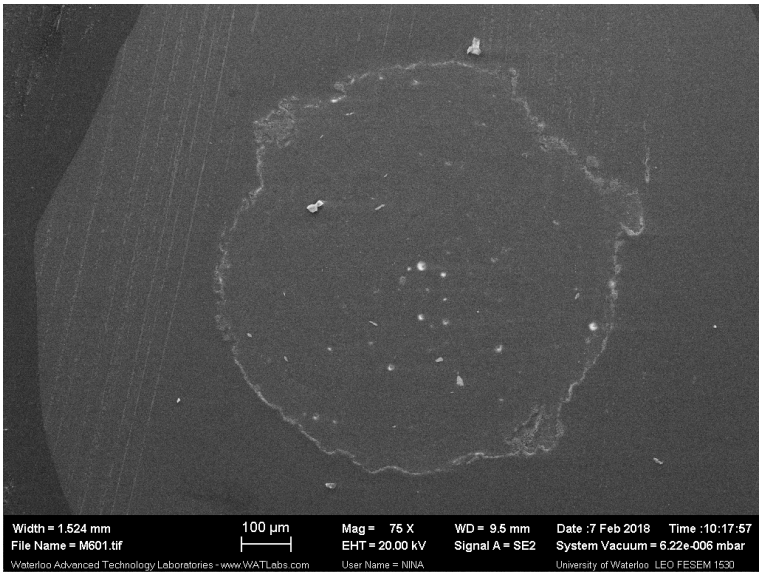

Figure A.6: M6: PMMA + bentonite nanoclay

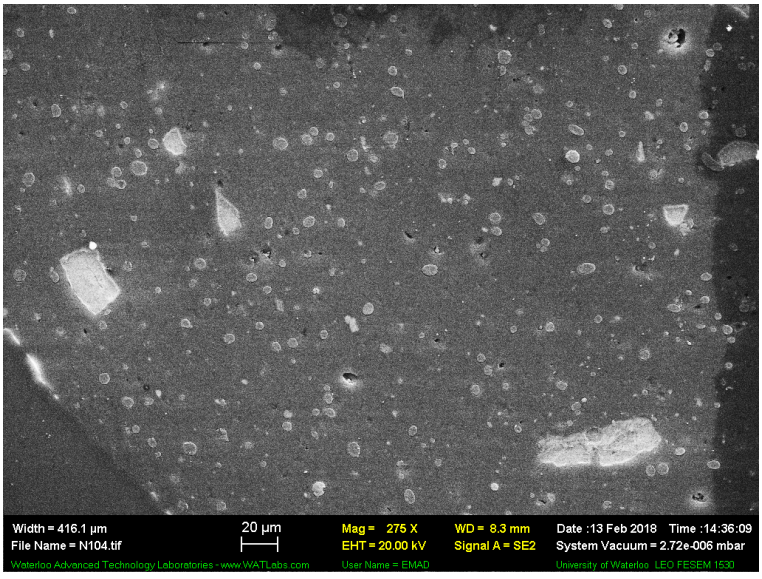

Figure A.7: N1: Nylon + TiO_2 NP

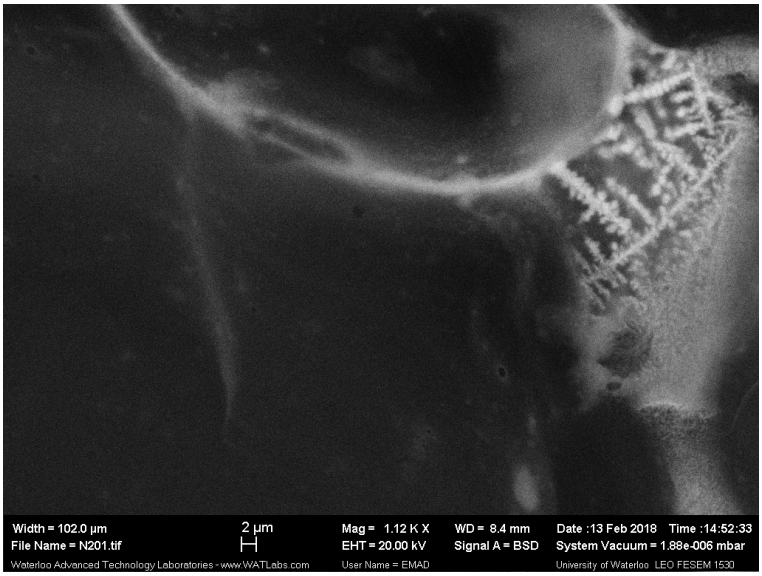

Figure A.8: N2: Nylon + TiO_2 NB

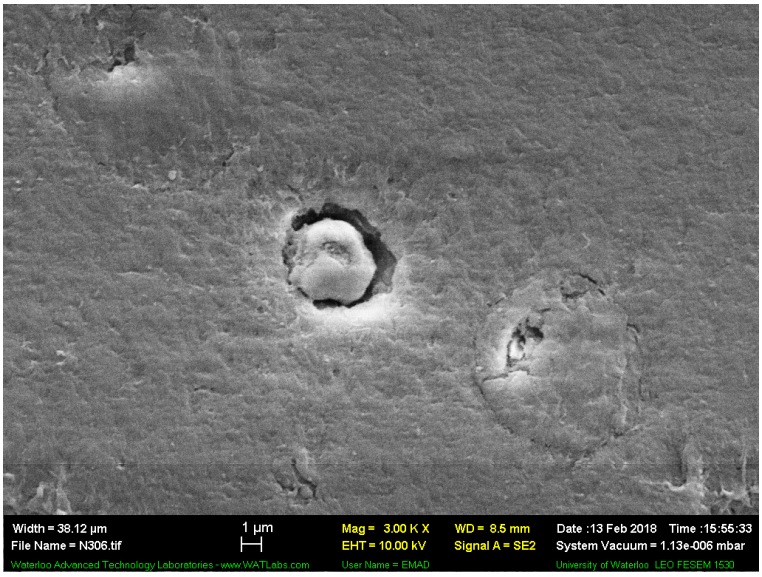

Figure A.9: N3: Nylon + TiO_2 NP + bentonite nanoclay

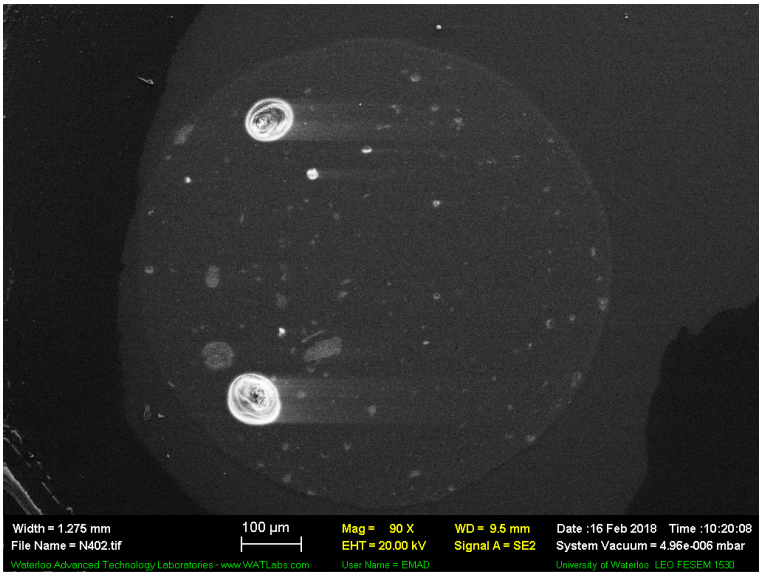

Figure A.10: N4: Nylon + TiO_2 NB + bentonite nanoclay

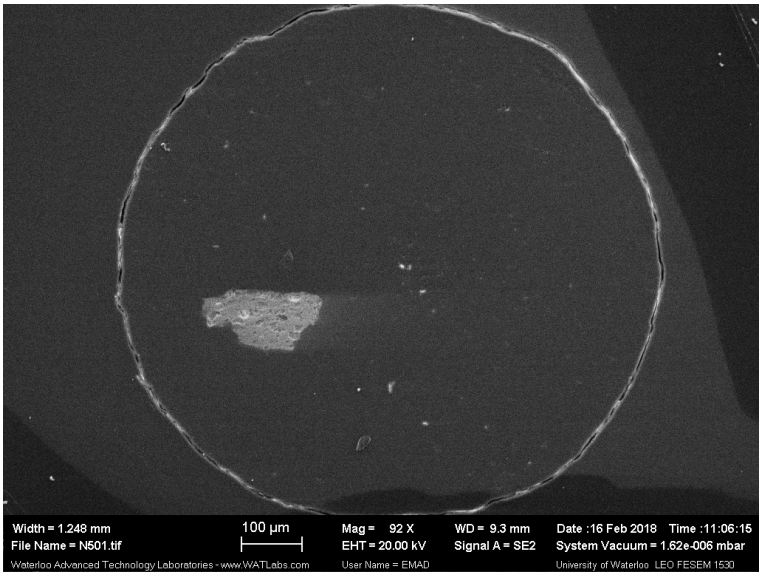

Figure A.11: N5: pure Nylon

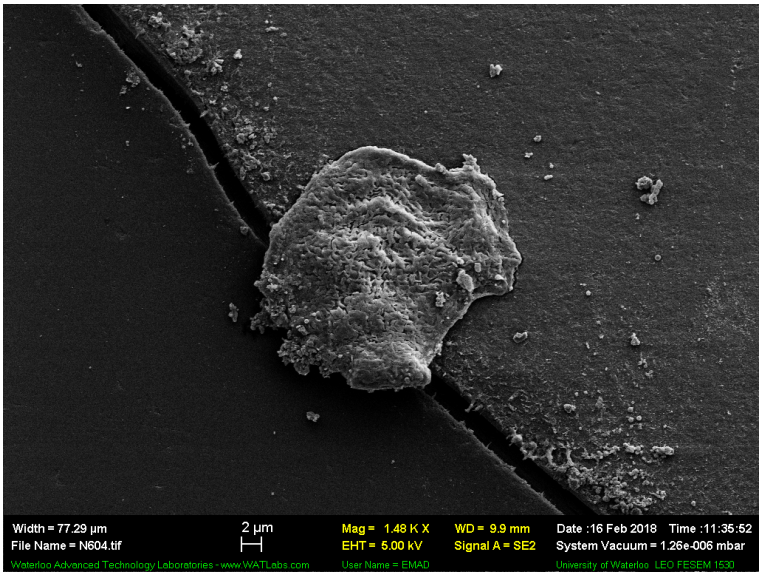

Figure A.12: N6: Nylon + bentonite nanoclay

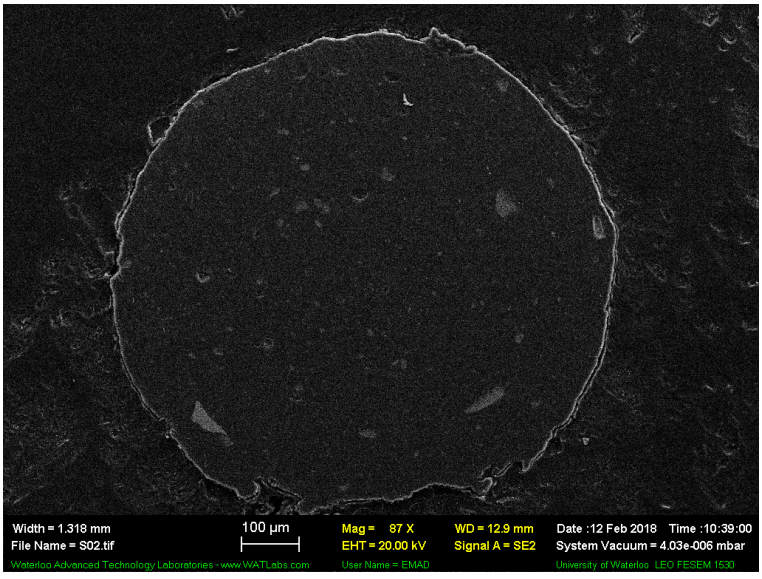

Figure A.13: S1: PSU + TiO_2 NP

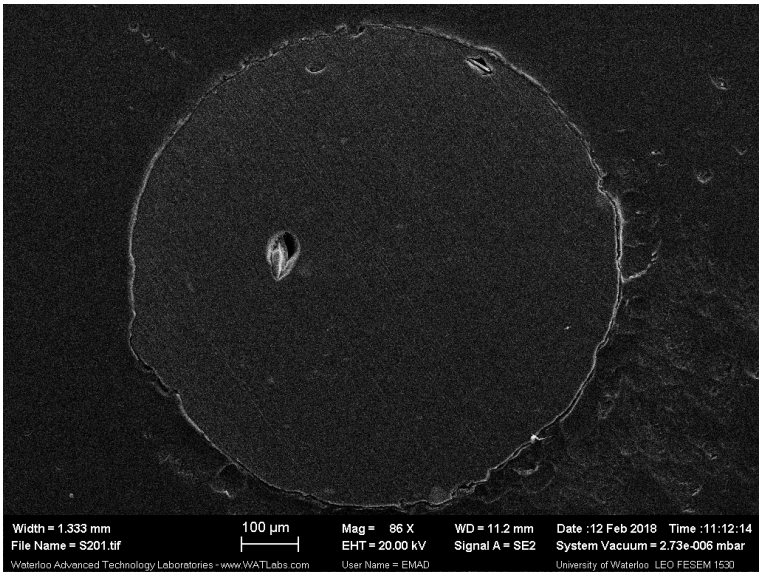

Figure A.14: S2: PSU + TiO_2 NB

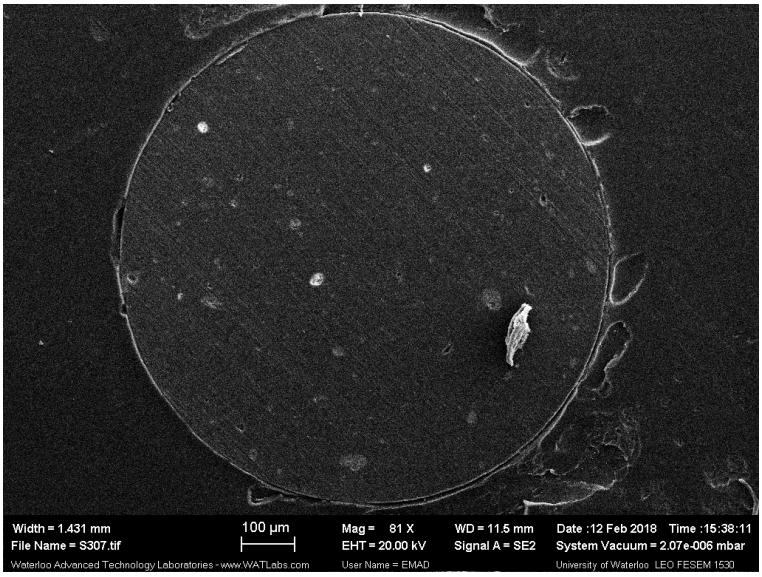

Figure A.15: S3: PSU + TiO_2 NP + bentonite nanoclay

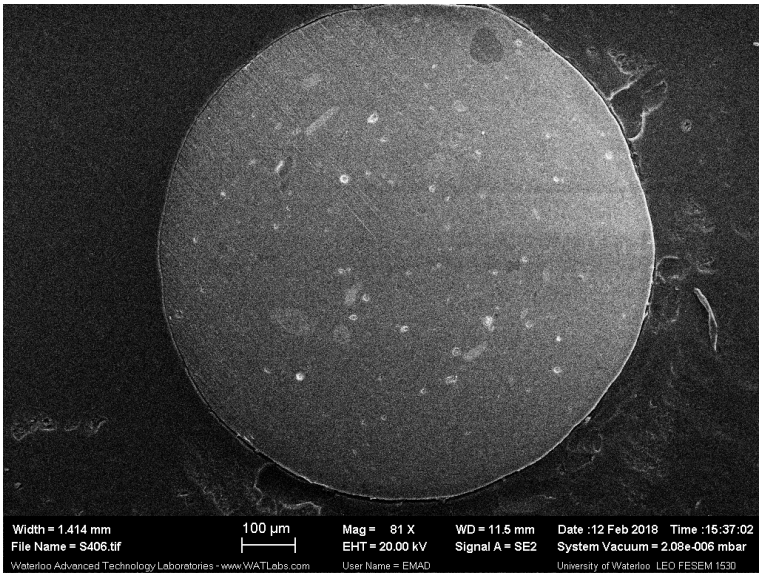

Figure A.16: S4: PSU + TiO_2 NB + bentonite nanoclay

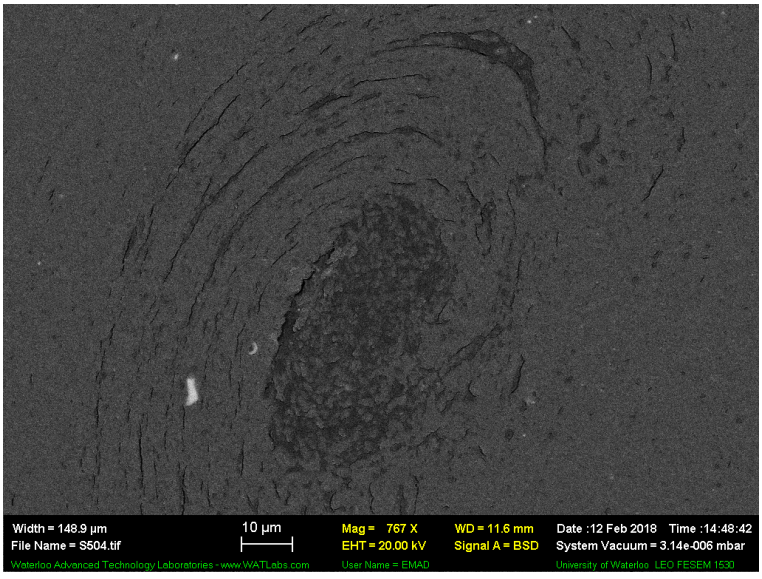

Figure A.17: S5: pure PSU

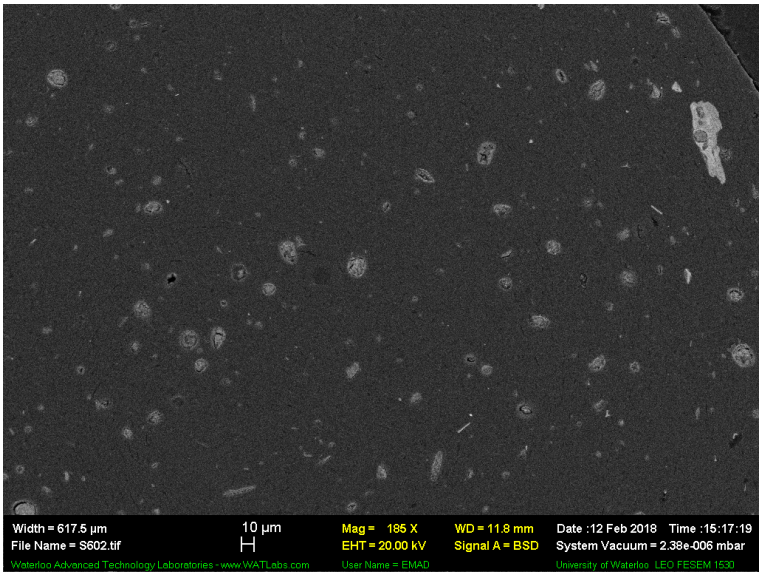

Figure A.18: S6: PSU + bentonite nanoclay

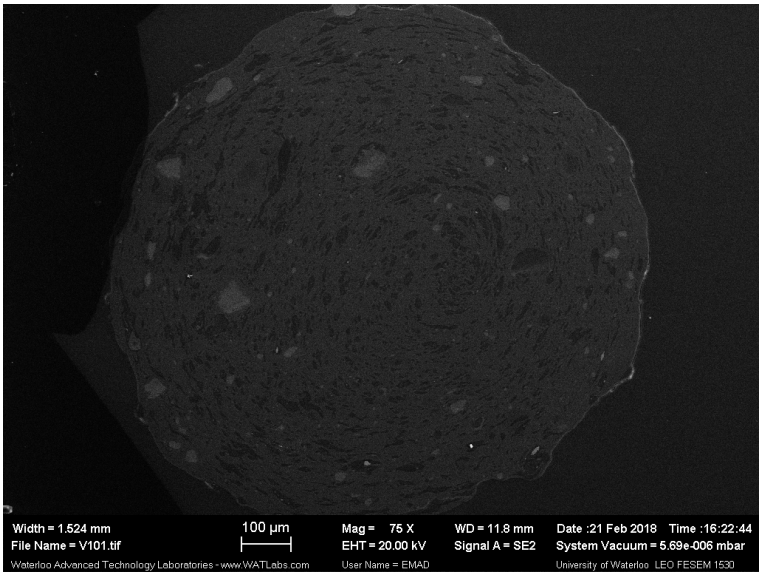

Figure A.19: V1: PVDF + TiO_2 NP

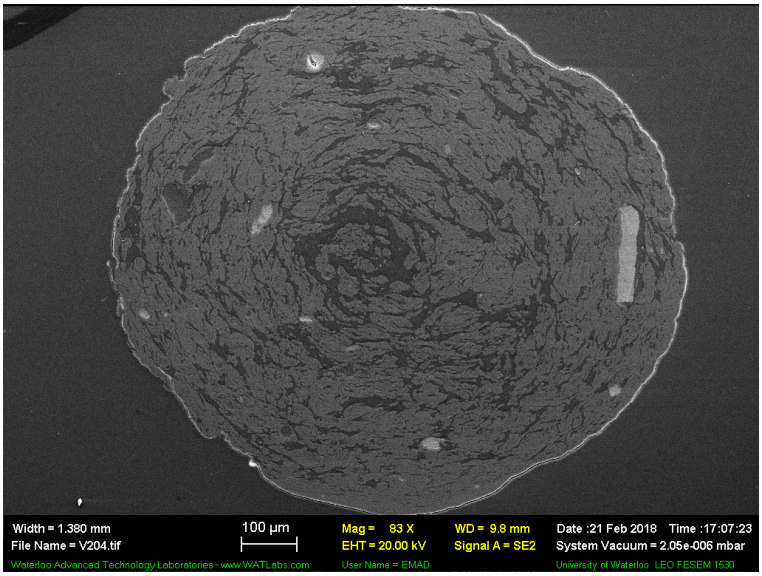

Figure A.20: V2: PVDF + TiO_2 NB

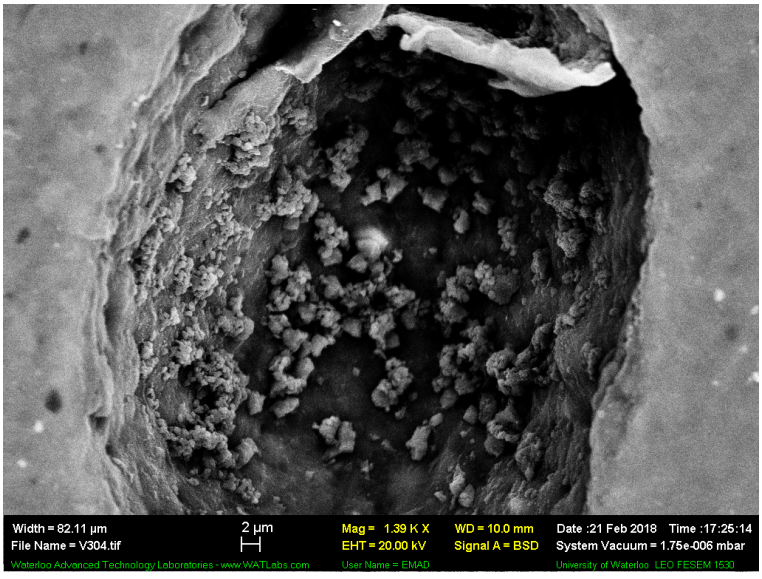

Figure A.21: V3: PVDF + TiO_2 NP + bentonite nanoclay

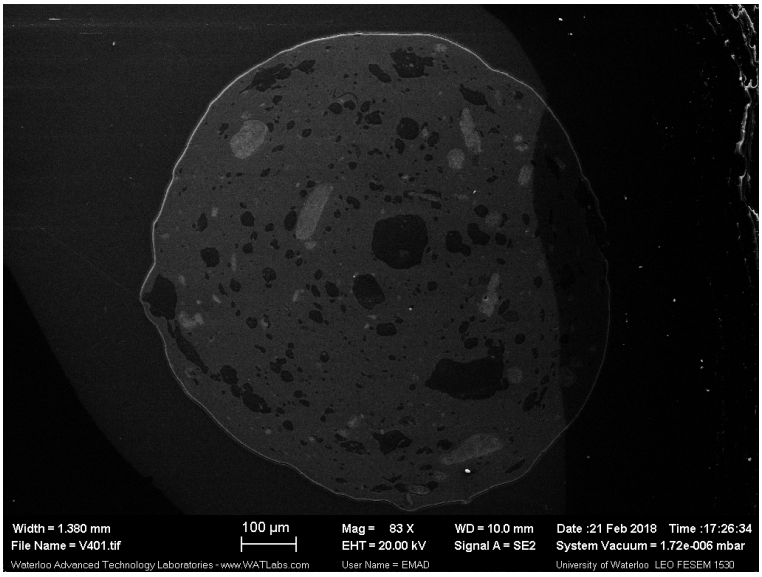

Figure A.22: V4: PVDF + TiO_2 NB + bentonite nanoclay

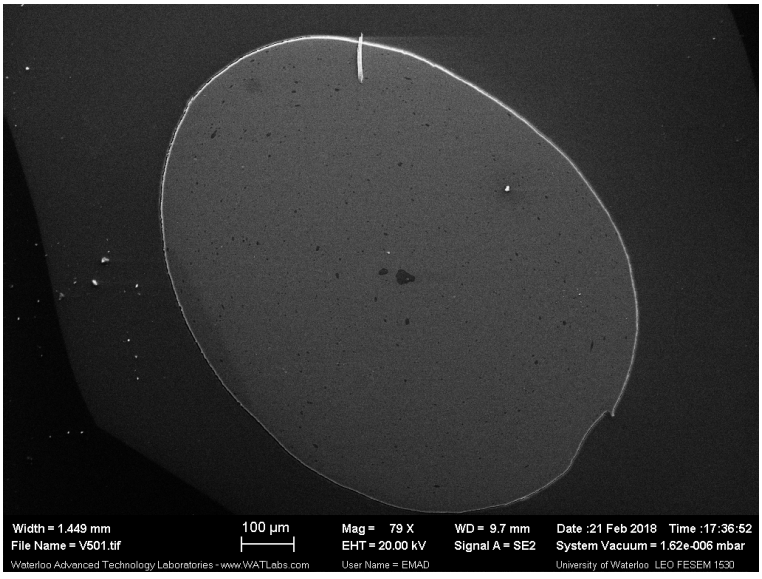

Figure A.23: V5: pure PVDF

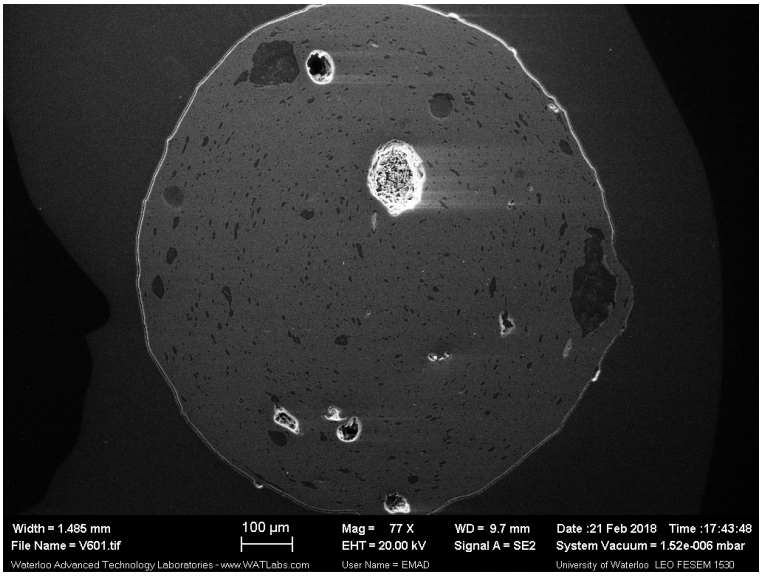

Figure A.24: V6: PVDF + bentonite nanoclay

A.2 Thermogravimetric analysis data

Below are the Weight over Temperature curves achieved from TGA:

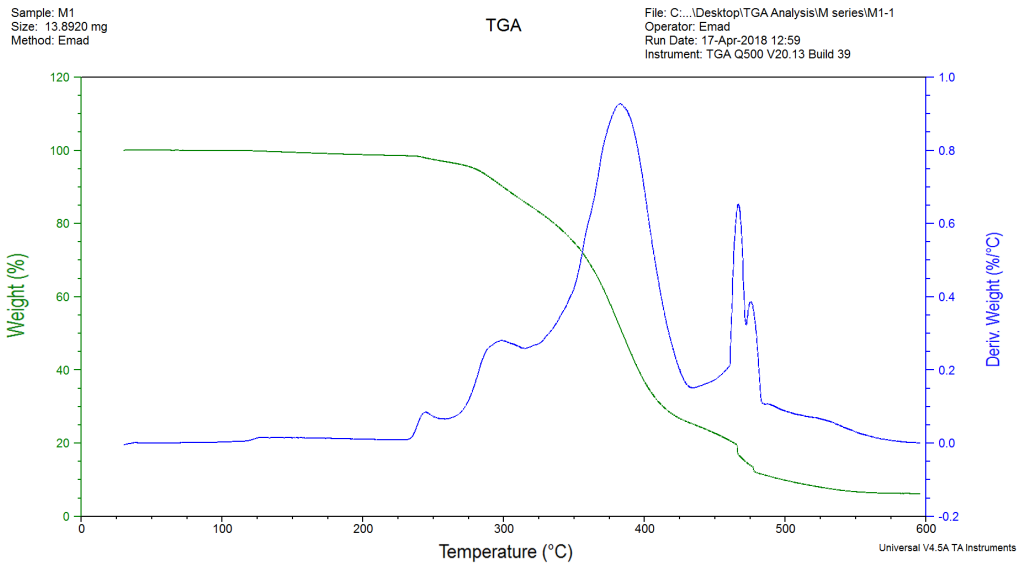

Figure A.25: M1: PMMA + TiO_2 NP

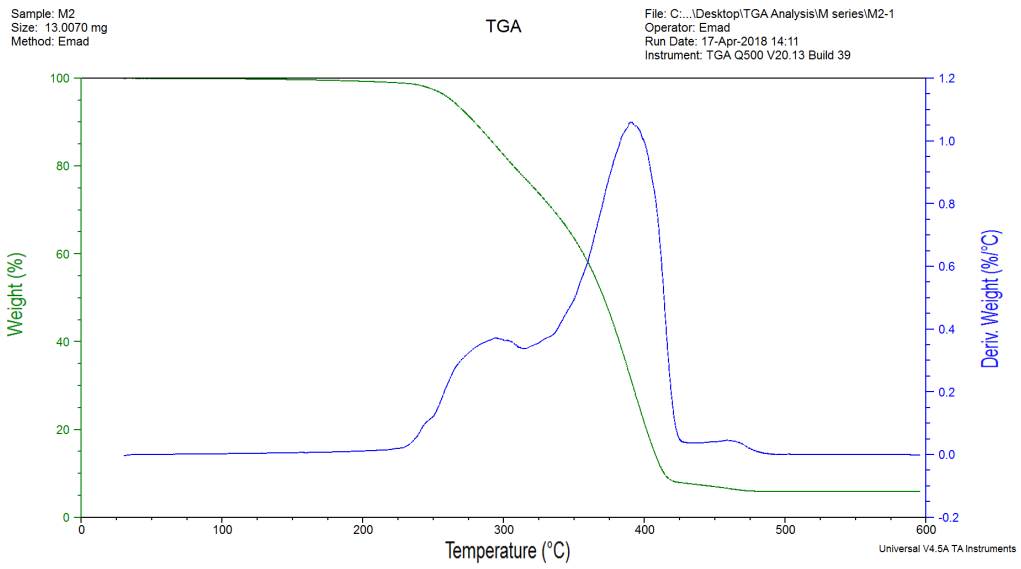

Figure A.26: M2: PMMA + TiO_2 NB

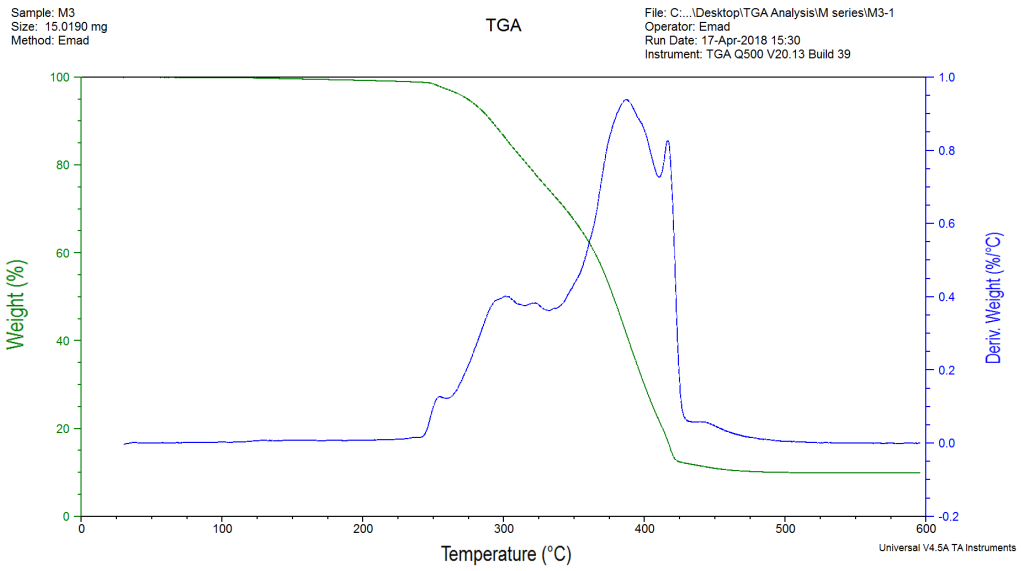

Figure A.27: M3: PMMA + TiO_2 NP + bentonite nanoclay

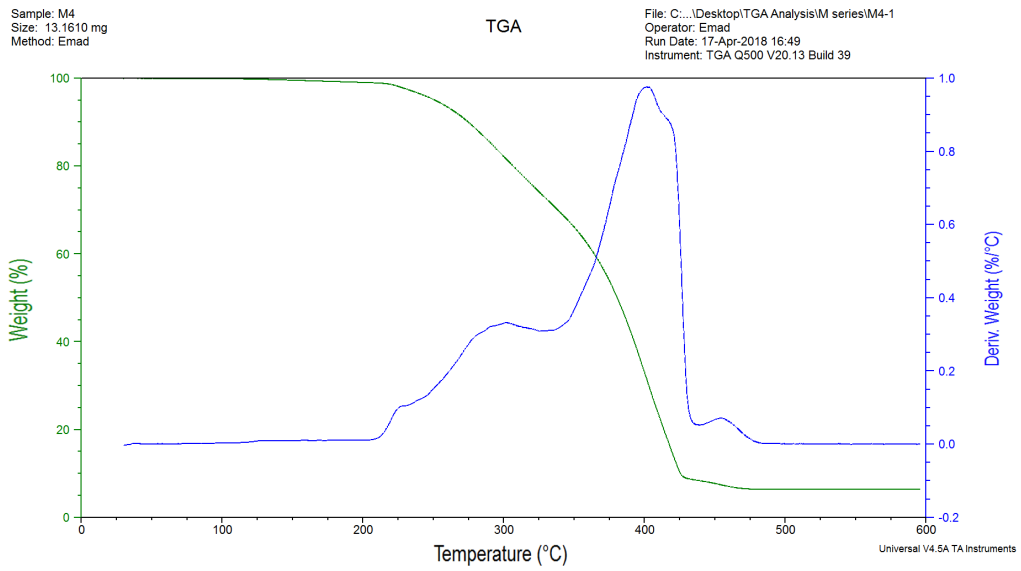

Figure A.28: M4: PMMA + TiO_2 NB + bentonite nanoclay

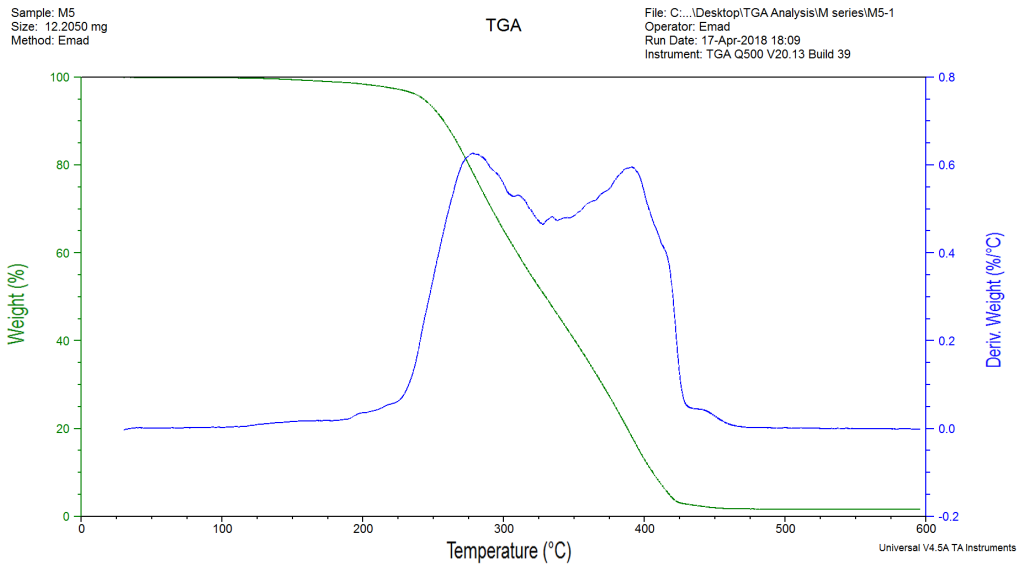

Figure A.29: M5: pure PMMA

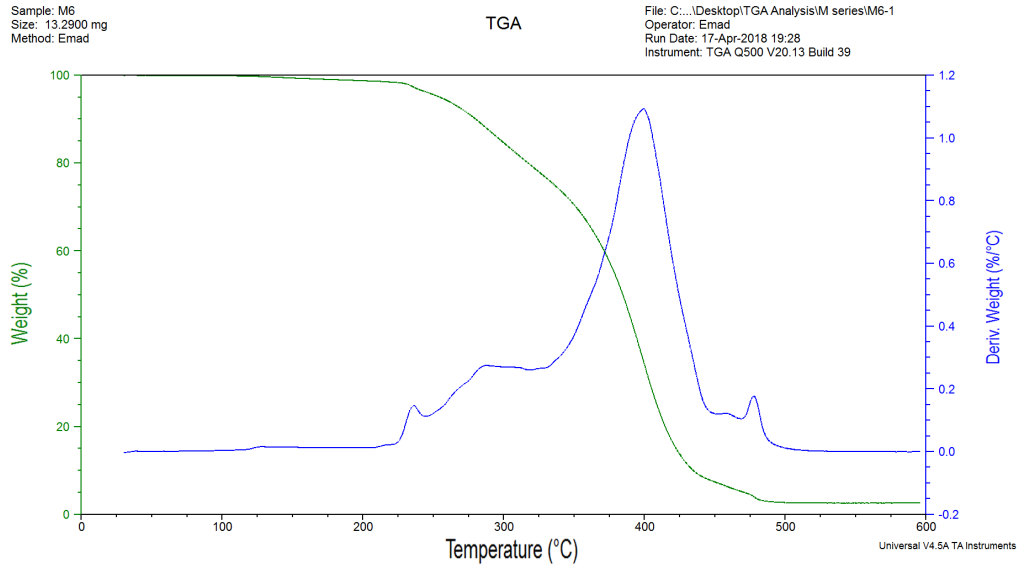

Figure A.30: M6: PMMA + bentonite nanoclay

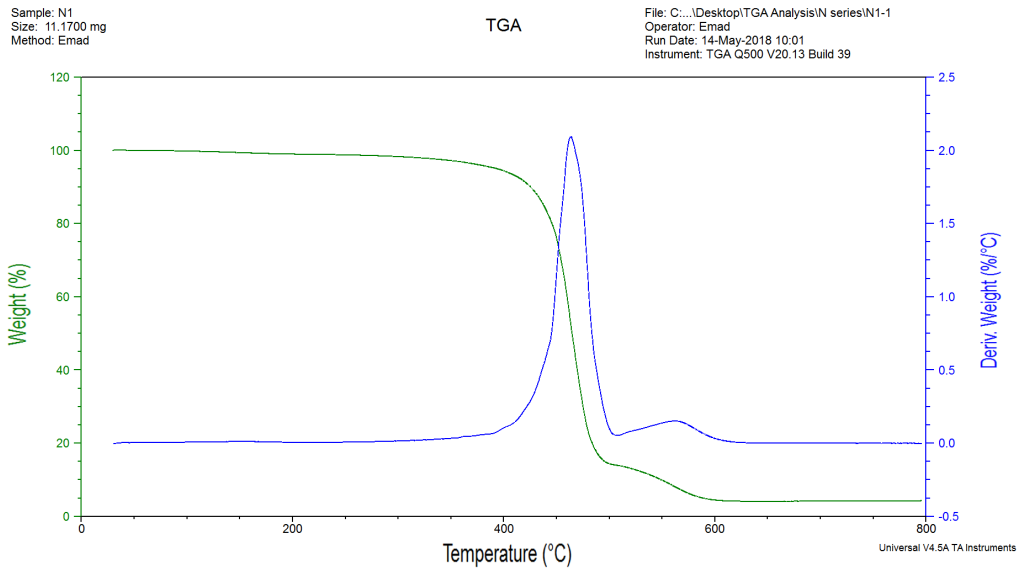

Figure A.31: N1: Nylon + TiO_2 NP

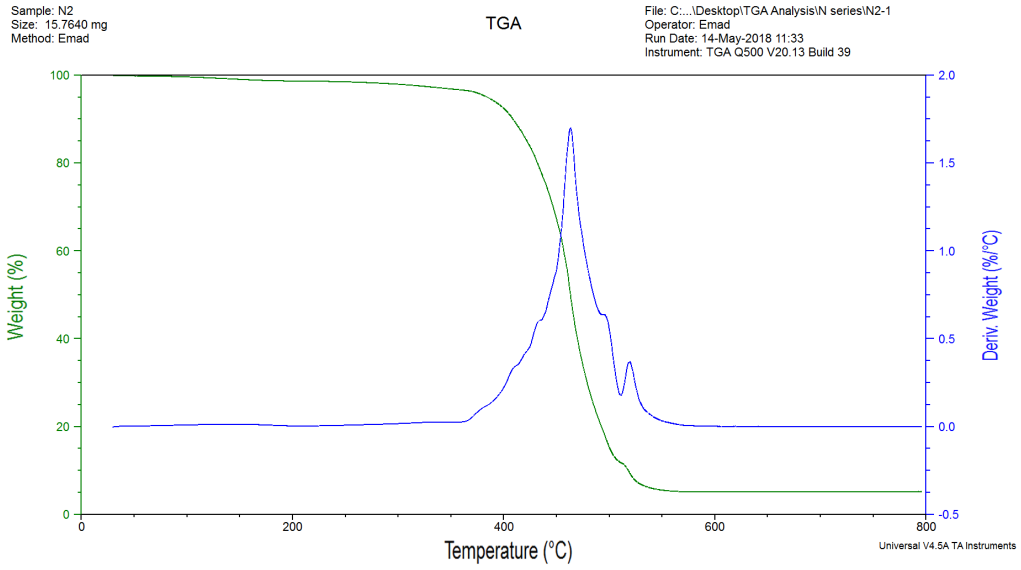

Figure A.32: N2: Nylon + TiO_2 NB

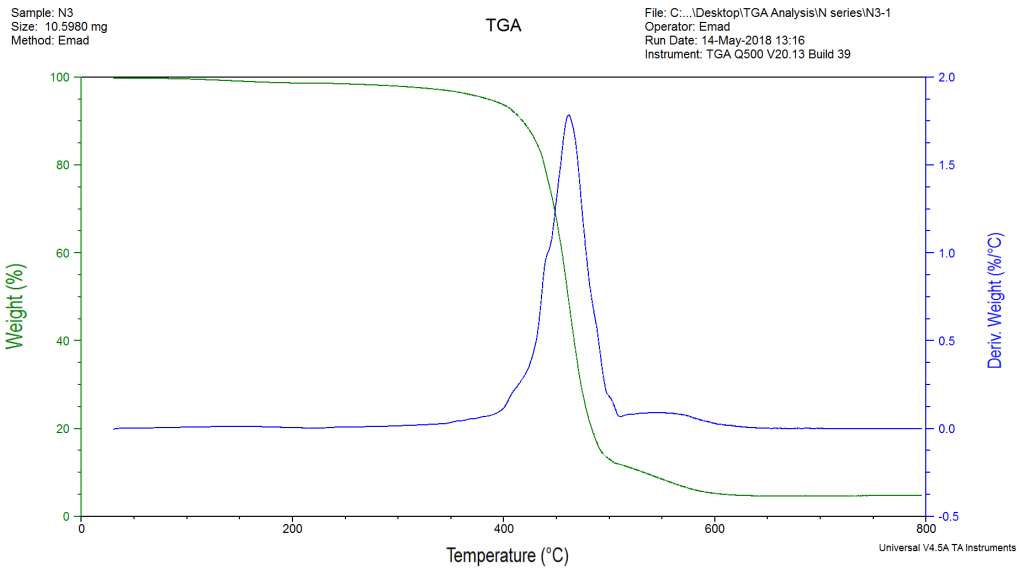

Figure A.33: N3: Nylon + TiO_2 NP + bentonite nanoclay

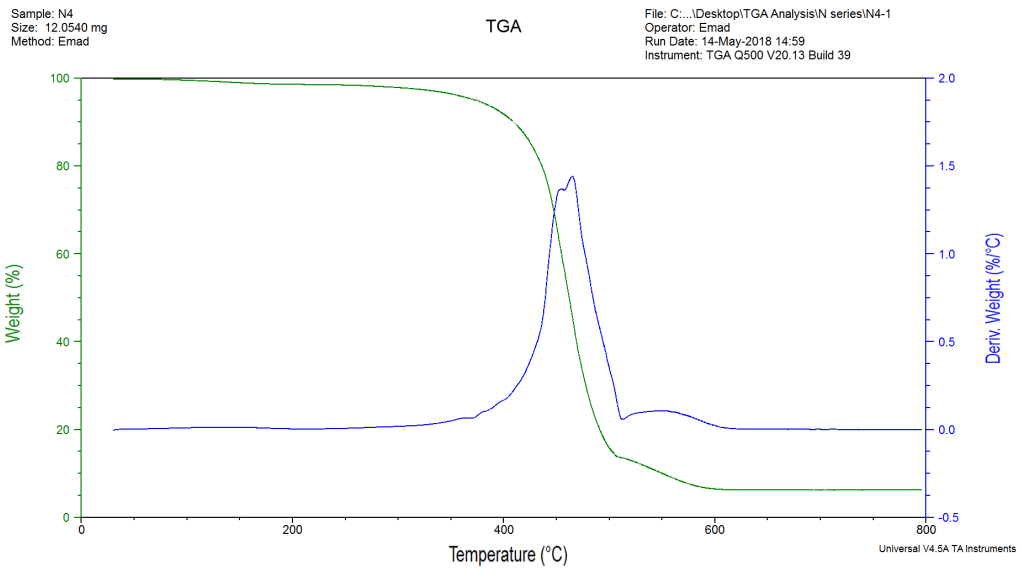

Figure A.34: N4: Nylon + TiO_2 NB + bentonite nanoclay

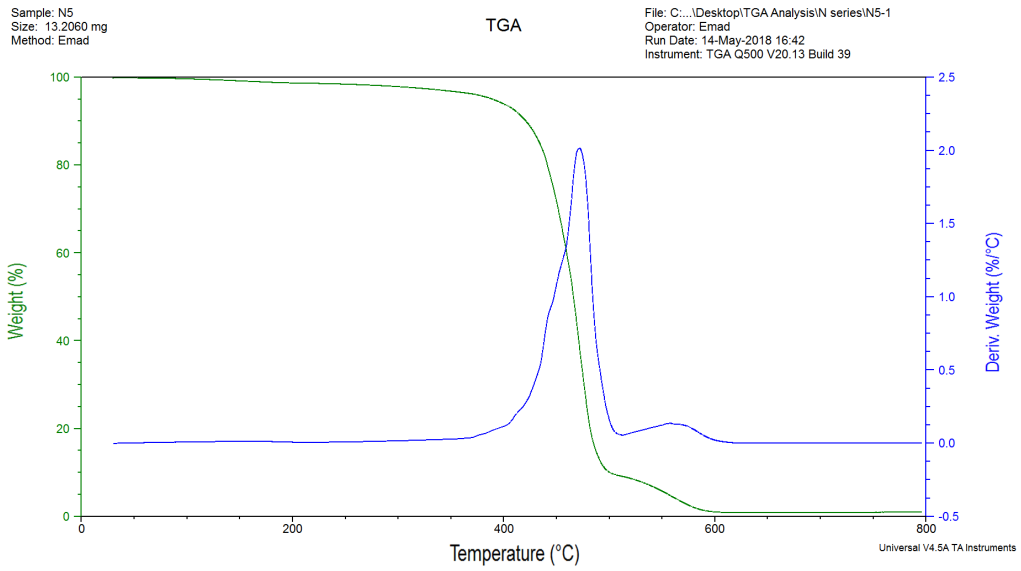

Figure A.35: N5: pure Nylon

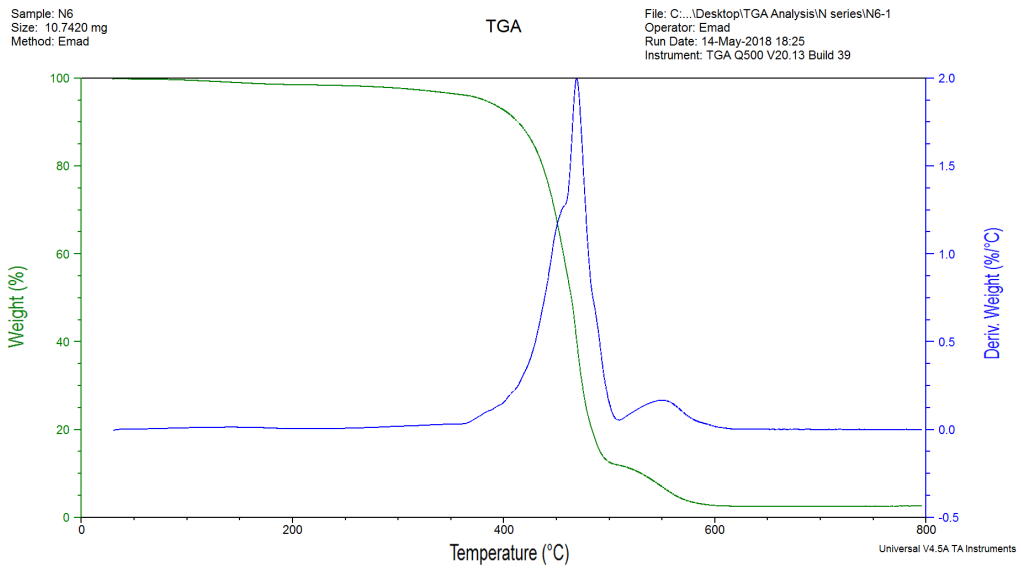

Figure A.36: N6: Nylon + bentonite nanoclay

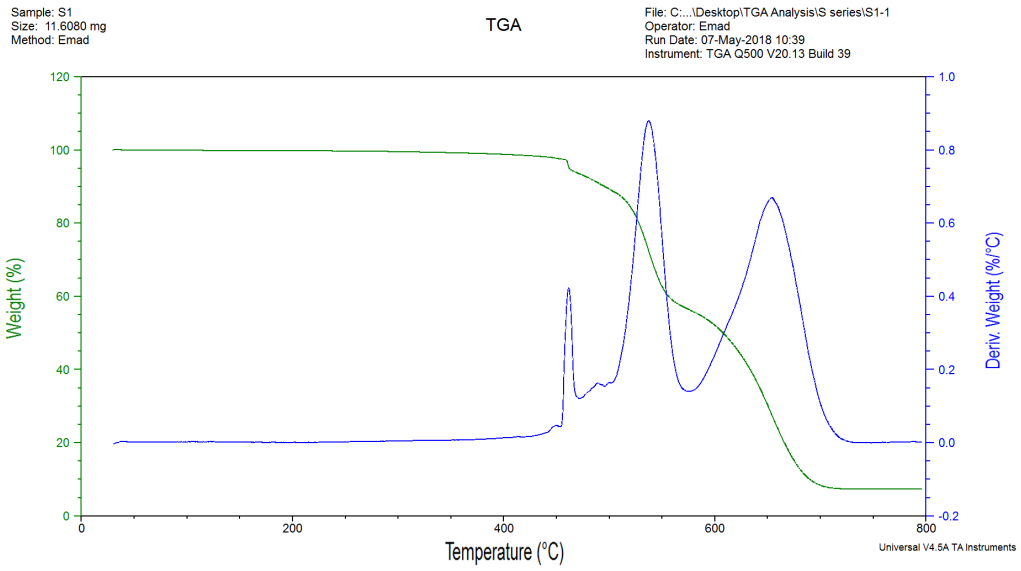

Figure A.37: S1: PSU + TiO_2 NP

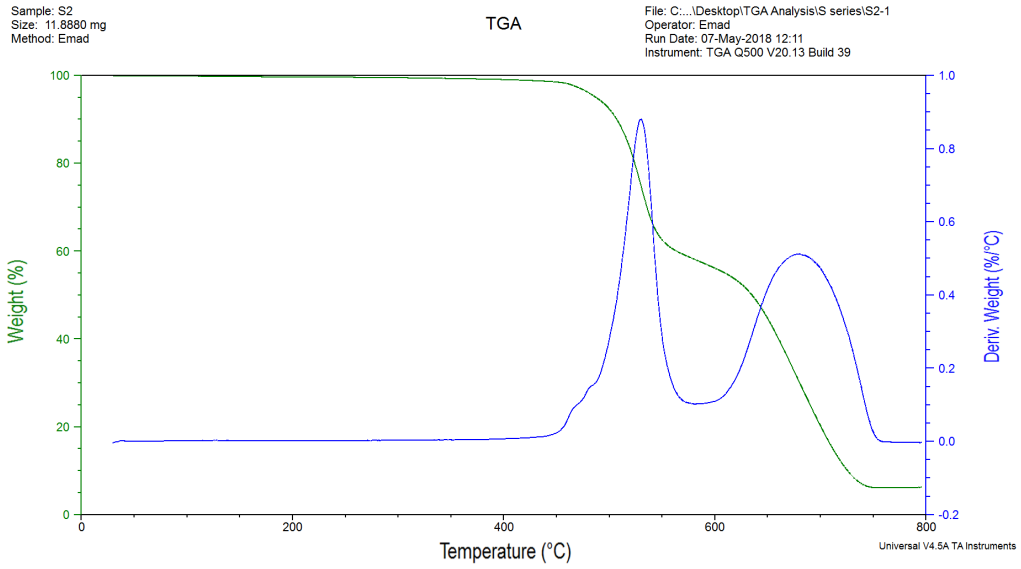

Figure A.38: S2: PSU + TiO_2 NB

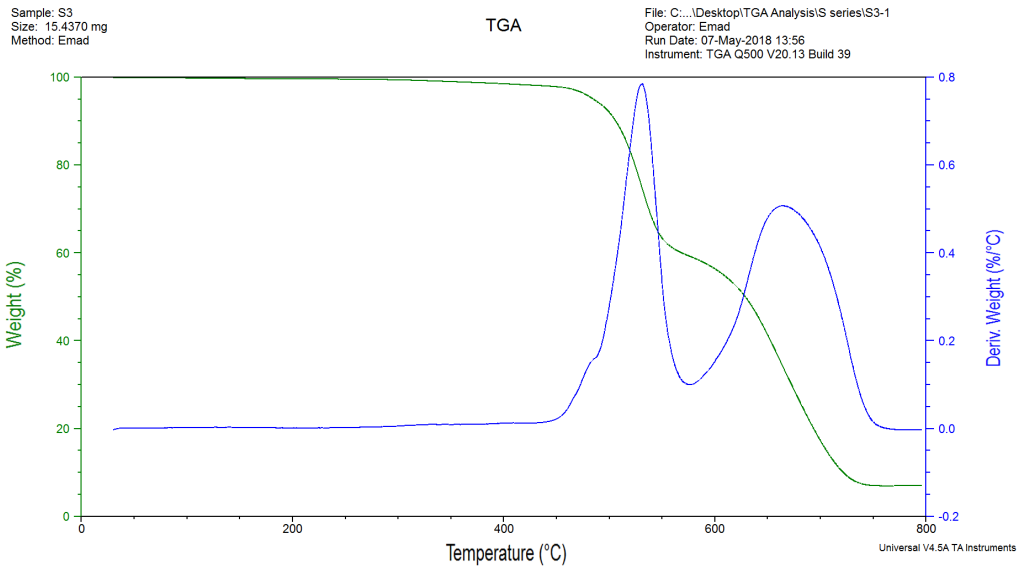

Figure A.39: S3: PSU + TiO_2 NP + bentonite nanoclay

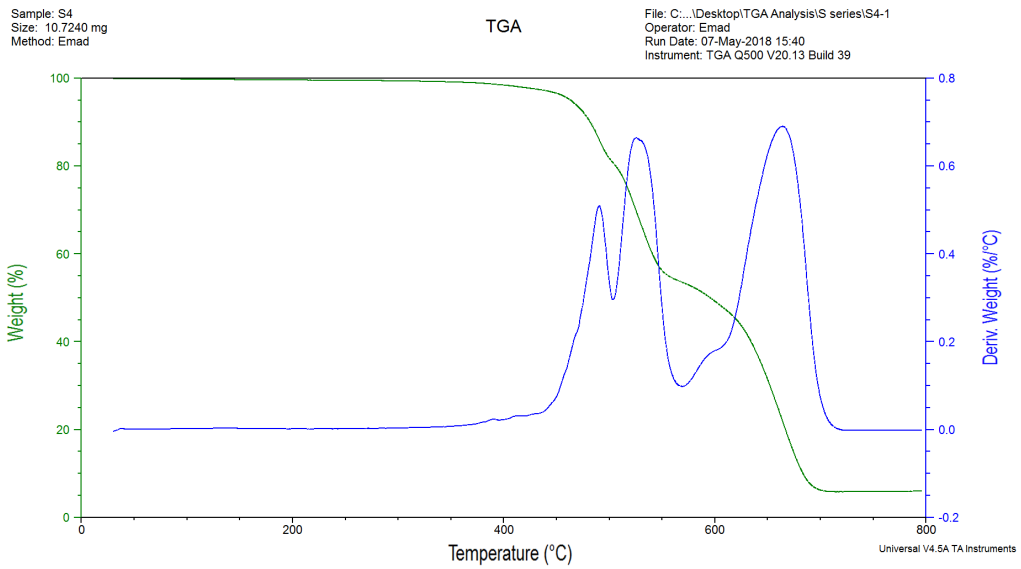

Figure A.40: S4: PSU + TiO_2 NB + bentonite nanoclay

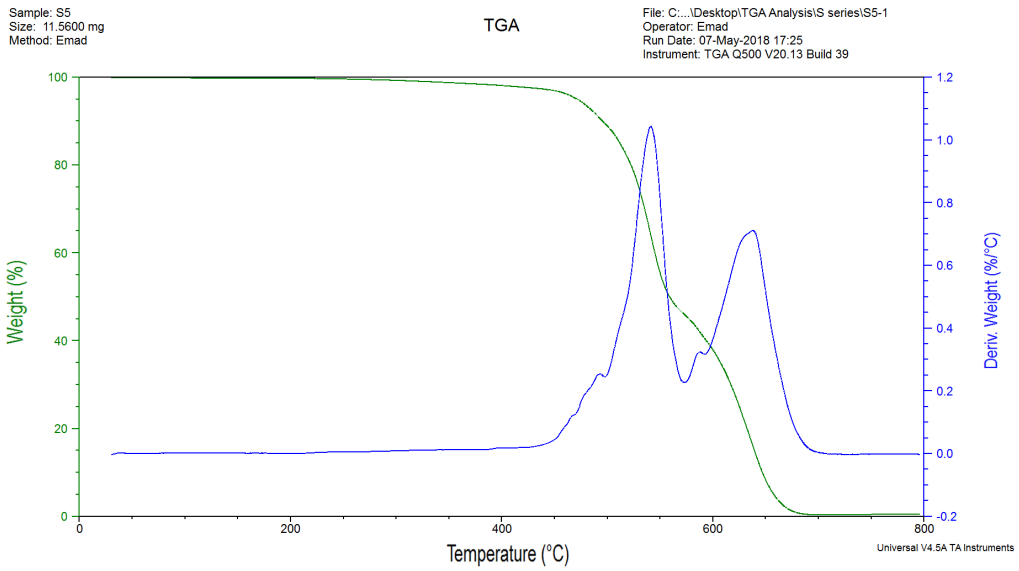

Figure A.41: S5: pure PSU

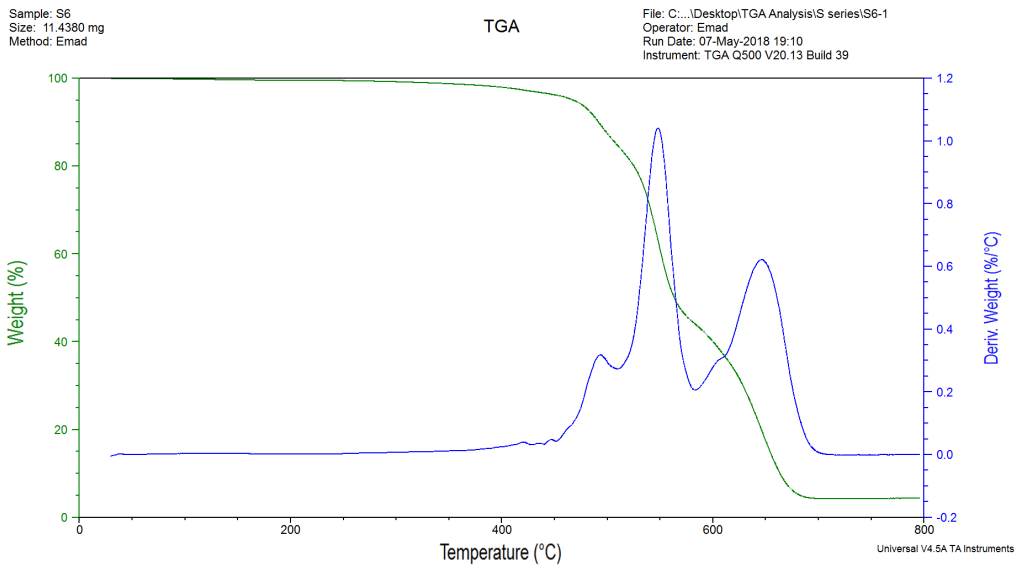

Figure A.42: S6: PSU + bentonite nanoclay

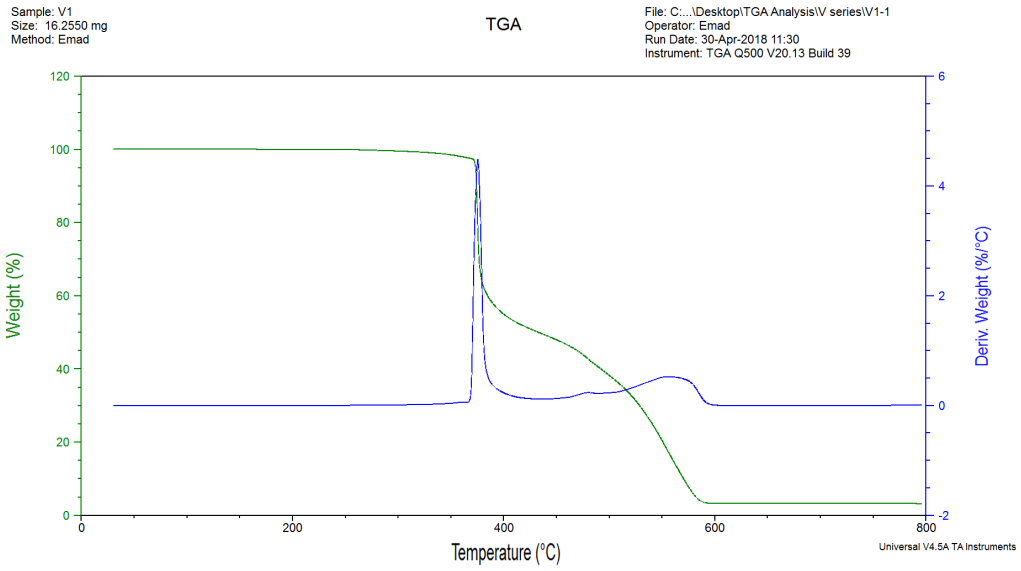

Figure A.43: V1: PVDF + TiO_2 NP

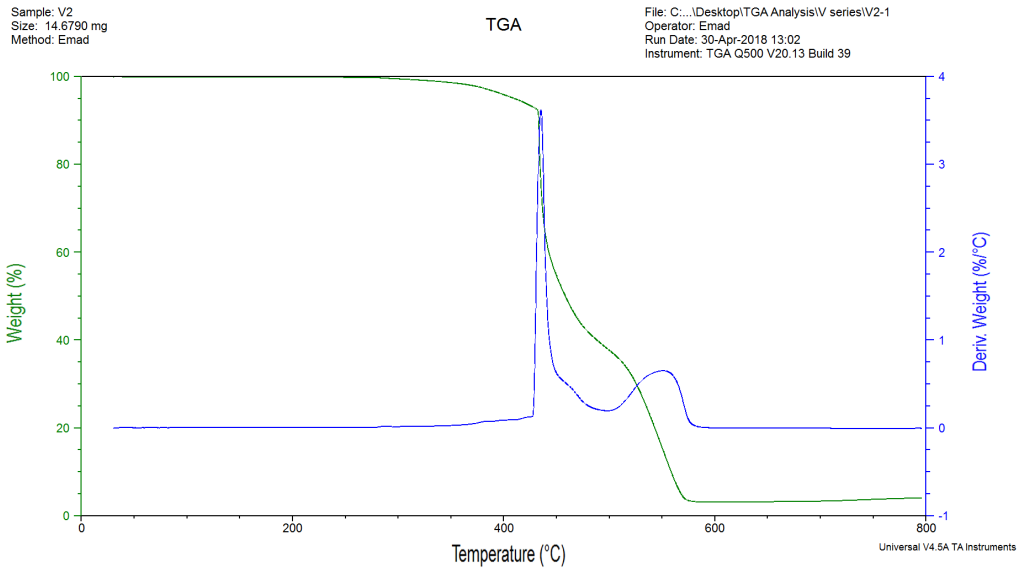

Figure A.44: V2: PVDF + TiO_2 NB

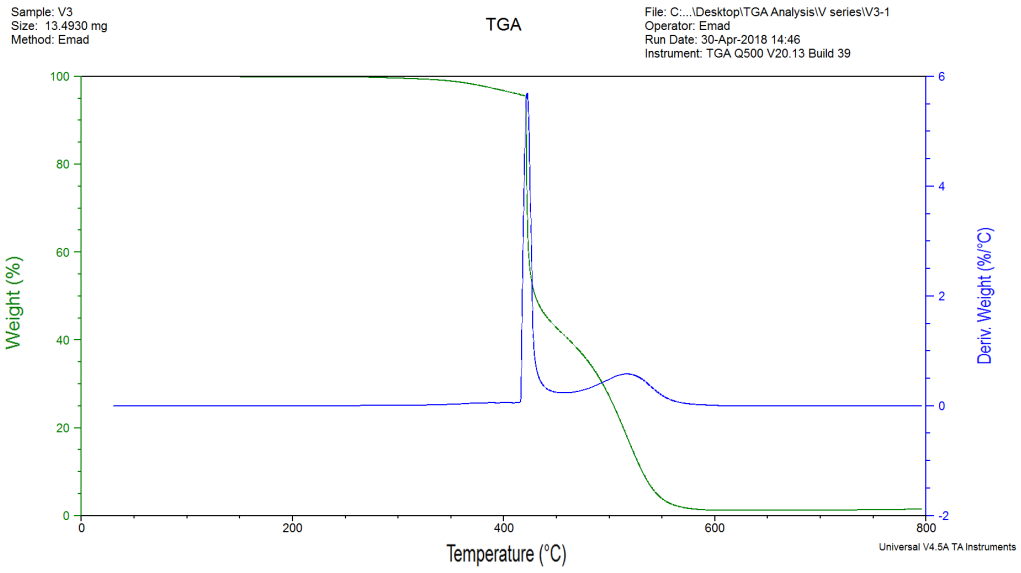

Figure A.45: V3: PVDF + TiO_2 NP + bentonite nanoclay

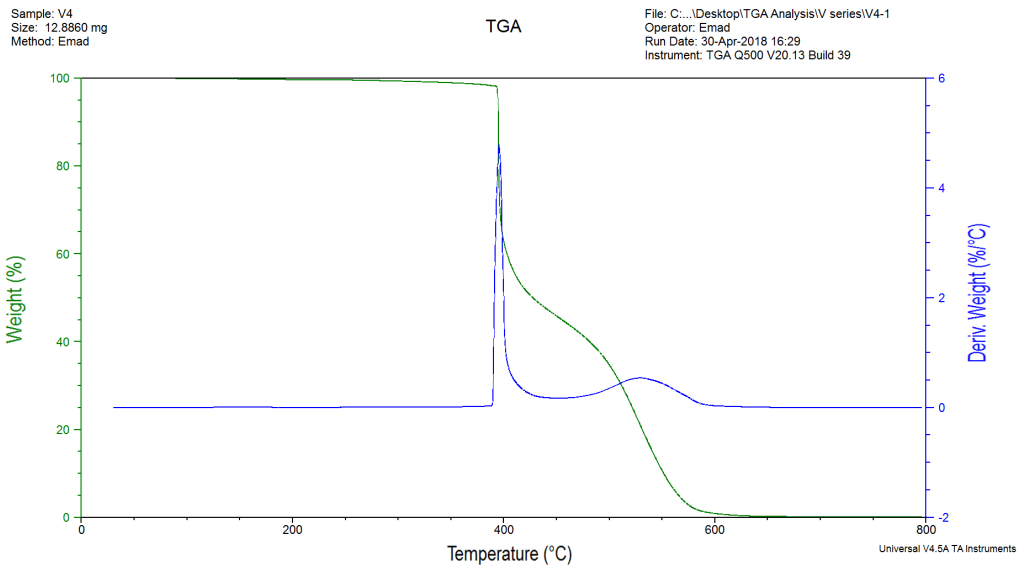

Figure A.46: V4: PVDF + TiO_2 NB + bentonite nanoclay

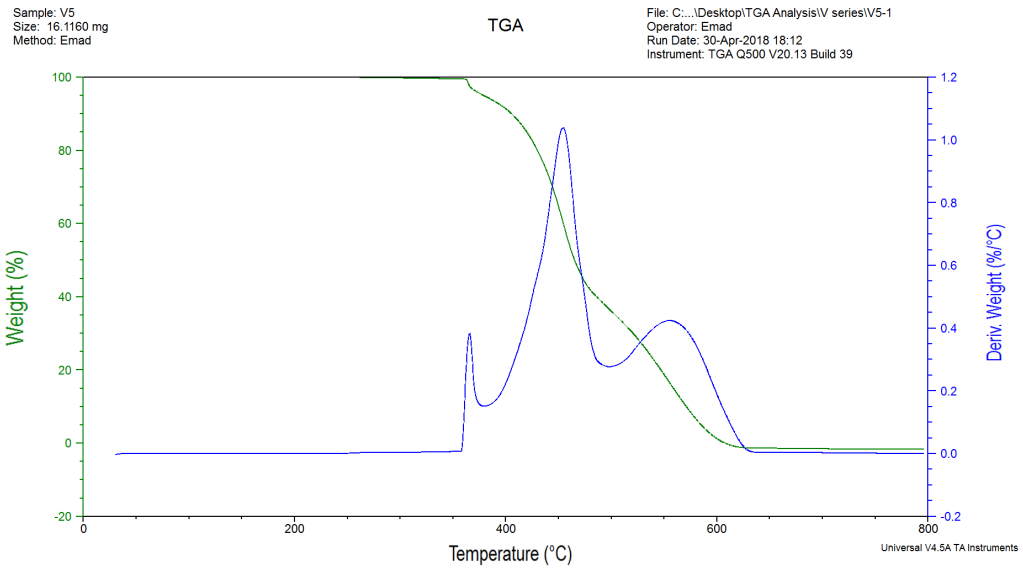

Figure A.47: V5: pure PVDF

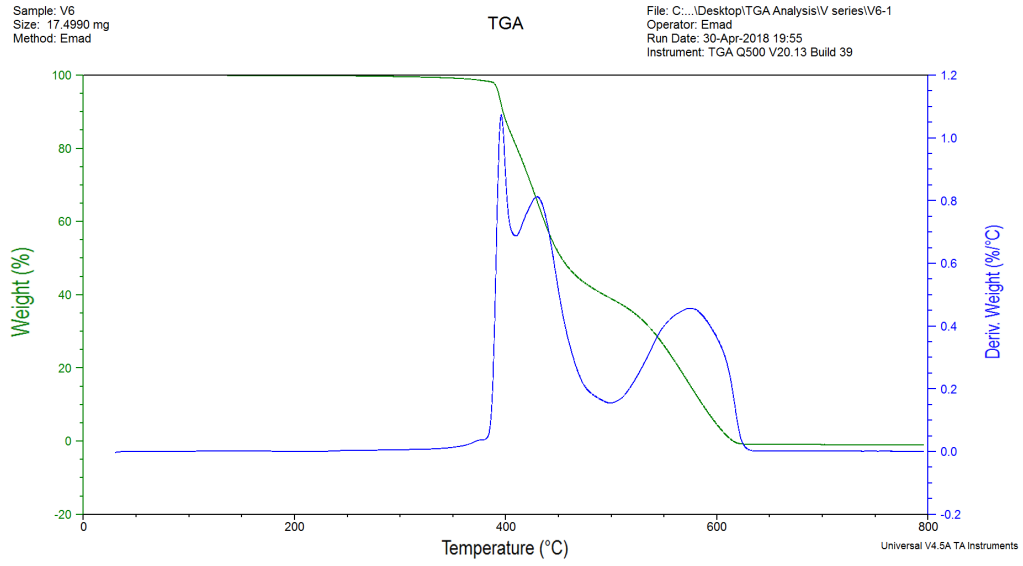

Figure A.48: V6: PVDF + bentonite nanoclay

Appendix B

B.1 Methylene blue degradation rates

Methylene blue degradation rates in the filaments of each polymer group are plotted in the following graphs:

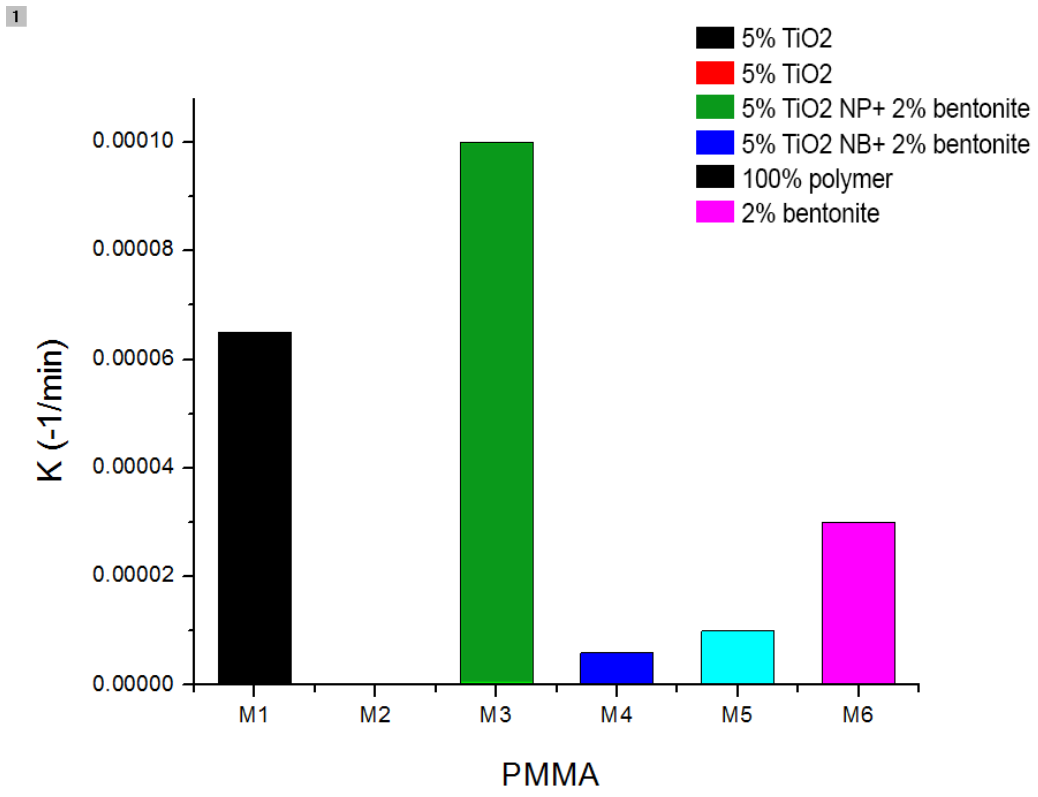

Figure B.1: Methylene blue degradation rates in the PMMA filaments after 5 hours

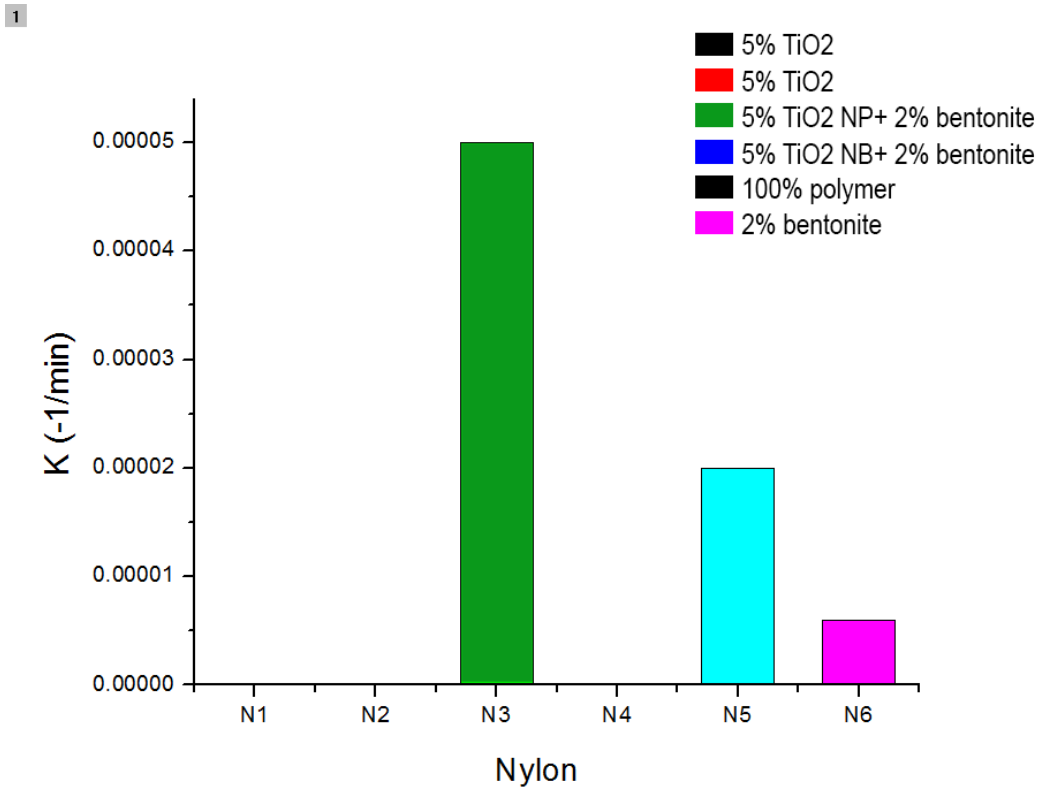

Figure B.2: Methylene blue degradation rates in the Nylon filaments after 5 hours

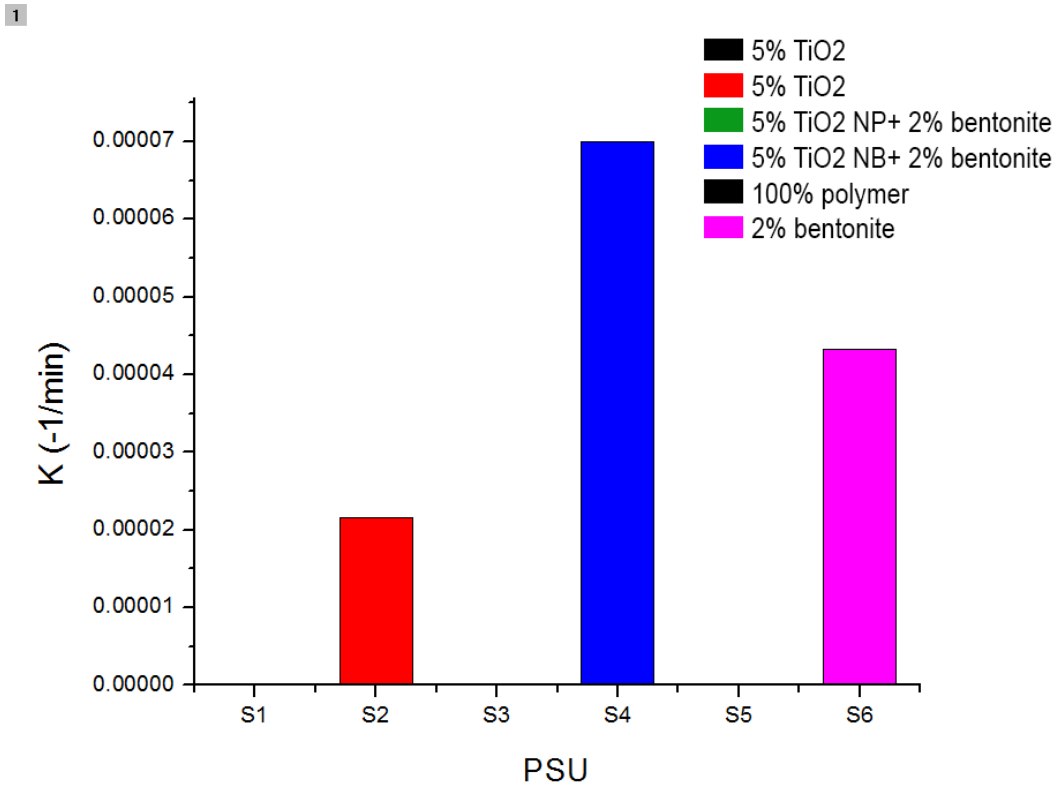

Figure B.3: Methylene blue degradation rates in PSU filaments after 5 hours

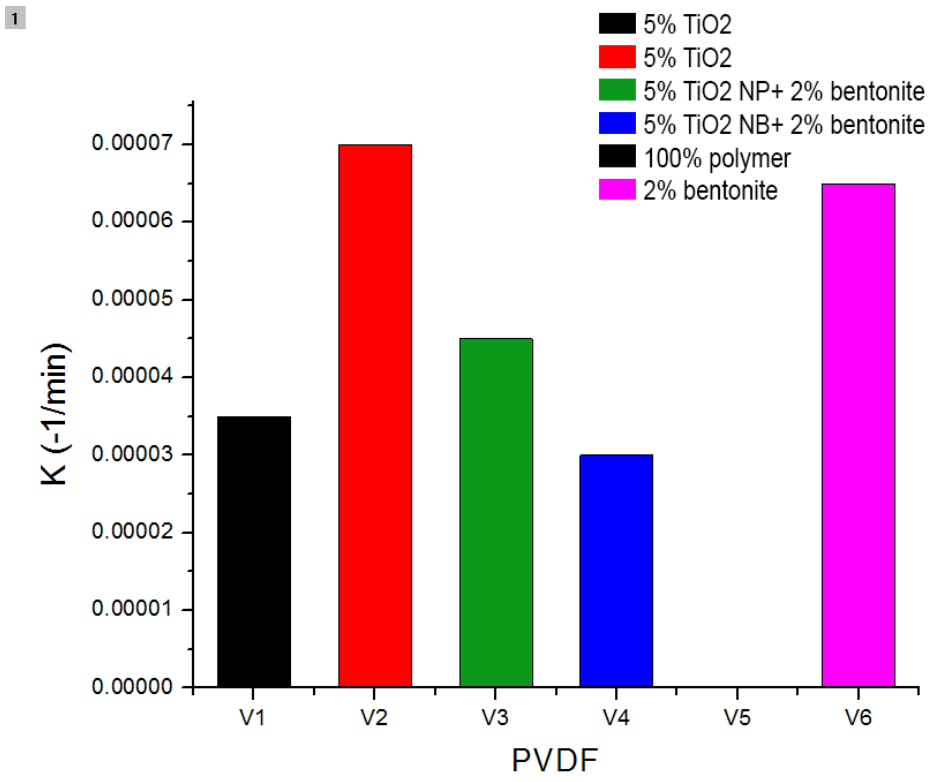

Figure B.4: Methylene blue degradation rates in PVDF filaments after 5 hours